A MULTISCALE MODELING APPROACH TO UNDERSTAND MECHANISM OF DEPOSIT CONTROL BY LUBRICANT DETERGENTS AND DISPERSANTS

A THESIS SUBMITTED TO
THE GRADUATE SCHOOL OF NATURAL AND APPLIED SCIENCES
OF
MIDDLE EAST TECHNICAL UNIVERSITY

BY

ESRA KAN

IN PARTIAL FULFILLMENT OF THE REQUIREMENTS
FOR
THE DEGREE OF MASTER OF SCIENCE
IN
POLYMER SCIENCE AND TECHNOLOGY

JULY 2022

Approval of the thesis:

A MULTISCALE MODELING APPROACH TO UNDERSTAND MECHANISM OF DEPOSIT CONTROL BY LUBRICANT DETERGENTS AND DISPERSANTS

submitted by **ESRA KAN** in partial fulfillment of the requirements for the degree of **Master of Science** i**n Polymer Science and Technology, Middle East Technical University** by,

Prof. Dr. Halil Kalıpçılar
Dean, Graduate School of **Natural and Applied Sciences** _____

Prof. Dr. Necati Özkan
Head of the Department, **Polymer Science and Technology** _____

Assist. Prof. Dr. Erol Yıldırım
Supervisor, **Polymer Science and Technology** _____

Examining Committee Members:

Prof. Dr. Mine Yurtsever
Chemistry, ITU _____

Assist. Prof. Dr. Erol Yıldırım
Chemistry, METU _____

Prof. Dr. İrem Erel Göktepe
Chemistry, METU _____

Assoc. Prof. Dr. Serhan Türkyılmaz
Chemistry, METU _____

Assist. Prof. Dr. Antoine Marion
Chemistry, METU _____

Date: 29.07.2022

I hereby declare that all information in this document has been obtained and presented in accordance with academic rules and ethical conduct. I also declare that, as required by these rules and conduct, I have fully cited and referenced all material and results that are not original to this work.

Name Last name : Esra Kan

Signature :

ABSTRACT

A MULTISCALE MODELING APPROACH TO UNDERSTAND MECHANISM OF DEPOSIT CONTROL BY LUBRICANT DETERGENTS AND DISPERSANTS

Kan, Esra
Master of Science, Polymer Science and Technology
Supervisor: Assist. Prof. Dr. Erol Yıldırım

July 2022, 101 pages

With the recent developments in high performance computing power, molecular modeling calculations to design and improve new generation additives for engine oils have reached a level that can support and guide experimental results. Control of insoluble nanoparticle aggregations in oil and on the engine pistons is the most important key performance parameter for lubricant oil additives. General consensus about the mechanism of deposit build-up is the self-aggregation of nanosized insoluble structures. Detergents and dispersants are the major additives to prevent aggregation in lubricant formulations provided by Lubrizol Corporation. Together with the base oil, they play a significant role to disperse and stabilize insoluble particles to control deposit formation. In this study, multiscale modeling methods were used to elucidate molecular mechanism of deposit control via detergents and dispersants by using density functional theory, molecular dynamics simulations of cells constructed by statistical sampling of large number of molecular configurations and coarse-grained simulations. The aim of this study is to understand the role of different groups such as bis-succinimide amine center and two polyisobutylene tails in dispersants as well as anionic sulfonate head group and alkyl tails in detergents. It

was demonstrated that the mechanism of deposit control can be explained by the interactions between constituents such as hydrogen bonding and hydrophobic-hydrophilic forces. We showed that nanoparticle aggregation is mitigated by intercalation of dispersant and detergent polar groups between the insoluble nanoparticles followed by the extension of hydrophobic tails into the oil phase that decreases coalesce further by forming a repulsive layer against the other nanoparticles.

Keywords: Dispersant, Detergent, Multiscale Modeling, Molecular Dynamics Simulation, Coarse-Grained Simulation

ÖZ

MOTOR YAĞLARINDA TORTU OLUŞUMUNUN DETERJANLAR VE DAĞITICILAR KULLANILARAK KONROL EDİLMESİ MEKANİZMASININ ÇOK ÖLÇEKLİ MODELLENMESİ

Kan, Esra
Yüksek Lisans, Polimer Bilim ve Teknolojisi
Tez Yöneticisi: Dr. Öğr. Üy. Erol Yıldırım

Temmuz 2022, 101 sayfa

Yüksek performanslı hesaplama gücündeki son gelişmelerle birlikte, motor yağlarında kullanılan yeni nesil katkı maddelerinin tasarlanması ve geliştirilmesi için moleküler modelleme hesaplamaları, deneysel sonuçları destekleyebilecek ve yönlendirebilecek bir düzeye ulaşmıştır. Motor yağında ve motor pistonlarında çözünmeyen nanoparçacık kümelenmelerini kontrol etmek, motor yağı katkı maddeleri için en önemli performans parametresidir. Tortu biriktirme mekanizması genel olarak nano boyutlu çözünmeyen yapıların kendi kendine kümelenmesi durumudur. Deterjanlar ve dağıtıcılar, Lubrizol Firması tarafından kullanılan motor yağı formülasyonlarında tortulaşmayı önleyen başlıca katkı maddeleridir. Baz yağ içerisinde, tortu oluşumunu kontrol etmek için çözünmeyen nanoparçacıkları dağıtmak ve stabilize etmek için önemli bir rol oynarlar. Bu tez çalışmasında, çok ölçekli modelleme yöntemleri kullanılmıştır. Deterjanlar ve dağıtıcılar aracılığıyla tortu kontrolünün moleküler mekanizmasını aydınlatmak için yoğunluk fonksiyoneli teorisi, çok sayıda moleküler konfigürasyonun istatistiksel olarak örneklenmesiyle oluşturulan hücrelerin moleküler dinamik simülasyonları ve kaba taneli simülasyonlar kullanmıştır. Bu çalışmanın amacı, dağıtıcılarda bulunan bis-süksinimid amin merkezi ve poliizobütilen kuyruk gruplarının yanı sıra,

deterjanlarda bulunan sülfonat kafa grubu ve alkil kuyruklarının rolünü anlamaktır. Tortu kontrol mekanizmasının, bileşenler arasındaki hidrojen bağı ve hidrofobik-hidrofilik kuvvetler gibi etkileşimlerle açıklanabileceği gösterilmiştir. Nanoparçacıklar arasına giren dağıtıcı ve deterjanların polar gruplarının parçacık kümelenmesini azalttığı, ayrıca hidrofobik kuyruklarının yağ fazı içine uzanarak, daha hidrofilik bir yüzeye sahip nanoparçacıklara karşı itici bir tabaka oluşturup kümelenmeyi daha da azalttığı gösterilmiştir.

Anahtar Kelimeler: Dağıtıcı, Deterjan, Çok Ölçekli Modelleme, Moleküler Dinamik Simülasyonlar, Kaba Taneli Simülasyonlar

To my beloved family…

ACKNOWLEDGMENTS

First of all, I wish to thank my supervisor Assist. Prof. Dr. Erol Yıldırım for his advice, guidance, encouragements and for introducing me this interesting area of research.

Computing resources used in this work were provided by the National Center for High Performance Computing of Turkey (UHeM) under grant number 1008192020. The numerical calculations reported in this paper were partially performed at TUBITAK ULAKBIM, High Performance and Grid Computing Center (TRUBA resources).

I would also like to thank Anıl Ağıral, Binbin Guo, and Eugene Pashkovski from Lubrizol Corporation (Lubrizol No. P2058871) to give me this great opportunity to work in this project.

I am also grateful to my lab mates for last two years full of enjoy, especially Tuğba Hacıefendioğlu Aydın, Deniz Budak and Oğuzcan Taneroğlu for their friendship and support in all matters.

I would like to thank my best friends İsmihan Altıparmak, Seda Sam, and Eylül Güllüoğlu for believing me and unconditionally supporting me.

I owe my special thanks to my love of my life, my husband, Güray Kan for always holding my hands, and making me believe to overcome all difficulties together. Thank you for not leaving me alone even for a moment during all the tiring times.

My final appreciations are for my lovely family. I would like to thank my mom Hülya Gürsoy, my dad İsmet V. Alparslan, my brother Atilla Erman Alparslan and sister-in law Betül Alparslan for their unconditional love, support and always believing me. Also, I would like to thank my other family, family of Kan, especially Günay Kan, Gürcan Kan for loving and supporting me like their own child.

TABLE OF CONTENTS

ABSTRACT v

ÖZ vii

ACKNOWLEDGMENTS x

TABLE OF CONTENTS xi

LIST OF TABLES xiv

LIST OF FIGURES xv

LIST OF ABBREVIATIONS xxii

LIST OF SYMBOLS xxiv

CHAPTERS

1 INTRODUCTION 1

1.1 Base Oil 1

1.2 Lubricant Deposit Control Additives 3

1.2.1 Detergent 4

1.2.2 Dispersant 6

2 EXPERIMENTAL CHARACTERIZATION 11

3 THEORETICAL AND COMPUTATIONAL CHEMISTRY 17

3.1 Quantum Mechanics Calculations (Electronic Structure Method) 20

3.1.1 Ab-initio Calculations 21

3.1.2 Density Functional Theory 21

3.2 Molecular Mechanics Calculations 23

3.2.1 Classical Monte Carlo Approximation 24
3.2.2 Molecular Dynamics (MD) Simulations 24
3.3 Coarse-Grained Simulations 27
3.4 Aim of the Study 28
4 COMPUTATIONAL METHODOLOGY 29
4.1 First Principle Calculations 30
4.2 Molecular Mechanics Methods 31
4.2.1 Calculation of Pairwise Interaction Energies based on the Molecular Mechanics Calculations 33
4.3 Coarse Graining Method 36
5 RESULTS & DISCUSSIONS 39
5.1 Molecular and Electronic Structures of System Components 39
5.1.1 Base Oil 40
5.1.2 Polyisobutylene-bis-succinimide (PIBSI) 41
5.1.3 Sulfonate Detergent 43
5.1.4 Insoluble Nanoparticle 44
5.2 Solubility Parameter Calculations 45
5.3 Validation of Computational Method and Force Field Approach 49
5.4 Interaction Energies 51
5.4.1 DFT Calculations 51
5.4.2 Pairwise interactions via Molecular Mechanics Methods 52
5.5 Solvation Free Energy Calculations 54
5.6 Monte Carlo Simulations 54
5.7 Molecular Dynamics Simulations 62

5.8 Coarse-Grained Simulations 84
6 CONCLUSION 93
REFERENCES 97

LIST OF TABLES

TABLES

Table 1.1. API base oil categories [3]. 3

Table 5.1. Solubility parameters of the base oil, polar and non-polar portions of dispersant, sulfonate, and Ca+2, and sulfonate. 46

Table 5.2. Hydrophobicity, SASA, TPSA, TASA, RPSA, RASA for the components of the system. 49

Table 5.3. Binary interaction energies. 53

Table 5.4. Coarse-grained interaction parameters mapped into the coarse-grained units. 85

LIST OF FIGURES

FIGURES

Figure 1.1. Molecular structures of (a) sulfonate, (b) phenate, (c) salicylate detergent. 5
Figure 1.2. a) Schematic representation of groups of dispersant molecule and mechanism, b) steric repulsion of engine oil contaminants surrounded with dispersant molecules. 7
Figure 1.3. Sludge particle growth demonstration, reproduced by permission of [8]. 8
Figure 1.4. Synthesis and structures of a) mono-, b) bis-, c) tris-succinimide dispersants. 9
Figure 2.1. Engine piston groove and lands. 11
Figure 2.2. Land cleanliness differences between a) in Group II base oil b) in Group II base oil with extra dispersant c) in Group III base oil environments. 12
Figure 2.3. Mean harmonic intensity averaged diameter of pistons a) detergent & dispersant effect b) base oil effect 12
Figure 2.4. SEM image of a) 2nd and 3rd land deposits and b) insolubles from drain oil. 13
Figure 2.5. XRD result of the drain insolubles. 13
Figure 2.6. Elemental analysis of a) land deposits b) drain insolubles. 14
Figure 2.7. XPS results of a) drain insolubles, b) land deposits. 15
Figure 2.8. TEM images of a) engine oil b) with extra dispersant. 16
Figure 3.1. Multiscale modeling of materials by using different time and length scales with the different methods. 19
Figure 4.1. Thermodynamic cycle. 36
Figure 4.2. Coarse-grained model of insoluble nanoparticle defined by coarse grained units. 38
Figure 5.1. Base oil structures with partial atomic charges. 40
Figure 5.2. PIB-bis-succinimide dispersant molecular structure. 41

Figure 5.3. a) Electrostatic Surface Potential, b) HOMO, c) HOMO-1, d) LUMO, and e) LUMO+1 structures of dispersant molecule. 42
Figure 5.4. Models of a) amine, b) succinimide, and c) isobutylene portions of PIBSI dispersant. 42
Figure 5.5. Molecular structure of polyisobutylene-bis-succinimide dispersant model. 43
Figure 5.6. Sulfonate detergent a) ESP surface, b) HOMO, c) LUMO structures and d) first principle, e) classical method calculations. 44
Figure 5.7. Ultrafine insoluble nanoparticle model. 45
Figure 5.8. The unit cell with 366 base oil molecules. 50
Figure 5.9. Density changes of base oil structure after 50000 step cell optimizations. 50
Figure 5.10. Interaction energies (kcal/mol) between components based on the DFT calculations. 52
Figure 5.11. A nanoparticle in a unit cell to calculate solvation free energy of nanoparticle. 54
Figure 5.12. The lowest energy cell geometry which agrees with first principle calculations with one nanoparticle and a) one dispersant molecule, b) one detergent molecule. 55
Figure 5.13. The lowest energy cell geometry which agrees with first principle calculations with two nanoparticles and a) one dispersant molecule, b) one detergent molecule 56
Figure 5.14. Packing of a) four nanoparticles in a unit cell with b) four dispersant molecules followed by c) base oil addition by Monte Carlo calculation. 56
Figure 5.15.a) Placing four nanoparticles in a unit cell, b) packing with 232 base oil molecules, and c) followed by four dispersant molecules. 57
Figure 5.16. Placing four nanoparticles in a unit cell, b) packing of 232 base oil molecule c) followed by ten sulfonate molecules and five calcium cations. 58

Figure 5.17. Two nanoparticle system packed with a) 261 base oil molecules b) base oil and two dispersant molecules c) base oil and six detergent molecules and 3 calcium cations. 59
Figure 5.18. Three nanoparticle system packed with 277 base oil molecules in a unit cell. 59
Figure 5.19. Three nanoparticle system with a) three dispersant and 237 base oil molecules, b) six dispersant and 213 base oil molecules, c) twelve dispersant and 190 base oil molecules. 60
Figure 5.20. Three nanoparticle system with a) six detergent and 252 base oil molecules, b) twelve detergent and 244 base oil molecules, c) eighteen detergents and 235 base oil molecules. 60
Figure 5.21. Four nanoparticle system a) in cubic cell, b) packing with 728 base oil molecules, c) packing with four dispersant and 697 base oil molecules. 61
Figure 5.22. Four nanoparticle system a) in cubic cell, b) packing with 728 base oil molecules, and c) packing with eight detergent molecules, four calcium cations and 717 base oil molecules. 61
Figure 5.23. a) The first, b) middle and c) final frames of MD simulations of aggregated four nanoparticles in empty unit cell for 2 ns simulation time. 62
Figure 5.24. a) The first, b) middle and c) final frames of MD simulations of aggregated 4 nanoparticles in unit cell packed with 697 base oil molecules for 2 ns simulation time. 62
Figure 5.25. MSD calculations of four nanoparticles in a) empty unit cell and b) unit cell with base oil. 63
Figure 5.26. a) The first, b) middle and c) final frames of MD simulations of separately placed four nanoparticles in empty unit cell for 2 ns simulation time... 64
Figure 5.27. a) The first, b) middle and c) final frames of MD simulations of separately placed four nanoparticles in unit cell packed with 581 base oil molecules for 2 ns simulation time. 64
Figure 5.28. Radial distribution function between hydrogen and oxygen atoms of nanoparticles. 65

Figure 5.29. Hydrogen bonding between nanoparticles shown as black dashed lines.....65
Figure 5.30. The first frame of MD simulations of two nanoparticles with 7 Å distance, b) the last frame of MD simulations of two nanoparticles with 2 Å distance.....66
Figure 5.31. Distance evolution graph of two nanoparticles in the unit cell with base oil.....67
Figure 5.32. a) The first frame of MD simulations of two nanoparticles with 7 Å distance and two dispersant molecules, b) the last frame of MD simulations of two nanoparticles with 9 Å distance with two dispersant molecules. Inset figures show detailed captures.....67
Figure 5.33. Radial distribution function between amine of dispersant molecules and hydrogen of nanoparticles.....68
Figure 5.34. Hydrogen bonding between nitrogen of dispersant amine group and hydrogen of nanoparticle hydroxyl group shown as black dashed lines.....68
Figure 5.35. a) The first frame of MD simulations of two nanoparticles with 8 Å distance, and b) last frame of MD simulations of two nanoparticles with 7 Å distance with six detergent molecules. Inset figures show detailed captures.....69
Figure 5.36. a) Distance distribution and b) RDF for the sulfonate head group and nanoparticle surface.....70
Figure 5.37. Hydrogen bonding between oxygen atoms in sulfonate head group and hydrogen atoms in nanoparticles surface for two nanoparticle system shown as black dashed lines.....71
Figure 5.38. a) The first frame of MD simulations of three nanoparticles with 5 Å distance, b) the last frame of MD simulations of aggregated three nanoparticles. Inset figures show detailed captures.....71
Figure 5.39. Distance evolution of the intermolecular distance between nanoparticles in three nanoparticle system.....72
Figure 5.40. Hydrogen bonding between nanoparticles shown as black dashed lines.....72

Figure 5.41. Distance distribution of randomly chosen distances between aggregated nanoparticles. 73
Figure 5.42. a) The first frame and b) the last frame of MD simulations of three nanoparticles with three dispersant molecules. Inset figures show detailed captures. 73
Figure 5.43. a) The first frame and b) the last frame of MD simulations of three nanoparticles with six dispersant molecules. 74
Figure 5.44. a) The first frame and b) the last frame of MD simulations of three nanoparticles with nine dispersant molecules. 75
Figure 5.45. MSD graphs of three nanoparticles for a) three, b) six, and c) nine dispersant molecule structures. 75
Figure 5.46. a) The first frame and b) the last frame of MD simulations of three nanoparticles with six sulfonate detergent molecules. Inset figures show detailed captures. 76
Figure 5.47. a) The first frame and b) the last frame of MD simulations of three nanoparticles with twelve sulfonate detergent molecules. Inset figures show detailed captures..... 77
Figure 5.48. a) The first frame and b) the last frame of MD simulations of three nanoparticles with eighteen sulfonate detergent molecules. Inset figures show detailed captures..... 78
Figure 5.49. RDF of oxygen atoms of detergent head group and hydrogen atoms at the nanoparticle surface. 78
Figure 5.50. Hydrogen bonding between oxygen atoms in sulfonate head group and hydrogen atoms at nanoparticle surface for two nanoparticle system, shown as black dashed lines. 79
Figure 5.51. MSD graphs of three nanoparticles for a) six, b) twelve, and c) eighteen detergent molecule structures. 79
Figure 5.52. a) The first frame of MD simulations of four nanoparticles with 8 Å distance, b) the last frame of MD simulations of four nanoparticles after 2 ns, c) last frame of MD simulations of four nanoparticles in base oil after 4 ns. 80

Figure 5.53. a) The first frame of MD simulations of four nanoparticles with 5 Å distance in 423 K, b) the last frame of MD simulations of four nanoparticles after 2 ns in 423 K, c) last frame of MD simulations of four nanoparticles in base oil after 2 ns in 823 K.....81
Figure 5.54. The first and b) the last frame of MD simulations of four nanoparticles with four dispersant molecules in 423 K.....81
Figure 5.55. RDF between hydrogen atoms in nanoparticle surface and a) nitrogen atoms amine portion b) oxygen atoms in succinimide portion.....82
Figure 5.56. Hydrogen bonding between a) the nitrogen atoms in dispersant amine group and hydrogen atoms in nanoparticles surface b) the oxygen atoms in dispersant succinimide group and hydrogen atoms in nanoparticles surface, shown as black dashed lines. 82
Figure 5.57. a) The first and b) the last frame of the MD simulation of four nanoparticles with eight sulfonate detergent molecules in cubic unit cell. 83
Figure 5.58. RDF between oxygen atoms in the head group of the sulfonate detergent and hydrogen atoms on nanoparticle surface. 83
Figure 5.59. Hydrogen bonding between oxygen atoms in the head group of sulfonate detergent and hydrogen atoms at the nanoparticle surface, depicted as black dashed lines.....84
Figure 5.60. Insoluble nanoparticle isosurface structures with a) 95% oil and 5% np, b) 90% oil and 10% np, c) 85% oil and 15% np, d) 80% oil and 20% np, e) 70% oil and 30% np, f) 60% oil and 40% np, g) 50% oil and 50% np ratios. 86
Figure 5.61. Insoluble nanoparticle isosurface structures with a) 85% oil and 15% np, b) 2% disp- 83% oil - 15% np, c) 5% disp- 80% oil - 15% np, d) 10% disp- 75% oil - 15% np, e) 15% disp- 70% oil - 15% np, and f) 25% disp- 60% oil - 15% np ratios. 87
Figure 5.62. Insoluble nanoparticle isosurface structures with a) 85% oil and 15% np, b) 2% det- 83% oil - 15% np, c) 5% det- 80% oil - 15% np, d) 10% det- 75% oil - 10% np, e) 15% det- 70% oil - 15% np ratios. 88

Figure 5.63. Insoluble nanoparticle isosurface structures with a) 10% disp - 85% oil - 5% np, b) 10% disp- 80% oil - 10% np, c) 10% disp- 75% oil - 15% np, d) 10% disp- 60% oil - 30% np ratios. 89
Figure 5.64. Insoluble nanoparticle isosurface structures with a) 10% sulf - 85% oil - 5% np, b) 10% sulf- 80% oil - 10% np, c) 10% sulf- 75% oil - 15% np, d) 10% sulf- 60% oil - 30% np ratios. 90
Figure 5.65. a) 2% detergent could not dissolve the 30% nanoparticles, b) 5% dispersant could not dissolve the 50% of nanoparticles. 91
Figure 5.66. Insoluble nanoparticle isosurface structures at a) 300 K, b) 450 K, c) 600 K temperatures. 91
Figure 5.67. The field density distribution of nanoparticles in oil without (a, b) and with (c, d) the depiction of polar amine center in dispersant and sulfonate head group. 92

LIST OF ABBREVIATIONS

ABBREVIATIONS

API: American Petroleum Institute

COMPASS: Condensed-phase Optimized Molecular Potentials for Atomistic Simulation Studies

DFT: Density Functional Theory

DLS: Dynamic Light Scattering

E: Energy

ESP: Electrostatic Potential

FTIR: Fourier Transform Infrared Spectroscopy

H: Enthalpy

HF: Hartree-Fock

MFT: Mean Field Theory

MW: Molecular Weight

MD: Molecular Dynamics

MSD: Mean Square Displacement

N: Number of particles

nm: Nanometer

NPH: Constant Pressure and Enthalpy

NPT: Constant Pressure and Temperature

NVE: Constant Volume and Enthalpy

NVT: Constant Volume and Temperature

P: Pressure

PAO: Polyalphaolefin

PAG: Polyalkyleneglycol

PIB: Polyisobutylene

PIBSA: Polyisobutylene succinic anhydride

PIBSI: Polyisobutylene succinimide

RDF: Radial Distribution Function

S: Stress

SEM: Scanning Electron Microscope

T: Temperature

TEM: Transmission Electron Microscope

TS: Tkatchenko-Scheffler

V: Volume

vdW: van der Waals

VI: Viscosity Index

WPD: Weight Piston Deposit

XPS: X-ray Photoelectron Spectroscopy

XRD: X-ray Diffraction Analysis

μm: micrometer

LIST OF SYMBOLS

SYMBOLS

$\hat{H}$: Hamiltonian operator

Ψ: Wave function

∇: Gradient

δ: Solubility parameter

μ_{xc}: Exchange correlation potential

χ: Flory-Huggins miscibility character

ΔG: The change in Gibbs Free Energy

CHAPTER 1

INTRODUCTION

The science of lubrication was born to reduce friction with the use of axles and bearings after the 17th century [1], [2]. In a lubrication system, there are moving surfaces under load and a lubricant between these surfaces. Both the physical and chemical properties of the lubricants are exploited by the industry. Reducing friction and wear is the most important function of lubricants.

1.1 Base Oil

Lubricating base oils are crude oil products that have been refined [3]. Base oils are main ingredients and carry out the primary function of lubricants. Base oils comprise a significant portion of lubricants. The remaining components of the lubricants are additives, a combination of compounds that contribute crucial properties to protect the engine's moving parts. Additives support the ability of base oil to protect engine bearings, piston rings, and other moving engine components.

The choice of base oils can have a significant impact on the lubricant's qualities. American Petroleum Institute (API) classifies the base oils at five groups. The properties of each group of base oils are different [4].

Base oils have four physical properties that determine how they perform in service [5]. These are pour point, viscosity, viscosity index and purity. First, the pour point is the lowest temperature at which an oil sample can be poured. The base oil to be selected should have the appropriate pouring point according to the usage. Viscosity is the resistance to flow. The Viscosity Index (VI) is the change in viscosity with temperature. High VI oils change viscosity less with temperature than a low VI oil.

The final physical property is purity. Components such as nitrogen and sulfur impair the purity. Their amount in the base oil should be limited [5].

Five classes of base oils are based on their structures and performance characteristics [1]. Group I, II and III, that are hydro-processed mineral oils, are refined from petroleum crude oil. Group I base oils have a sulfur content greater than 0.03% by weight, a saturate content of less than 90%, and a VI between 80 and 119. They are widely utilized in industrial and marine lubricants, as well as in older engine oils. Both Group II and III are hydro-processed oils with similar purity and 99% saturates. For Group II base oils, hydro-treating is a common method for production which is a process that requires adding hydrogen to base oil at high temperatures in the presence of a catalyst in order to stabilize the base oil's most reactive components, improve color, and extend its service life. The major distinction between Group II and III is that Group III has a VI of 120 or above. Group II which used in this study dominates the base oil supply, particularly in North America [2].

Group III base oils are frequently hydrocracked which is more severe form of hydro-processing. It is performed by introducing hydrogen into the base oil, at temperatures and pressures that are higher than those used in ordinary hydro-treating. Sulphur, nitrogen, and aromatics are all eliminated to a large extent [2].

Group IV oils are mainly polyalphaolefins (PAOs) that are a type of synthetic base oils. Group IV base oils can be produced with a VI of up to 140 by combining different alpha olefins [1]. Base oils in Group V are those that are not in Groups I, II, III, or IV. Since, this group includes naphthenic base oils, different synthetic esters, polyalkyleneglycols (PAGs), phosphate esters, and others. Base oil categories are shown in Table 1.1. below, according to API.

Table 1.1. API base oil categories [3].

Base Oil Category	Sulphur (%)		Saturates (%)	Viscosity Index
Group I	>0.03	and/or	<90	80 to 120
Group II	<0.03	and	>90	80 to 120
Group III	<0.03	and	>90	>120
Group IV	PAO Synthetic Lubricants			
Group V	All other base oils not included in Group I, II, III, IV			

1.2 Lubricant Deposit Control Additives

Lubricants can be designed with a variety of components, depending on the needs of the application. Some intended features can be increased with base oil selection, while others can be improved with additives. Engine oil additives are made to preserve a variety of engines, including those used in heavy trucks, passenger cars, and ships, as well as smaller engines found in recreational vehicles. The property of automotive lubricants, particularly engine oils, to suspend undesired particles from thermal and oxidative degradation is one of their most important qualities. When by-products of fuel combustion, pass through piston rings into the lubricant, side products formed due to the reactive species and lubricant oxidation. The oxidation products are thermally unstable and decompose into highly polar compounds. They also have a tendency for forming surface deposits and clogging engine rings. First, deposits cause malfunctioning in tight surfaces, such as those between pistons and cylinder walls, and it hinders oil flow to sections that require lubrication [3].

The dispersant and detergent are oxidation inhibitors and more importantly, they are the main deposit control additives in lubricant oil. Dispersants have the ability to inhibit the production of high-temperature deposit formations by the aggregation of insolubles, while detergents have the capability to disperse and suspend contaminants [4].

In an engine environment, these additives deal with two basic deposits: soot and sludge. Soot is produced by diesel engines, due to incomplete oxidation of the fuel upon ignition [5], [6]. As a result of the accumulation of soot, oil thickening issues arise. These ultrafine granular and abrasive particles have a diameter of less than 100 nm, yet they aggregate over time into larger particles with a diameter on the order of 1 μm to depending on the time their polar surface is exposed to the oil. Sludge is commonly generated in the lubricant of gasoline passenger car engine oils, which is not as large as soot in size. It sourced from the thermal oxidation of oil, as well as the fumes that contained partially burned fuel. Both soot and sludge increase the viscosity of the oil, which is harmful for engine rings. Soot and sludge, that are insoluble particles and carbon-rich or metallic by nature, are the result of incomplete fuel oxidation during ignition [5].

1.2.1 Detergent

Since the 1940s, detergents have been used in engine oil applications as lubricant additives [5]. These lubricant additives became named as 'detergents' as a result of their cleaning capability, chemical affinity and structural similarity to aqueous detergents, such as those used in laundry soaps. Detergents are also called as metallic soaps [7]. Detergents are metal salts of organic acids that improve lubricant compositions by providing corrosion protection, deposit prevention, and a variety of other advantages. They are chemical compounds that chemically neutralize deposits that form under high-temperature environments, or as a result of burning sulfur-containing fuels or other materials that produce acidic combustion products [4]. Alkyl benzenesulfonic acids, alkylphenols, carboxylic acids, and alkenyl phosphonic acids are some of the common acids used to synthesize detergents. The amount of metal used, may be equal to or greater than the stoichiometric amount required to neutralize the acid function completely. The detergents are termed 'neutral' when the metal cation is present in the stoichiometric amount. They are termed as 'basic, overbased, or superbased' when they are present in excess [3][8]. The amount of

overbasing, as well as the size and shape of the component, have an impact on detergent performance [5]. This study will not include any research into over-based structures.

Detergent type and concentration are highly depending on the application such that different combinations might be required to achieve optimum performance and cost. Sulfonate-, phenate- and salicylate-type detergents incorporating calcium carbonate are the most widely used in Lubrizol Corporation formulations as shown in Figure 1.1. This thesis is the product of a Technology Transfer Office Project carried out with the collaboration of Lubrizol Corporation. In addition, the experimental results were shared by the company, and they shared their valuable experiences on this subject.

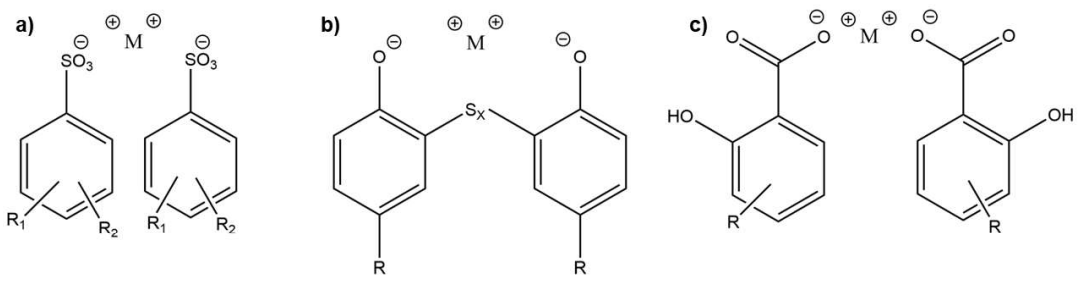

Figure 1.1. Molecular structures of (a) sulfonate, (b) phenate, (c) salicylate detergent.

This study focused on the metal salt detergents, specifically on the sulfonic acids (sulfonates) that have more applications compared to alkylphenol (phenates), or alkyl salicylic acids (salicylates) for the inhibition of deposit formation. One of the key groups of lubricant additive components that helps enhance the performance and life of the engine are alkyl aryl (alkaryl) sulfonate detergents. Alkaryl sulfonates are significant engine oil detergents that clean and protect the engine against rust [9]. Their detergent activity contributes in the neutralization of acids created during fuel combustion, which can cause engine damage. Alkaryl sulfonates are formed by neutralizing an alkaryl sulfonic acid. Alkaryl sulfonic acid have a benzene ring with sulfonic acid substituent groups and long-chain alkyl substituent groups, with a base metal, typically calcium hydroxide, to form the corresponding metal salt as depicted

in Equation 1.a and 1.b. Mg^{2+} and Ca^{2+} are the most commonly used divalent metals [5].

$$A - H + M - OH \rightarrow A - M + H_2O \quad (1.a)$$

$$acid\ substrate + metal\ hydroxide \rightarrow neutral\ metallic\ detergent + water \quad (1.b)$$

The main role of the detergent helps keep small particles suspended so that they can be removed by the oil filter and not build up any deposits and aggregates in the engine.

1.2.2 Dispersant

Soot is a common by-product of internal combustion engines. Organic oxides as a product of combustion are transformed to polymers and cross-linked random organic structures as the ageing process progresses. This results in the formation of insoluble materials and eventually deposits. When it stays longer in the lubricant, it can cause some problems in engine environment. Dispersants are molecules that are used to disperse or suspend deposit-forming contaminants such as soot and sludge, which cause increased viscosity, abrasive wear, and filter clogging problems. Dispersants have polar central group and non-polar tail group(s). The polar group in the middle of dispersants connects with polar deposits and keeps them suspended in the oil according to theory, while the non-polar tail group is predicted to establish a barrier that prevents small groups of contaminants from creating bigger aggregates [10], [11]. Long polar groups capture organic deposits and maintain them distributed in the liquid phase [12]. Due to the steric and electrostatic interactions, the particles and associated dispersions are unable to agglomerate. Typically, the polar group of the dispersant contains oxygen or nitrogen especially in the alcohol and amine form that can form hydrogen bonds with the polar groups.

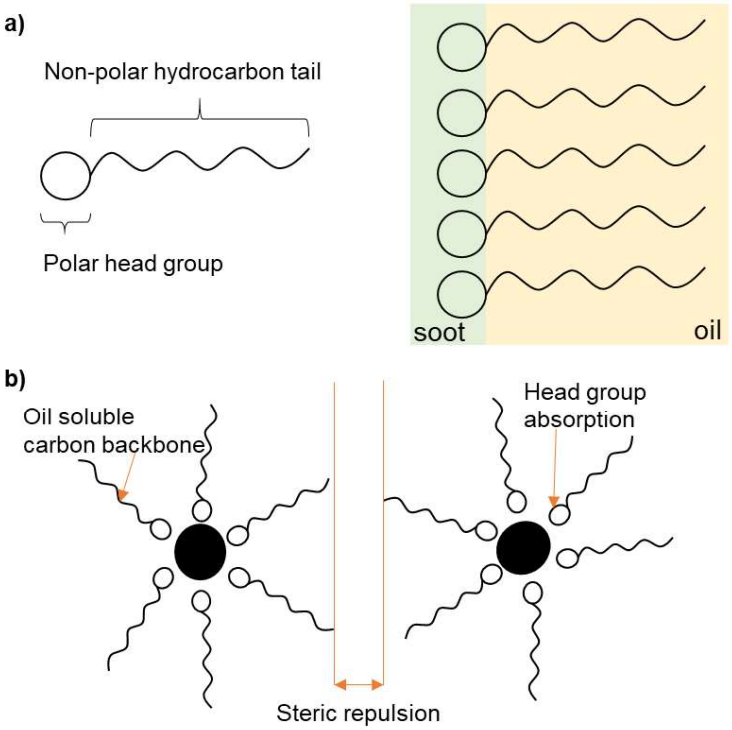

Figure 1.2. a) Schematic representation of groups of dispersant molecule and mechanism, b) steric repulsion of engine oil contaminants surrounded with dispersant molecules.

It was proposed by experimentalists that dispersants work through a steric stability mechanism to prevent agglomeration. In steric stability mechanism, the tail acts as a hydrophobic barrier layer to prevent attraction between insoluble particles, once the polar group has been adsorbed onto the fine particle's surface. As shown in Figure 1.2. for the single tail dispersant, this differentiates the small particles and prevents them from interacting each other and growing in size[5], [13], [14].

Dispersant activity was determined to be dependent on the concentration and that is the reason why dispersants have one of the highest additive rates in a lubricant oil recipes. The effect of dispersant ratio on performance is highlighted in Figure 1.3. After a 288 hours duration, particle development in three different drain oils were demonstrated in Figure 1.3. The dispersant concentrations in these formulations were 1.0, 2.3, or 5.0 mole percentage, demonstrating that higher ratios prevent particle development more successfully [5].

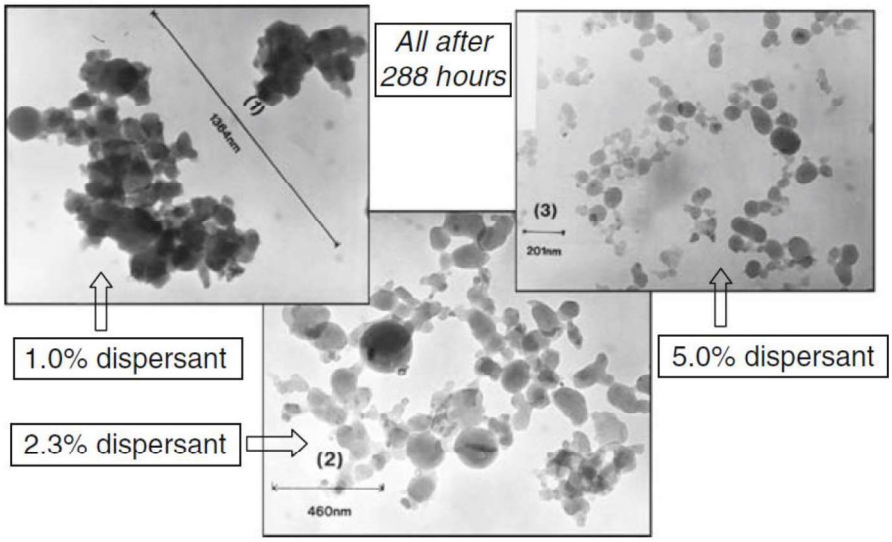

Figure 1.3. Sludge particle growth demonstration, reproduced by permission of [8].

Ashless dispersants are generally derived from hydrocarbon polymers, usually polybutene. Ashless dispersants, as their name implies, do not leave any ashes in the engine. Succinimides are the most widely utilized dispersants in today's engine oil formulations. The most prevalent dispersants utilized in the oil industry today are polyisobutylene succinimide based ones. A polyamine head and a polyisobutylene (PIB) stabilizing tail with one, two or three succinimide bridges form these structures. The reaction of a polyisobutylene succinic anhydride (PIBSA) with a polyamine result in the creation of polyisobutylene succinimide dispersants. The number of amine groups in the chain, reacting with PIBSA, is a critical key parameter in succinimide production. The three syntheses for common succinimide amine based dispersant structures using the normal ratios of these reactants were demonstrated in Figure 1.4.

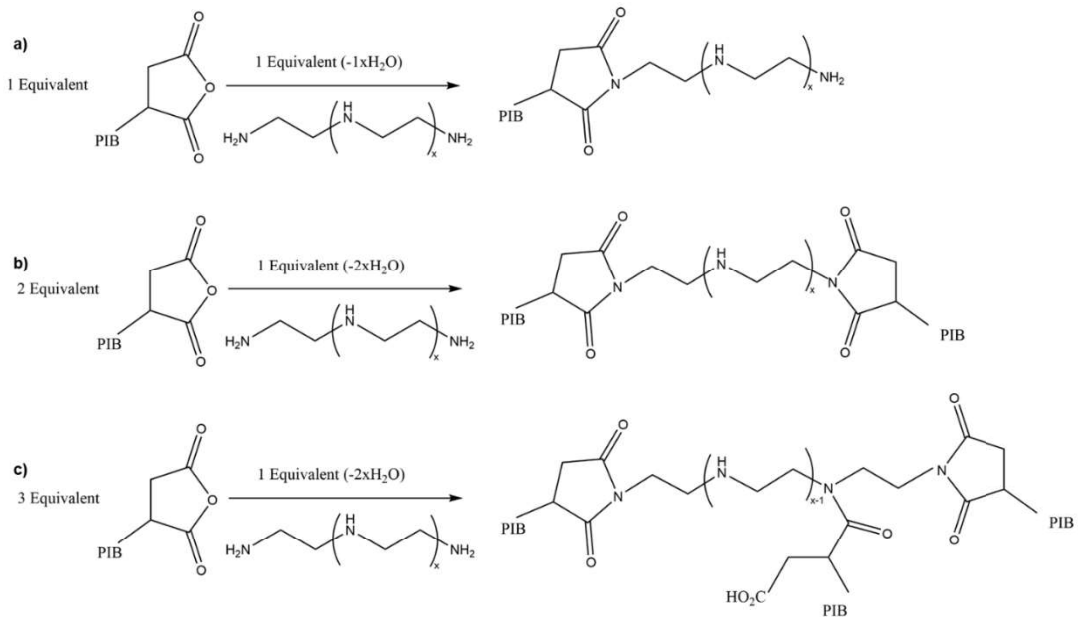

Figure 1.4. Synthesis and structures of a) mono-, b) bis-, c) tris-succinimide dispersants.

The ratio of a typical polyamine to PIBSA changes from 1:1 to 2:1 to 3:1, resulting in mono-, bis, and tris-succinimides, respectively. The primary amine preferentially reacts with the PIBSA unit and water in each case to create an imide group. After all the primary nitrogen atoms have been consumed in the tris model, a secondary amine can open up the additional anhydride group to generate an amide. In fact, depending on the polyamine utilized, branching and cyclic species are present in varying proportions. The reduced models given in Figure 1.4. will be used in this study.

Bis-succinimide and tris-succinimide, with PIB tails at 1000 to 2000 g/mol MW, are the most common type of dispersants. The type of amine group in center, PIB size, and amount of succinimides (bis vs tris) can all be controlled. Future lubricant standards and new engine hardware require the development of new dispersant technologies, for which our calculations can provide a roadmap. In this study, polyisobutylene-bis-succinimide will be used as a dispersant having two PIB tails at 1000 g/mol weight and six amine groups in the middle of the chains to elucidate dispersion mechanism.

CHAPTER 2

EXPERIMENTAL CHARACTERIZATION

To understand how dispersants and detergents work for deposit control and gain insights on dispersants and detergents mechanism of action fundamentally, some experimental results were used as guideline in modeling the nanoparticles, dispersant, and detergent. These experimental results were provided by Lubrizol Corporation. The output of the research may give some directions for developing next generation dispersants and detergents.

Dispersancy and deposit tests have strong correlation with IIIH Weighted Piston Deposit rating (WPD). Higher WPD number indicates cleaner pistons (Figure 2.1). IIH indicates that, the Sequence IIIH Test is a dynamometer lubricant test that uses a fired engine to evaluate car engines lubricants for high-temperature performance characteristics such as oil thickening, varnish deposition, and oil consumption.

Figure 2.1. Engine piston groove and lands.

3rd land cleanliness is critical for working principal of engines. As given in Figure 2.2, when piston grooves were examined; in first engine environment Group II base oil, in the second engine environment Group II base oil with extra dispersant, in the third engine environment Group III base oil were used for deposit control on engine rings.

Figure 2.2. Land cleanliness differences between a) in Group II base oil b) in Group II base oil with extra dispersant c) in Group III base oil environments.

With Dynamic Light Scattering (DLS), which is often used to characterize suspensions of separate nanoparticles or aggregates for a variety of analytical reasons such as checking product specifications or evaluating dispersion processes[15], mean harmonic intensity averaged diameters of insoluble nanoparticles from drain oil are measured where the results were given in Figure 2.3.

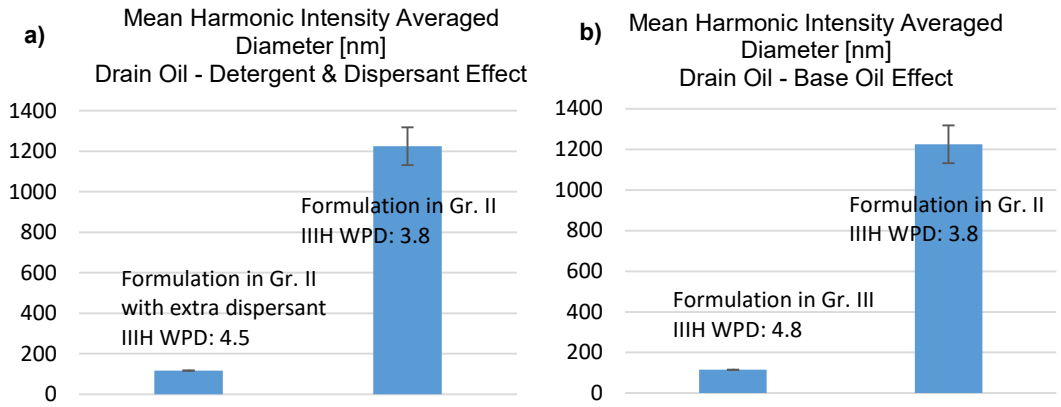

Figure 2.3. Mean harmonic intensity averaged diameter of pistons a) detergent & dispersant effect b) base oil effect.

WPD numbers of three pistons are determined as 3.8, 4.5, 4.8, respectively. This indicates that 3rd piston is cleaner than 2nd, 2nd piston is cleaner than 1st piston. Although the usage of Group III base oil gave better results for deposit control, Group II base oil usage is more abundant for passenger car lubricant oils. Especially with extra dispersant in Group II, deposit accumulation is mitigated.

In the case of lubricant oil samples from the engine environment were examined by Company, samples were characterized by FTIR, XRD, XPS, DLS, Zeta Potential, Electron microscopy, Focused Beam Reflectance, Probe Microscopy, and elemental

analysis. Land deposits and drain oil insolubles were both investigated to see differences and similarities between them.

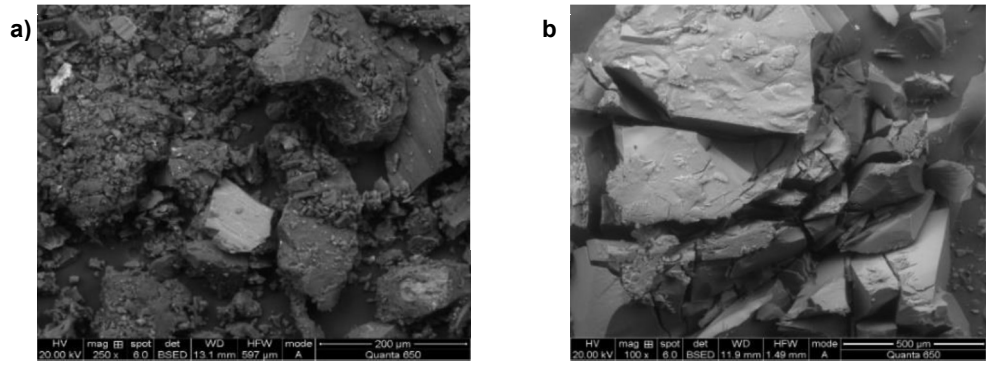

Figure 2.4. SEM image of a) 2nd and 3rd land deposits and b) insolubles from drain oil.

In Figure 2.4, 2nd and 3rd land deposit and drain oil insolubles, SEM images were given. Similar morphological structures were observed from the deposit formation and drain insoluble particles images.

XRD analysis, given in Figure 2.5, indicates that deposits are primarily amorphous carbon with traces of silicon carbide.

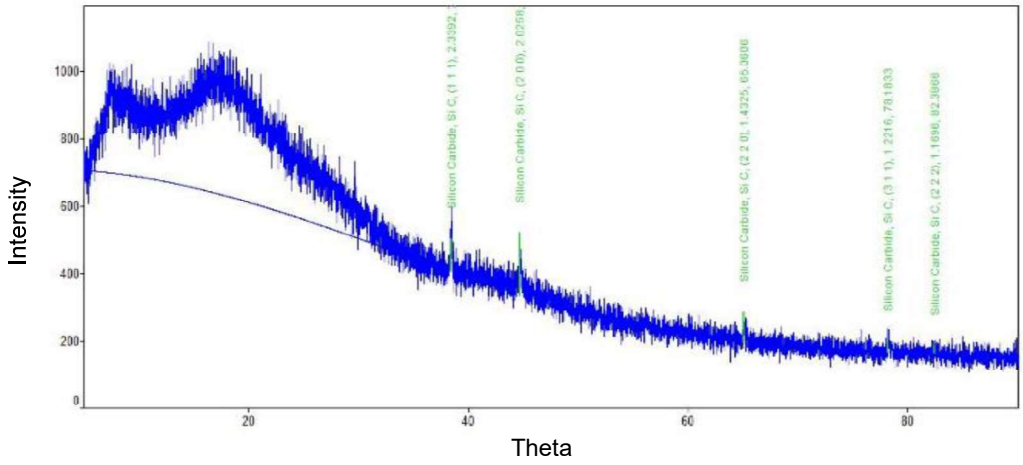

Figure 2.5. XRD result of the drain insolubles.

Elemental composition analysis showed that land deposits have 72% carbon 25% oxygen as mole ratio. The remaining portion mostly composed of magnesium, phosphorus, sulfur and very small proportions are zinc, calcium, sodium, aluminum, copper and silicon. For the drain insoluble particles, elemental composition gave the fact that, there were 74% carbon and 23% oxygen by number of atoms which we used in the modeling step. There is a small proportion of other elements shown in Figure 2.6. For nanoparticle composition, it was accepted that nanoparticle mainly contains 74% of carbon and 23% of oxygen and rest is metal atoms sourced from additives.

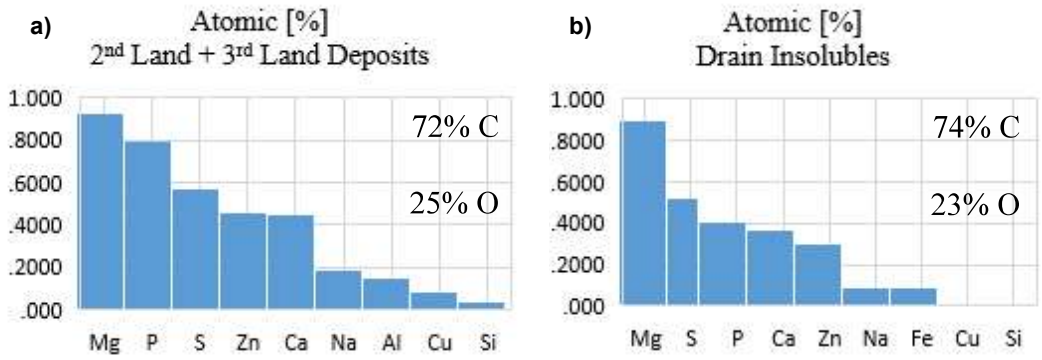

Figure 2.6. Elemental analysis of a) land deposits b) drain insolubles.

This measurement promotes the idea of deposit and drain insolubles are similar structures and have almost the same composition since almost the same ratios were obtained.

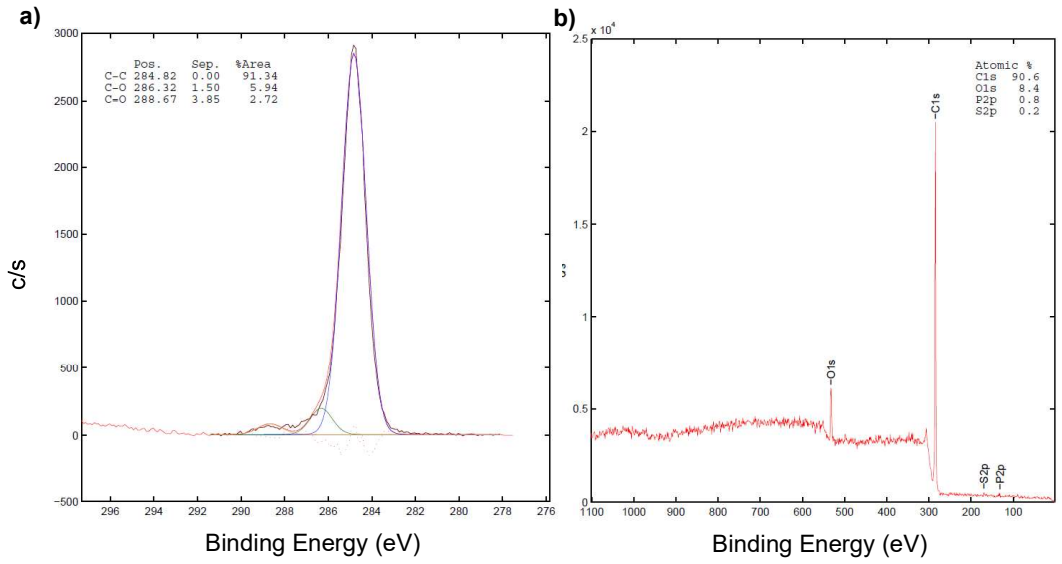

Figure 2.7. XPS results of a) drain insolubles, b) land deposits.

XPS results given in Figure 2.7 demonstrated that surface is formed mostly by carbon and oxidized carbon chain structures.

All the characterization methods pointed out that samples from the engine environment and drain insoluble particles, which were causing deposits on the engine pistons, have similar molecular structures.

It is proposed that aggregation of drain insoluble nanoparticles creates larger insolubles in the engine oil which will form deposits that clog the piston lands. For foresight, controlling the generation and colloidal stabilization of insolubles at initial stages can be the key for the deposit control.

For further understanding and elucidating the role of dispersant, the difference was shown by using TEM. In the second sample given in Figure 2.8, extra dispersant was added to the oil. Dispersion of insolubles showed significant improvement by adding extra dispersant. This was the first time to display the contribution of dispersant in oil.

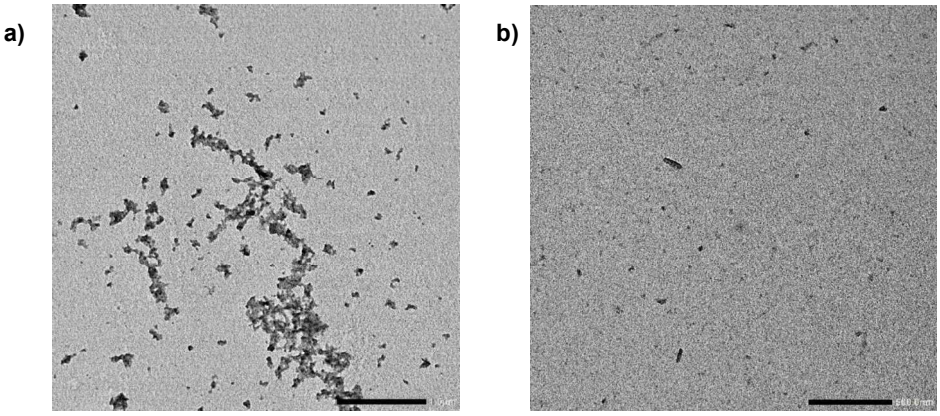

Figure 2.8. TEM images of a) engine oil b) with extra dispersant.

Both detergents and dispersants have a similar role to disperse insoluble particles in the engine oils. As a result of these observations on the dispersant mechanism, the working mechanism of detergents were also studied with computational methods. The working mechanism of detergent and dispersant were unknown at molecular level and aggregation have never been studied theoretically in the literature. The results of experimental data, such as C/O ratio in the insoluble nanoparticles, have been utilized as a source of computational chemistry studies. In the light of these experimental results provided by the Lubrizol Corporation, this computational study and thesis were conducted as a part of collaboration between Technology Transfer Office of METU and Lubrizol Corporation.

CHAPTER 3

THEORETICAL AND COMPUTATIONAL CHEMISTRY

Chemistry studies the structures of matter such as atoms, molecules, electrons, and nuclei. It also examines the composition, reactivity and physicochemical properties of matter. Since there are many different compounds with different compositions and different nuclear positions in nature, nowadays scientists focus on chemistry with enthusiasm to design new molecules and their inter- or intramolecular interactions.

Theoretical chemistry is a branch of chemistry in which mathematical approaches are utilized to describe chemical processes using laws of physics. One of the well-known goals of theoretical chemistry is to discover the most stable spatial distributions of atoms in molecules. Furthermore, theoretical chemistry can be used to determine a molecule's chemical and physical properties, such as relative energy, dipole moment, spectroscopic properties such as vibrations, descriptors such as hardness, softness, reactivity as well as photochemical properties such as excited state properties.

There are only numerical solutions found by solving several mathematical equations in multi particle (complex) systems in theoretical chemistry. Powerful and fast computers can answer these types of mathematical equations. Computational chemistry is a relatively new discipline of chemistry that has emerged as a result of the technology of computers. Rather than establishing a new method, the fundamental goal of computational chemistry is to acquire results for chemical issues using the existing quantum chemistry and molecular mechanics methods. As a result, computational chemistry is considered as a computer application branch of relatively older theoretical chemistry. Despite the fact that computational and theoretical chemistry are sometimes regarded as separate disciplines, there is a strong link between them. As a result of computational calculations, theoretical approaches can

be developed, while new theoretical approaches support computational topics [16]. In 1986, the theoretical chemist Henry Schaefer said that “It is clear that theoretical chemistry has entered a new stage, with the goal of being no less than full partner with experiment”, and emphasize the increasing importance of the theoretical chemistry besides the chemical experiments [17].

In computational chemistry, important results for the molecules consisting of hundreds of atoms depending on the given accuracy can be extracted. However, the challenge is to choose convenient theoretical methods for complex systems to be studied and evaluate them.

Multiscale modeling is relatively new area involves processes at different scales. Processes at different scales are governed by different physical laws. As an example, quantum mechanics and classical mechanics have different length and time scales. While Newton Laws are used for molecular dynamical structures, Schrödinger equation is defined to the systems in quantum mechanics models where electronic properties of structures are used with much more details [18]. Small-scale models should use theories that provide more detailed and more accurate information about the system. As the size of the system increases, information loss occurs, however there is an opportunity to run longer and large-scale simulations. In addition, the boundaries between different scales vary depending on the system [19]. Time and length scale of multi-scaling approach can be summarized as in Figure 3.1.

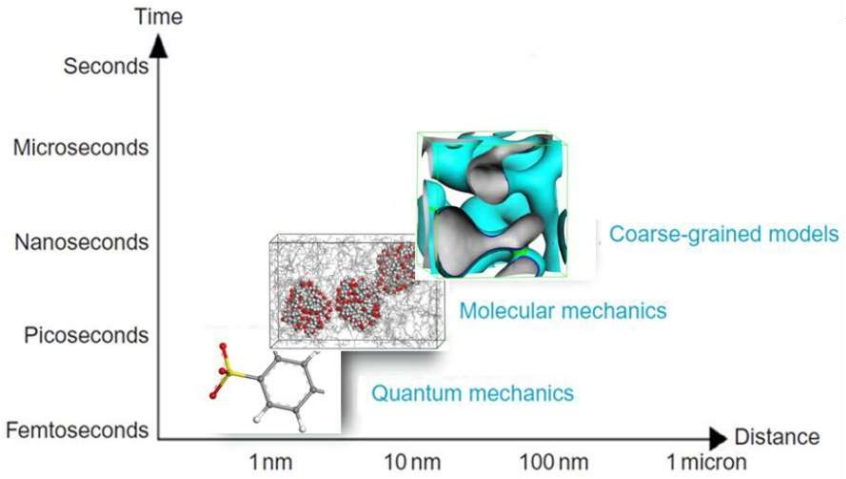

Figure 3.1. Multiscale modeling of materials by using different time and length scales with the different methods.

Requirements for parallel computation for larger scale system sizes have increased due to the complexity and number on calculations per simulations such as integrating the equations of motion. From this perspective, computational chemistry experiments have shifted from large-scale complex tests to multiscale modeling methods to also reduce information losses in large-scale computations. In multiscale models, while moving from each scale to the next, the small-scale system is verified, and the models are prepared for the larger system [20].

Some of the advantages of multiscale modeling can be ordered as follows: Multiscale modeling reduces product development time, produces more realistic system with accurate designs, reduces the number of large-scale model experiments which have higher computational costs, assists in the development of new materials [20].

Multiscale modeling simulations can be classified at three main methods: quantum mechanics calculations, molecular mechanics calculations and coarse-grained simulations [21].

3.1 Quantum Mechanics Calculations (Electronic Structure Method)

First principle quantum chemical methods cover ab-initio and density functional theory. The Nobel Prize in chemistry was awarded to Walter Kohn and John Pople, demonstrating the great potential and significance of first-principles quantum chemical studies in today's chemistry research. Walter Kohn's contribution was the introduction of the new density functional theory (DFT) approach, whereas John Pople's contribution was the development of the quantum chemical procedures for more systematic and practical use in chemistry [22]–[24].

First principles quantum chemical calculations have generally been unsuitable for larger molecules due to their high processing requirements. However, the findings of simpler methods, such as the force-field based molecular mechanics method, vary greatly depending on the parametrization. Because first principles approaches do not require empirical calibration of parameters, they can be used for any molecular system or property, even if no experimental data is available. Therefore, they have the potential to produce more accurate results than classical methods, considerably increasing the accuracy of computational research in this field [22]. In addition, the motions of electrons are considered in quantum chemistry (or electronic structure method), which concern the computation of molecular electronic structures that are not covered in classical methods.

Quantum mechanical methods are based on the solution of the time independent Schrödinger Equation (Equation 2 and 3) [25], [26].

$$\hat{H}\Psi = E\Psi \tag{2}$$

$$\hat{H} = -\frac{h^2}{2m}\nabla^2 + V(r) \tag{3}$$

Where Ψ is the wave function and the Hamiltonian operator $\hat{H}$ is the sum of the kinetic energy and the potential energy of the system. From the first principles, the Schrödinger wave equation describes the motions of electrons and nuclei in a chemical system. In a stationary quantum system, the Schrödinger equation defines

the spatial probabilities corresponding to the energy levels [27]. The electron distribution also known as orbitals and their energies in the molecule can be represented as the wave function, which is a mathematical function. As an example, the electron distribution along the molecule can be used to determine polar and nonpolar parts of a molecule. In addition, since the Schrödinger equation can only be solved accurately for the hydrogen atom, all quantum chemical approaches must be approximate.

Two groups of quantum chemical first principle methods were used widely: the pure 'ab-initio' methods and Density Functional Theory (DFT) which is used in this study.

3.1.1 Ab-initio Calculations

Ab-initio term means "from the beginning" in Latin. It calculates system parameters from the bottom up with no experimental input in the equations except atom types. These calculations use only Schrödinger equation, physical constants, and atomic numbers in the chemical systems. The Hartree–Fock (HF) method is the most basic ab-initio method. Local deviations of the electron distribution are ignored in the HF approach because each electron only sees the average field of the other electrons. As a result, HF excludes electron correlation, which lowers the reliability of the approach [22], [28], [29]. Post-HF methods such as Moller-Plesset, Coupled Cluster, Configuration Interaction are very accurate as well as highly computationally expensive methods.

3.1.2 Density Functional Theory

Density Functional Theory (DFT) is an alternative ab-initio calculation method in which the total energy is defined in terms of total electron density rather than the wave function, where electron correlation is still considered.

The DFT is in fact based on two studies that Hohenberg and Kohn in 1964 and Kohn and Sham in 1965 [30], [31]. The first Hohenberg-Kohn theorem prove that, the external potential energy and consequently the total energy and all of the system's attributes is a unique functional of the ground state electron density, $n_0(r)$. Consequently, the total energy function, E(n), can be expressed in Equation 4 as follows:

$$E(n) = F(n) + \int drV_{ext}(r)n(r) \tag{4}$$

Where n is the function of electron density, F is internal electronic energy and V_{ext} is external potential energy.

According to the second Hohenberg-Kohn theorem, minimizing the energy functional with respect to the electron density gives the system's ground state energy as in Equation 5.

$$\frac{\delta E(n(r))}{\delta n(r)} \Big|_{n=n_0} = 0 \tag{5}$$

Hohenberg–Kohn theorem states that the actual electron density corresponding to the complete solutions of the Schrödinger equation is the one that minimizes the energy of the overall functional. All the properties can be calculated when the ground state electron density is known according to the theorem.

Kohn–Sham theorem is the very important part of the modern DFT calculations [31]. The Kohn-Sham potential, commonly abbreviated as V(r) is the local effective (fictitious) external potential that the non-interacting particles move in to define the Kohn-Sham equation. They have the single particle character of the Schrödinger equation. The Kohn-Sham equation main principle is to build the single-particle potential V(r) such that the density of the non-interacting system is equal to the density of the interacting system (Equation 6).

$$\left\{-\frac{\nabla^2}{2} + V + \mu_{xc}[\rho]\right\}\Phi_i = \varepsilon_i \Phi_i \tag{6}$$

Where the term μ_{xc} is the exchange-correlation potential.

In summary, the main principle DFT is to characterize a molecular system directly through its density rather than first determining the electronic wave function. However, the functional form of the energy density is unknown. As a result, the common technique is to estimate it using various model functionals. B3LYP is one of the most extensively used model functionals [32]. Fitting to atomic or molecular data is a typical method for determining the precise form of density functionals. Thus, DFT is not exactly an ab-initio method, although is referred as such [33]. Since DFT is computationally more efficient than all electron correlated ab-initio techniques, it can be used to study larger molecular systems. However, one of the primary weaknesses of density functionals is their inability to account for accurate dispersion energy resulting from the correlation between changes in the electron distribution of nearby molecules. This problem has recently been solved by dispersion corrections [34].

3.2 Molecular Mechanics Calculations

These methods usually use a force field, which is a parametric function of the locations of the nuclei, can be utilized to determine the energy of a molecular system in any spatial distribution. These parameters include atomic mass and charges, Lennard-Jones parameters, equilibrium values of bond lengths, bond angles, dihedral and inversion angles. Classical methods are computationally efficient and typically used on larger molecular systems.

Monte Carlo and Molecular Dynamics type classical simulations are the most used approaches for molecular mechanics calculations in complex systems.

3.2.1 Classical Monte Carlo Approximation

The Monte Carlo method is a mathematical problem solving technique. The method is simply a statistical approach to the analysis of differential equations, which can be found in a variety of natural science fields [35]. It is a class of numerical computation algorithms which are used to obtain several numerical results with a large number of repeated random samplings. Monte Carlo models predictive systems based on random numbers. It is an approach used in the fields of static simulations, distribution functions, numerical analysis, atomic and molecular physics.

The approximation involves using a large, but finite number of interacting particles to approximate distribution by using energy and structure criteria. One may undertake a limited number of experiments to come up with a sample of a probable origin. As an example, in Metropolis Monte Carlo method [35], trial configurations are generated without any bias. To illustrate, the probability of displacing a molecule from 10 to 11 Å in the x direction is the same as the probability of displacing a molecule from 11 to 12 Å. Obviously, the probability of displacing a molecule from 10 to 11 Å in the x direction could equally be halved, provided twice as many of these attempts are accepted. It is also possible to generate trial configurations in such a biased way such as configurational bias Monte Carlo method.

3.2.2 Molecular Dynamics (MD) Simulations

Molecular dynamics (MD) simulation is a computational approach of a general view of statistical mechanics. MD simulations are used to determine equilibrium and dynamic parameters of complicated systems that cannot be calculated analytically as a complement to experiment.

Molecular dynamics simulation is a classical Newtonian method for studying the structures and characteristics of materials at the atomic level. It calculates particle positions over time using the classical Newton's law of motion. The length scale of

molecular dynamics simulations is around tens of nanometers, and the simulation time scale is tens of nanoseconds.

Surfactants and aggregates have been studied using molecular dynamics simulations throughout the past decade. The interactions between particles in molecular dynamics simulations are driven by a special type of potential energy function, often known as a force field, that includes both bonded (bond length, bond angle, dihedral, etc.) and non-bonded (van der Waals and Coulombic) interactions or parameters.

The force fields can be investigated in three class. Class I force fields, quadric force fields, do not include bond stretching and angle bending correlations which are simpler forms of the calculations. Some of the examples of Class I force fields are AMBER, CHARMM, GROMOS, OPLS. Class II force fields include the potential energy for bonds and angles by cubic and/or quartic terms. They also include intramolecular forces and cross-terms that describe the coupling of adjacent bonds, angles, and dihedrals. Bond and angle vibrations can be reproduced more accurately by using higher-order terms and cross terms to describe interactions. Some of the examples of Class II force fields are PCFF, COMPASS [36], UFF [37], MM2, MM3. Class III force fields add special effects such as polarization, stereo-electronic effects, electronegativity effects to their calculations for use in organic chemistry. AMOEBA, DRUDE are the examples of them [38], [39].

To study deposit control by Lubrizol detergents and dispersants in base oil, COMPASS force field was selected in this thesis study due to its parametrization of all functional groups including anionic phenyl sulfonate, calcium cation, succinimide group and all functional groups of insoluble nanoparticles. It is the abbreviation of Condensed-phase Optimized Molecular Potentials for Atomistic Simulation Studies and indicates a breakthrough in force field approaches in terms of technology. It is one the first ab-initio force field that can accurately predict gas phase and condensed phase features for a wide range of molecules and polymers. It is also the first high quality force field which include both organic and inorganic material parameters.

For MD simulations, a sensitive simulation protocol is applied to ensure not only the equilibrium phases and time integration, but also proper application of boundary conditions, positioning of solvent and particles, and the computation of non-bonded terms. This sensitive simulation protocol is also useful for monitoring the temperature and energy fluctuations for detecting systematic deviations or sudden change, which could signal numerical difficulties. Choosing the appropriate summation method and ensemble is a part of this sensitive protocol. The Ewald summation method [40] is a way of calculating non-bond energy in periodic systems. Because the inaccuracy associated with cut-off approaches is substantially bigger in an infinite lattice, crystalline materials are the best candidates for Ewald summation. The approach can also be used on amorphous solids and liquids.

The constant energy surface of a phenomenon can be explored by applying Newton's equations of motion. On the other hand, the most natural events occur when a system is subjected to environment changes such pressure and heat exchange. Under these conditions, the system's total energy is no longer conserved, needing the use of more complex molecular dynamics. Keeping some state variables (energy (E), enthalpy (H), number of particles (N), pressure (P), stress (S), temperature (T) and volume(V)) constant, different statistical ensembles were created. The mean or change of these quantities in the ensemble created can then be used to compute a variety of structural, energy, and dynamic properties. There are generally four ensembles are available in simulation software packages: constant temperature and pressure (NPT), constant energy and volume (NVE), constant pressure and enthalpy (NPH), constant temperature and volume (NVT). In this study NVT ensemble system was used. Controlling the thermodynamic temperature gives the constant temperature and volume ensemble (NVT), also known as the canonical ensemble. When conformational searches of models are performed without periodic boundary requirements, this ensemble is appropriate. In periodic boundary conditions, volume, pressure, and density are identified and constant-pressure dynamics can be performed by using barostats such as Berendsen, Andersen and Langevin. To control temperature of the system, there are some thermostat methods. Nosé dynamics [41]–

[43] is a methodology for doing constant temperature dynamics that creates real canonical ensembles. The Nosé-Hoover formalism is based on Hoover's simplified reformulation, which eliminates time scaling and produces real-time trajectories with equal time intervals.

3.3 Coarse-Grained Simulations

Coarse-Grained (CG) models can cover length and time beyond the all-atom model, since all-atom MD simulations usually takes a longer time and length to characterize materials and examine their behavioral properties. Molecular simulations have generally more widespread applications at all atom models, which limits the simulation in terms of length at nanometers and simulation time to nanoseconds. To prevent these limitations, coarse-grained simulations are developed in the last two decades. CG models were shown to be particularly effective in extending the length scale to micrometers and time scales to microseconds accessible by simulations. The main purpose of coarse graining is to reduce the degrees of freedom. Thus, the number of the variables and the number of interactions between the system decreases [44]. It eliminates time and length limitations as the infinite number of possible interactions are both reduced and cut-off distances changes in coarse-grained simulations. Here, it is crucial to relate coarse-grained results as closely as possible to lower scale simulations by better mapping and bridging [45].

To create coarse-grained molecular models, chemically bonded atoms are combined into beads or other type of units, and the effective coarse-grained interactions are derived by averaging over the small details of the atomistic models [46]. Units are defined as virtual particles formed by the grouping of fine particles [47]. This model reproduces the thermodynamic and structural properties of the atomic model in a new analytical dimension [44]. Four-six heavy atoms or fine particles can be represented by one bead according to most of the models. For example, a coarse-grained water particle, that is, one bead, contains four water molecules [45].

The CG model is kept relatively simple to promote applications for observable sizes. It is made to be quick, precise, useful, and flexible. There are only a few different levels of interaction among the few known categories of coarse-grained units. There are several different approaches to coarse graining. In this study, the dynamic mean-field density functional method was used as method. The Mean Field Theory (MFT) examines how high-dimensional random models behave. The function of MFT is to substitute an average interaction, commonly referred to as a molecular field, for all interactions in every particle. This process reduces the number of calculated particles that are affected. Due to the simplicity of MFT problems, it is possible to get a lower computing cost [48]. Moreover, dynamic mean-field density functional method is more suitable for fluids such as oil phases.

3.4 Aim of the Study

From the experimental analysis shared by the Lubrizol Corporation, it was found that deposits are build-up by aggregation of nanosized insoluble particles in the engine grooves and pistons. Dispersant and detergent have significant role to disperse and stabilize these insoluble particles. The results provided by the company were used as input and guideline in this thesis study.

The objective of this study was to understand molecular mechanism of nanoparticle aggregation and the role of different functional groups on detergent and dispersant molecules such as amine and succinimide groups of dispersant molecules and sulfonate head group of detergent molecules to mitigate this aggregation. Thus, computational chemistry methods were applied to elucidate molecular mechanism. In Chapter 4, computational methods at different scales and qualities were explained that were used for multiscale modeling. These methods were first principle calculations, molecular mechanics calculations, and coarse-grained models. In Chapter 5, all thesis study results were presented and discussed in detail.

CHAPTER 4

COMPUTATIONAL METHODOLOGY

In the fields of soft matter and fluid science and engineering, molecular modeling and simulations are important instruments. Experimentally observed micromolecular structure, dynamics, thermodynamics, and microscopic and macroscopic features can all be predicted and explained using these computational methods. Simulations can help inform, guide, and complement activities in materials design and discovery, thanks to recent increases in computational power.

This increased power of computational simulations must be used properly. In addition, it is necessary to obtain meaningful results and to ensure the validity and reproducibility of these simulations on lubricant oils in this study.

It was demonstrated in this thesis how recent improvements have transformed this discipline from a descriptive to a predictive approach in order to better understand the deposit control mechanism. It was also be demonstrated how to model the properties and functions of lubricant oils under realistic limitations. To characterize the physics and chemistry that regulate the properties and processes of lubricant oils under realistic temperature and pressure circumstances, a suitable linkage of electronic-structure theory and statistical approaches is required. For instance, electrostatic potential surface of detergent head group is determined from electronic-structure theory. Additionally, mixing energies of dispersants and detergents with ultrafine nanoparticles are calculated from statistical methods. Regardless of the technology used to combine the individual scales, a key feature of a true multiscale simulation methodology is that the constituent models at various resolution levels are consistently linked. This scale-bridging necessitates the deliberate construction of individual models to ensure thermodynamic and/or structural consistency.

Starting with first-principles calculations and transferring their precise results to parametrize higher-scale methods like MD simulations would require a careful transition among distances and methods. Each step toward a larger scale needs an increase in system size, length scale, and time scale, as well as a simplification of theoretical models by losing as little accuracy as possible. Mainly MD simulations and supporting DFT calculations were performed in order to explain the mechanism of deposit control by using dispersants and detergents, to evaluate interactions, mixing energies, and free energy of solvation. At last, coarse-grained simulations were performed for investigating larger time and length scale experiments.

4.1 First Principle Calculations

DFT was used to compute molecular properties such as frontier orbitals, atomic charges and pairwise interaction energies between the base oil and additives of lubricant oils with the components of insoluble particles in order to explain observed aggregations and to identify phase organizations such as PIBSI blocks or detergent head and tail groups. To define very accurate interactions, short model oligomers representing lubricant components was used such as phenyl sulfonate head group and alkyl tail with six carbon atoms.

From a vast number of molecule configurations sampled by statistical sampling method, energetically advantageous starting structure pairs with possible strong interactions will be identified. At least five initial structures were determined for each pairwise interaction type. B3LYP exchange-correlation functional with DNP level was used to determine lowest energy structures and interaction energies to evaluate pairwise interactions. Tkatchenko-Scheffler (TS) [49] parameters were applied for vdW dispersion corrections since noncovalent forces, such as hydrogen bonding and van der Waals (vdW) interactions are important in deposit formation. Interactions of detergents and dispersants with model particles were calculated by using same method to understand effect of competitive interactions. The accurate DFT based pairwise interactions between different groups on insoluble particles,

base oil, dispersants, and detergents shed light on the general self-organization in the system as well as helpful to prepare initial structures for the MD simulations.

4.2 Molecular Mechanics Methods

After first principle calculations, molecular mechanics methods were applied to the periodic systems with multi-components of the engine oil which forms the main body of this thesis study.

At first, an insoluble nanoparticle was modelled, which was one of the most challenging parts of the study. It was constructed many times manually, first as a 2-3 nm sized rigid spherical amorphous SiO_2 type particle, then the structure was changed to softer amorphous random structure at the same size, since experimental studies points out the flexibility of the sooth and sludge. Due to the inflexible nature of the nanoparticle structure, the errors related to the bond lengths and energy jumps of the nanoparticles were avoided by modeling new structure in the first simulations. In addition, aggregation these nanoparticles were tested both in vacuum and oil to validate accuracy of the model. Other important test criteria such as carbon/oxygen ratio and high temperature stability were also tested for the insoluble particle model.

In the molecular mechanic methods, COMPASS force field gave better result and validated by three criteria. First of all, it covers parameters for all functional groups, including anionic sulfonate head group and assign very similar atomic charges with DFT calculations. Secondly, it reaches 0.86 g/cm^3 experimental density in constant pressure simulations of pure oil cells. At last, COMPASS force field recreates pairwise interactions observed in DFT calculations successfully, such as aggregation of nanoparticles, hydrogen bonding between amine groups and insoluble particle surface. Cut-off distance at 12.5 Å was used for the van der Waals interactions and the electrostatic energy calculated by using the Ewald summation method with accelerated convergence with COMPASS force field.

Many different MD simulations were performed including cells only with base oil; cells only with nanoparticles in vacuum; cells with base oil and nanoparticles; cells with base oil, different number of nanoparticles and different number of detergent molecules; cells with base oil, different number of nanoparticles and different number of dispersant molecules. To generate initial structures for MD simulations, Monte Carlo type statistical calculations were performed to pack oil molecules and additives into a cell where insoluble nanoparticles were already added. As an example, into a unit cell with only nanoparticle, dispersant and detergent molecules were packed by Monte Carlo method by 2000 steps followed by molecular minimization, separately at different numbers. By this way, cell structures with the lowest energies among the 2000 cells were found where the dispersant and detergent molecules are at their most probable positions on the nanoparticle. Packing simulations were then repeated for these cells for the addition of base oil to the cells with insoluble nanoparticles coordinated detergent and dispersant structures at the surface. The aim of these two step addition was to find out where dispersant and detergent molecules would most likely position on the nanoparticle in the base oil matrix.

The unit cells containing different numbers of nanoparticles, base oil, detergent, and dispersant were minimized for 5000 steps, followed by MD simulations. MD simulations with 2 ns total simulation time and 1fs steps were performed at NVT ensemble with Nose thermostat at experimental engine temperature, 423 K, to equilibrate dispersant-detergent-base oil-model particle interface.

Some of these structures were also simulated in the LAMMPS program by exporting cells and simulation parameters in ".car" and ".mdf" formats and results were evaluated visually in the VMD program.

Distances at final structures, radial distribution functions (RDF), mean square displacements (MSD), and length evolution with time analysis were made to examine the aggregation behavior of nanoparticles in the simulated structures and to

determine the working mechanisms of detergents and dispersants in the base oil, and to express them quantitatively.

4.2.1 Calculation of Pairwise Interaction Energies based on the Molecular Mechanics Calculations

χ (chi), is a thermodynamic property that describes the miscibility character of the two constituents like modeled insoluble nanoparticle and dispersant/detergent. The free energy of mixing (ΔG_{mix}) per mole for molecules is derived using Flory Huggins Theory in Equation 7. It is assumed that the detergents and particles are randomly distributed, and all lattice sites are occupied. The volume fractions of the components (Φ_i) and the degree of oligomerization of component i, n_i are used to compute the ΔG_{mix} of lattice sites [50].

$$\frac{\Delta G_{mix}}{RT} = \frac{\phi_i}{n_i} \ln \phi_j + \chi \phi_i \phi_j \tag{7}$$

The combinatorial entropy is indicated by the first two terms. Because this contribution is always negative, a mixed state is preferred over pure components. The last term represents the free energy resulting from the interactions. This term favors a mixed state if the interaction parameter χ is negative. By calculating the thermodynamic parameter χ, the miscibility behavior of the detergent or dispersant with nanoparticles, which has a significant impact on aggregation, can be analyzed.

As an example, interaction parameter between particle and detergent were calculated from the difference between solubility parameters (δ) as given in the Equation 8, where V_{avg} is the average volume of molecules and $\delta_{Particles}$ and $\delta_{Detergent}$ are the solubility parameters of model particles and detergents, respectively. The solubility parameters of model particles and detergents are $\delta_{Particle}$ and $\delta_{Detergent}$, respectively.

$$\chi = \frac{V_{ref}(\delta_i - \delta_j)^2}{RT} \tag{8}$$

If the difference in $(\delta_i-\delta_j)^2$ between two constituents is more than 4 J/cm^3, they are considered to be immiscible. Solubility parameters will be computed using the molar cohesive energy, E_{coh}, which is calculated by subtracting the total non-bond energies of isolated ($E_{isolated}$) and periodic ($E_{periodic}$) states, as shown in Equations 9 and 10. The cohesive energy density is E_{coh}/V, while the amorphous cell volume is V. MD simulations in amorphous cells in the NVT ensemble will be used to calculate these energies [51]. One by one, the amorphous cells for every dispersant-detergent-base oil-model particle were built.

$$\delta = \sqrt{\frac{E_{coh}}{V}} = \sqrt{e_{coh}} \tag{9}$$

$$E_{coh} = E_{isolated} - E_{periodic} \tag{10}$$

Free energy of solvation will be calculated for nanoparticle in base oil with detergent and dispersant, via the coupling parameter and thermodynamic integration method. After cell packing and geometry optimization, the free energy of solvation was calculated using a three-step thermodynamic integration sequence. As the first step of the free energy of solvation calculation, the model with either detergent, dispersant or base oil is discharged in the vacuum. The ideal contribution to the free energy of solvation, which is represented as the free energy change, will then be determined. Following that, the model particle will be contacted to detergent, dispersant, and base oil, and the Van der Waals (vdW) free energy change for discharged interaction will be determined. Last, the electrostatic impact to the solvation free energy will be calculated by charging up the solvated and discharged model particle in the detergent, dispersant, and base oil. As a result, total free energy of aggregate solvation by detergent, dispersant, and base oil is computed as the sum of contributions from the ideal term, vdW, and electrostatic solvation free energies.

The modified Flory-Huggins Theory can then be used to predict the miscibility behavior of the sulfoxides with detergent, dispersant, and base oil with model particle. The compatibility of detergent, dispersant, and base oil with model nanoparticles were investigated using statistical mechanics methods to calculate

binary interaction energies in vacuum. The mixing energy (E_{mix}) between detergent-dispersant-base oil and model particles, denoted as i and j, was computed using a Flory-Huggins model and force field-based molecular mechanics approaches to accomplish that aim. For each pair of detergent, dispersant, and base oil, and aggregates, Monte Carlo-type minimizations of a large number of cluster interactions were performed to get the number of surrounding components, known as coordination numbers, Z_{ij}, and the binding energies, $<E_{ij}>$. The average binding energy was computed by producing 10^8 configurations at room temperature using the average of the weighted distribution function, $P_{ij}(E)$ as shown in Equation 11, and the coordination numbers, Z_{ij}, were obtained by generating 10^6 clusters.

$$\langle E_{ij} \rangle = \frac{\int dEEP_{ij}(E)e^{-E/RT}}{\int dEP_{ij}(E)e^{-E/RT}} \tag{11}$$

E_{mix} is defined as the free energy difference due to attraction between the mixed lubricant components and the model nanoparticles as shown in Equation 12.

$$E_{mix} = \frac{1}{2}\left(Z_{ij}\langle E_{ij}\rangle_T + Z_{ji}\langle E_{ji}\rangle_T - Z_{ii}\langle E_{ii}\rangle_T - Z_{jj}\langle E_{jj}\rangle_T\right) \tag{12}$$

Thermodynamic cycle method was used to calculate the solvation free energy (ΔG). In this method, atomic charges on a solute molecule in a vacuum (ideal gas) are removed (ΔG_{id}) as a first step, solute molecule without any atomic charge is brought into the vdW contact with the solvent which is base oil in our case (ΔG_{vdw}), finally, the charges on the solvated molecule are added again to calculate electrostatic free energy (ΔG_{el}) as demonstrated in Figure 4.1. The total free energy of solvation calculated by addition of these factors in Equation 13:

$$\Delta G = \Delta G_{ideal} + \Delta G_{vdW} + \Delta G_{electrostatic} \tag{13}$$

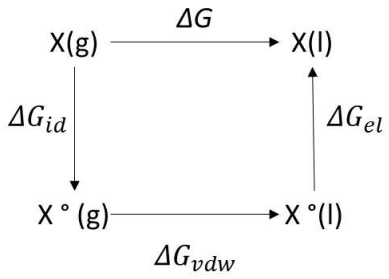

Figure 4.1. Thermodynamic cycle.

There are vdW and electrostatic interactions between a solute molecule and the solvent. In thermodynamic cycle, both can be turned on and off at the same time in by removing charges, however this can cause instabilities since opposite charges can collapse if the van der Waals repulsion that protects them is weakened. However, by eliminating the charges before trying to scale the van der Waals interactions, the problem can be avoided [52]. This method can be thought of as a thermodynamic cycle in which the gas molecules' charges are first removed, then the gas molecule is coupled to the solvent using just van der Waals contacts, and finally the charges are turned back on the solvent environment.

4.3 Coarse Graining Method

Mesoscale modeling utilizes classical simulation techniques to coarse-grained systems without compromising the underlying molecular level interactions. Coarse graining methods are generally similar to all-atom molecular dynamics simulations where the basis of the simulation technique is calculating the dynamics of a system by integrating the equations of motions of all the units in the system. The major disadvantage of all-atom molecular dynamics simulations and some of the coarse graining methods, such as Dissipative Particle Dynamics [53] or Martini type [47] coarse-grained force fields, is that they include many small scale fluctuational motion of atoms than is necessary for an understanding of many physical processes. This process requires high performance computer processor speeds and large

memory capacities that currently limit its applicability to a few microseconds of molecular motion.

We used a faster method in this study for the numerical calculation of dynamic mesoscopic phenomena in copolymer melts in three dimensions was developed by Fraaije et al.by adapting mean-field density functional theory to coarse-grained simulations [54]. An important aspect of this method is the time-integration of functional Langevin equations, where the thermodynamic driving forces are adapted from a Gaussian chain molecular model. Different than other coarse graining methods, it is a phase dependent simulation more than spherical bead or repeating unit dependent model. This method still finds interactions for mesoscale units, capturing the essential physics of the system under study [54], however the units are field densities instead of beads. In the dynamic coarse-grained variant of mean-field density functional theory, which states that there is a one-to-one mapping between the distribution functions of the system, the densities, and an external potential field. In this method, a real system, that is, a system with interactions, can be equated to an ideal system, that is, one with no interactions, using an effective external potential created by other fields. This theory can be used for the large model description of fluids such as oil matrix system where every phase is moving and self-organizing in an external field. The chain is the fundamental building block of the model in this method. In this description, the intra-chain correlations can, in principle, be treated by any suitable model. In practice, a Gaussian chain model is utilized because it allows a factorization of the interactions, hence is computationally more efficient. The non-interacting Gaussian chains are hence the ideal system, and any inter-chain, that is, non-bonded, interactions are treated as non-ideal. Inter-chain reactions enter into the effective external potential. Unique to the implementation we used, a further factorization of this external potential into an electrostatic and dispersive contribution. We need only interaction parameter and structure of the system to study phase organization. The solubility parameters can be used to derive Flory-Huggins interaction values as given in Equation 8.

Where V_{ref} is a reference volume, taken to be the molar volume of one of the specified units for coarse graining that is actually the mean volume of the two units. Then we converted Flory-Huggins parameters into mean-field density functional theory input by Equation 14:

$$\nu^{-1}\varepsilon_{ij} = \chi_{ij}RT \tag{14}$$

where $v^{-1}E_{IJ}$ is the input parameter. The values of the terms are greater than zero will tend to cause phase separation and lower than zero will give phase mixing. In the coarse graining of the system, insoluble nanoparticles were created as dendrimer like structures since it is not possible to generate random amorphous structures in this method. Every 4-6 heavy atoms were mapped into one coarse grained unit. Each nanoparticle is created by four types of beads where O is the neutral center, A is the nonpolar group, P is the polar group such as ester or ether, R is the highly polar group such as alcohol or carboxylic acid. Nanoparticle is defined as $O_1[A_3P_1A_3R_1]_5$ in the coarse-grained simulations (Figure 4.2). Dispersant is defined as $T_{18}N_6T_{18}$ where T represents the non-polar PIB tail, and N represents the bis-succinimide polar center. Detergent is defined as T_4S_1 in coarse grained simulations where S represents phenyl sulfonate head group and T represents the alkyl tail. Both PIB and alkyl tail of sulfonate were represented by same T unit with different chain length since they show similar hydrophobicity and interactions with other units. Base oil unit is represented by nonpolar B and oil molecule is represented B_4 in the simulations.

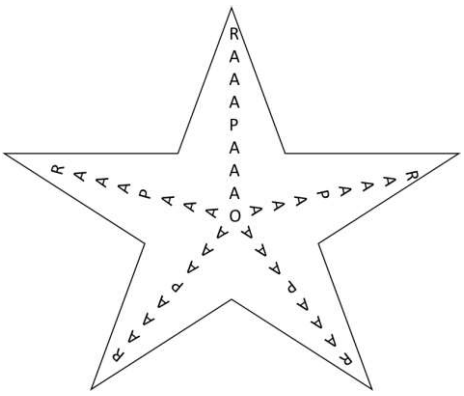

Figure 4.2. Coarse-grained model of insoluble nanoparticle defined by coarse grained units.

CHAPTER 5

RESULTS & DISCUSSIONS

Computational methods at different scales were used to obtain theoretical results. In addition, literature research was carried out as a first step to model initial structures and to determine the most suitable software, methods and algorithms that are used in this study. The results of the experimental studies such as TEM and XPS data were used as roadmap to understand the aggregation mechanism, to solve working mechanisms of the detergent and dispersant which create colloidal imbalance to prevent aggregation. The first step of the simulations was to generate initial structures of the base oil, dispersant and detergent that were used in the calculations.

5.1 Molecular and Electronic Structures of System Components

To be able to model structures observed in the experimental study that are mainly base oil, insoluble nanoparticle, dispersant, detergent; it is necessary to determine accurate structures. For this purpose, base oil, dispersant, and detergent structures were constructed in accordance with the structures used in the literature and data sheets provided by the company.

In this study, six different atoms were present in these structures: carbon, hydrogen, oxygen, sulfur, nitrogen, and calcium that are all well-defined in the first principle and classical methods. In this thesis, atoms are depicted in different colors in the figures for the rest of this text such that: gray balls are carbon atoms, white balls are hydrogen atoms, red balls are oxygen atoms, yellow balls are sulfur atoms, dark blue balls are nitrogen atoms and green balls are calcium cations. Molecules or atoms are given as line, as ball and stick, as all-stick or as CPK style depending on the best visualization of the simulation cell. Generally, nanoparticle structure was given in

CPK, dispersant and detergent were given in ball and stick, base oils were given in line styles.

5.1.1 Base Oil

Group II oils was used as base oil in all calculations. In the production of Group II base oils, feedstock is converted to saturates, which are high in isoparaffins. Average carbon number of isoparaffins and naphthenic groups are between 20 – 25 [55]. Groups II base oils have distinct forms of branching at positions 2, 3, and 4, as well as at the carbon chain's center at positions 6 and 7. When compared to structures with branching in the middle of the chain, which impose mobility limits, configurations with methyl branching at the terminal end of the chain provide more molecular mobility or flexibility at low temperatures. High VI properties are favored by structures with branching at 2, 3, and 4 locations [55]. In addition, it is also known experimentally that there is an alkene structure in the base oil structure and little amount of branching. In the light of these information, the base oil structure has been built and given in the Figure 5.1, with the formulation of $C_{24}H_{48}$, and molecular weight 336.64 g/mol. Both small percentage of alkene and branching factors were considered in our model. Atomic charges were calculated for geometry optimized structures by Merz-Kollman based ESP algorithm at B3LYP/6-311g(d) level [56].

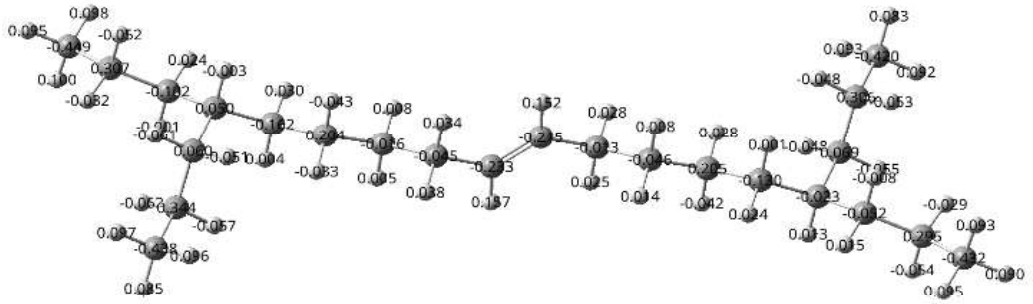

Figure 5.1. Base oil structures with partial atomic charges.

Base oil is highly neutral and non-polar except the small polarity at the end groups.

5.1.2 Polyisobutylene-bis-succinimide (PIBSI)

In this study, polyisobutylene-bis-succinimide was used as dispersant in all calculations (Figure 5.2). Bis- version of succinimide are common besides tri- or mono- derivatives. Straight chain amine group between C_8-C_{18} of bis-succinimides are made with polar groups of various diameters and nitrogen contents [57]. Typical molecular weight of PIB portion at the two tails is approximately 1000 – 2000 g/mol. Typical polyamine structures at the center are with 6-7 nitrogen and 2.5-3 weight % dispersant in oil. Amine groups were bridged to the PIB tails via bis succinimide linkage. 18 isobutylene repeating units with MW of 1009.90 g/mol was used in our model.

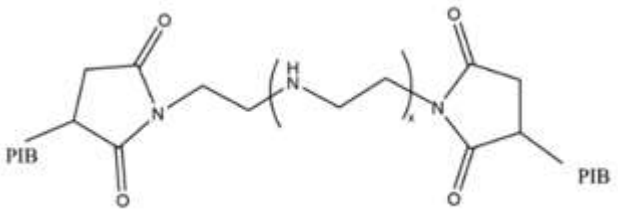

Figure 5.2. PIB-bis-succinimide dispersant molecular structure.

Polyisobutylene-bis-succinimide dispersant have three main groups: polyisobutylene (PIB) tails, bis-succinimide group ($C_4H_5NO_2$) bridge and amine central groups. Electrostatic Potential Surface (ESP) and frontier orbitals are shown in Figure 5.3. In ESP surface, electron rich to electron poor regions were depicted from red to blue, respectively. As indicated in Figure 5.3, especially oxygen atoms in succinimide and nitrogen atoms in amines have the highest electron density depicted as red in color. Amine hydrogens and carbons in bis-succinimide were the electron deficient groups. According to these results, succinimide and amine groups were polar structures, however poly-isobutylene tails are highly non-polar tails. HOMO-LUMO orbitals were also concentrated on the amine groups and bis-succinimide, respectively, which is a strong indication for potential polar interactions as well as susceptibility towards nucleophilic-electrophilic attacks to those groups.

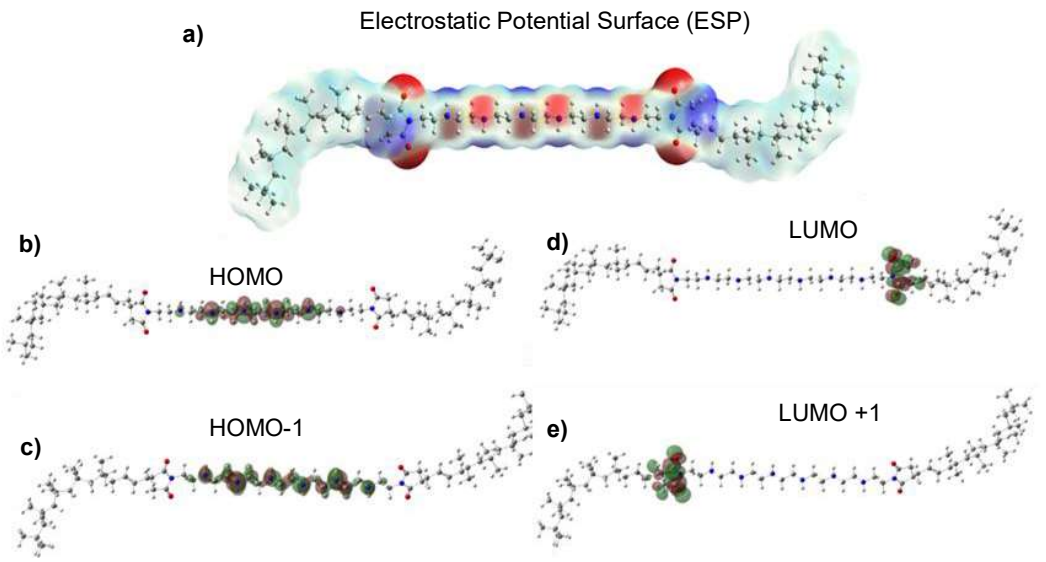

Figure 5.3. a) Electrostatic Surface Potential, b) HOMO, c) HOMO-1, d) LUMO, and e) LUMO+1 structures of dispersant molecule.

Amine center was built with six amine molecules connected to each other with ethyl groups as given in Figure 5.4. Partial atomic charges are calculated according to DFT calculations at B3LYP/6-311 level that supports polarity of the central amine-bis-succinimide group.

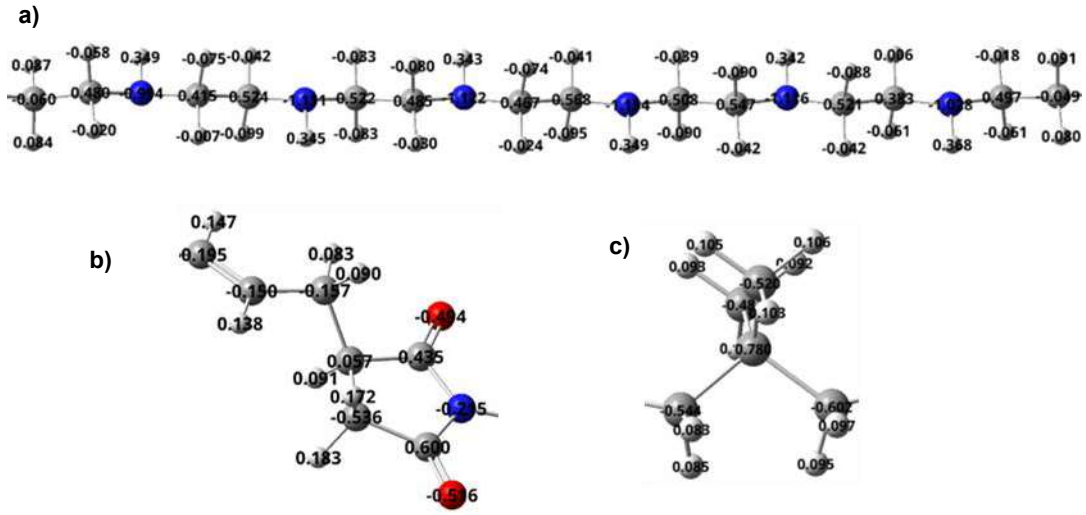

Figure 5.4. Models of a) amine, b) succinimide, and c) isobutylene portions of PIBSI dispersant.

Polyisobutylene-bis-succinimide dispersant real version was modelled for classical simulations as given in Figure 5.5 with 18 PIB repeating units on each side. Dispersant has 2610.61 g/mol molecular weight with $C_{174}H_{342}N_8O_4$ chemical formula.

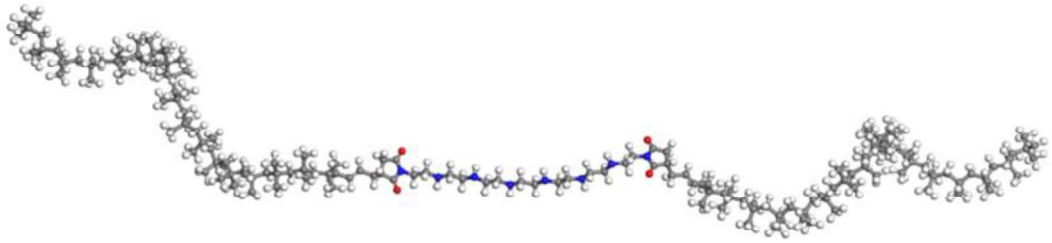

Figure 5.5. Molecular structure of polyisobutylene-bis-succinimide dispersant model.

5.1.3 Sulfonate Detergent

Sulfonate, which has the most widespread industrial usage, was studied as detergent in this study. Besides sulfonate, salicylate and phenate are the other commonly used detergents in passenger car formulations that will not be included in this study. The hydrophilic anionic group of the sulfonate-based detergent has negatively charged sulfonate head groups and a single alkyl chain as tail. Typical commercial sulfonate systems have significantly linear chains between C_{15}-C_{36} [58]. In the direction of these knowledge, sulfonate detergent structure was modelled as in Figure 5.6 with an alkyl tail with 20 carbons and phenyl sulfonate anionic head group. The chemical formula is $C_{26}H_{45}SO_3$, with 437.70 g/mole molecular weight, relatively smaller in size compared to the dispersant.

ESP surface for sulfonate detergent model was given in Figure 5.6 which show that all electron rich part is concentrated on the phenyl sulfonate head group. Partial atomic charges according to first principle calculations and classical methods based on the COMPASS force field provided close results. HOMO is on the head group and LUMO was on the alkyl tail as expected.

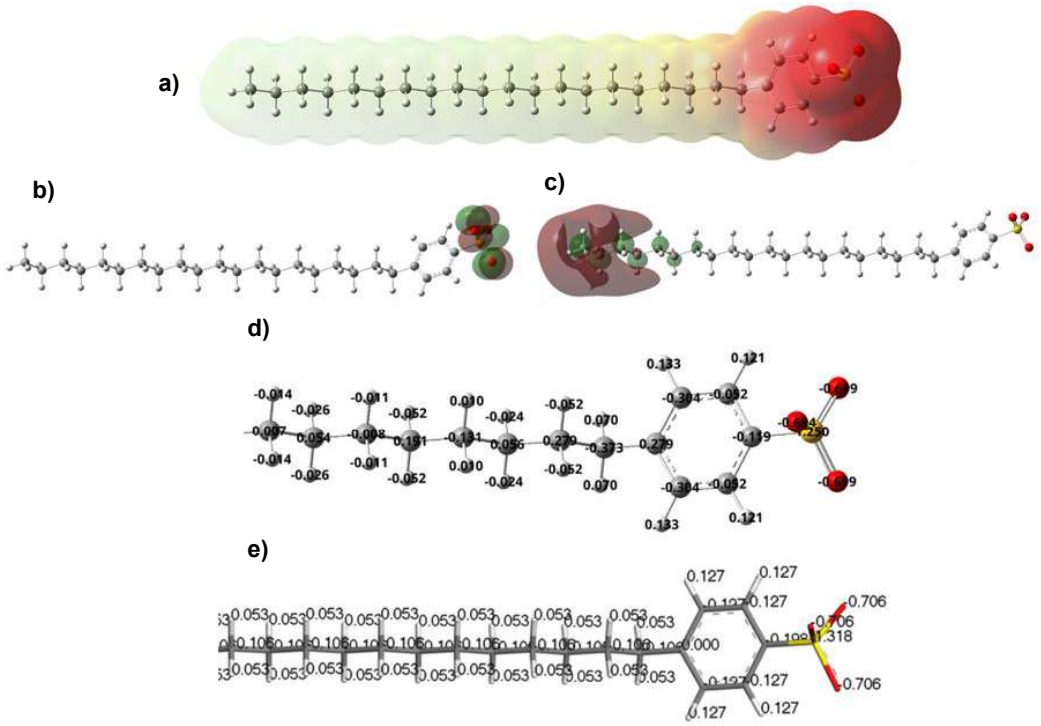

Figure 5.6. Sulfonate detergent a) ESP surface, b) HOMO, c) LUMO structures and d) first principle, e) classical method calculations.

5.1.4 Insoluble Nanoparticle

One of the biggest challenges in this study was to model the ultrafine insoluble nanoparticles which aggregate to form deposits in the engines. From the results provided by Lubrizol Corporation, it is known that this nanoparticle may have many functional groups that primary-secondary-tertiary alcohols, ketone, aldehyde, carboxylic acid, ester and ether groups. From elemental analysis, approximately 75% carbon and 25% oxygen atoms were provided in the structure which have oxygen mostly distributed particle surface. Their size is less than 5 nm, they inner structure is mainly amorphous, and they have spherical structure.

Since there is no such a molecular information about this aggregated ultrafine particle structure in the literature, this model was created manually according to the experience and measurements. This is the very first study to model insoluble nanoparticle in the literature.

It has been modeled many times manually and constructed in a way that does not give errors due to close bond distances, satisfy convergence criteria for both force and energy, having negative total energy and free energy, appropriate for chosen force field by computational methods, having experimental C/O ratio, self- with each-other. To check the validation of the initial structure, energy was decreased by annealing (heating-cooling) cycles that gave stable amorphous nanoparticle. In the modeled nanoparticle, oxygen was mainly distributed on the surface and designed in accordance with the elemental analysis as shown in Figure 5.7. Chemical formula is $C_{300}H_{559}O_{100}$ and it has 5766.57 g/mol molecular weight with approximately 2.2 nanometer diameter.

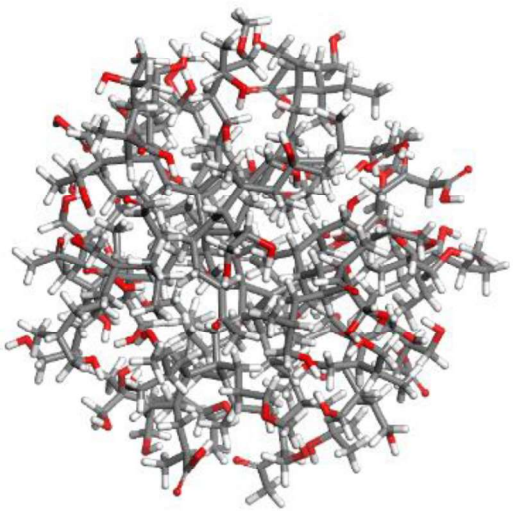

Figure 5.7. Ultrafine insoluble nanoparticle model.

5.2 Solubility Parameter Calculations

After modeling all structures in the oil, the first step is to calculate the interactions and mixing of these parts with each other. The simplest way to do this is to calculate the solubility parameter. Solubility parameters (δ) that are close to each other mix, those that are far away do not mix generally.

Table 5.1. Solubility parameters of the base oil, polar and non-polar portions of dispersant, sulfonate, and Ca+2, and sulfonate.

	van der Waals contribution Solubility parameter ($(J/cm^3)^{0.5}$)	**Electrostatic contribution Solubility parameter ($(J/cm^3)^{0.5}$)**	**Total solubility parameter ($(J/cm^3)^{0.5}$)**
Base oil	17.013	0.874	17.407
Dispersant (polar portion)	20.341	11.233	23.637
Dispersant (non-polar portion)	12.304	0.414	12.671
Sulfonate and Ca^{+2}	10.436	49.213	50.445
Sulfonate detergent	18.991	23.442	30.439

Solubility parameters for all structures were calculated in three steps. In the first step, 20 amorphous periodic cells were constructed. 30-60 molecule were packed into each cell depending on the cell size that should be larger than two times cut-off distance. In the second step, geometry optimizations for all the cells were performed for at least 5000 steps until the energy and force convergence. In the third step, solubility parameters (vdW and electrostatic contributions) were calculated as average for the cells (Table 5.1).

As indicated previously, polar group of the dispersant is amine and succinimide, non-polar group is polyisobutylene tail. During calculation of the solubility parameter, vdW contribution and electrostatic contribution to the solubility were also calculated separately. Electrostatic interactions were important for polar groups of the molecules. As an example, non-polar part of dispersant has almost zero electrostatic contribution. Next, base oil has also almost zero electrostatic contribution due to its non-polar structure. It was determined that the solubility parameters of the non-polar group of dispersant and oil as well as the polar group of the dispersant and sulfonate head group have close values to each other.

These results promoted the idea that non-polar tail of the dispersant and detergents may extend into the base oil while amine and succinimide prefer to interact with the polar surface of the nanoparticle.

The solubility parameter of the nanoparticle has not been calculated because it was not possible to construct high number of nanoparticles samples into the many cells. However, it was known that its surface is formed by oxygen rich functional polar groups. These calculations led us to investigate the interactions of the dispersant with other components.

Hydrophobicity and surface properties of the components were calculated in terms of octanol-water partition coefficient (AlogP), solvent accessible surface area (SASA), total polar surface area (TPSA), total apolar surface area (TASA), relative polar surface area (RPSA), relative apolar surface area (RASA). Alog P is a measure of hydrophilicity or hydrophobicity of a molecule. It shows how easily an analyte partitions between the aqueous water and organic phases such as octanol. A more polar, hydrophilic chemical will have a lower log P (even negative), indicating that it prefers to reside in the aqueous phase [59]. In other words, calculated log P value in water vs. a simple organic compound can be used to predict its solubility properties in other aqueous and organic solvents [60]. The log P of non-polar, hydrophobic molecules will be highly positive, indicating that they will partition into an organic phase. Ghose and Crippen's approach was used to calculate the Alog P, theoretical approach [61]. Each atom in the molecule was assigned to a class in this atom-based approach, with additive contributions.

To examine the hydrophilic and hydrophobic interactions, dispersant and nanoparticle structures were divided into consistent parts since they are large structures and consists of groups with different polarities. Dispersants were represented by amine repeating unit that is dimethyl amine and hexamer of this group, bis-succinimide, polyisobutylene (PIB) monomer and PIB_{18} at about 1000 g/mol; detergents were represented by sulfonate group, phenyl sulfonate group; functional groups on the insoluble nanoparticle surface were represented by

carboxylic acid substituted (Nacid), ketone substituted (Nketone), alcohol (Nalcohol) and dialcohol (Nalcohol2) substituted branched alkane groups as given in DFT calculations. Base oil was represented by alkyl group with two short branching and one alkene groups ($C_{24}H_{48}$) similar with DFT calculations. Calculations showed that oil and PIB groups were the most hydrophobic group with the highest apolar surface area. Sulfonate head group of detergents, amine group and bis-succinimide groups of dispersants were the most hydrophilic groups that can be coordinated polar groups on the nanoparticle surface. It should be noted that although the sulfonate head group was highly hydrophilic with highest relative polar surface area, detergent was as hydrophobic as base oil at overall due to the alkyl tail with 20 carbon atoms (Table 5.2).

Table 5.2. Hydrophobicity, SASA, TPSA, TASA, RPSA, RASA for the components of the system.

Structures	AlogP [63]	SASA	TPSA	TASA	RPSA	RASA
Oil molecule	10.47	794.41	0.00	794.41	0.00	1.00
CH_3COOH	-0.20	212.70	122.97	89.74	0.58	0.42
CH_3OH	-0.36	170.74	69.06	101.68	0.40	0.60
Nacid	2.71	346.28	76.50	269.77	0.22	0.78
Nketone	2.15	314.80	47.36	267.44	0.15	0.85
Nalcohol	2.14	323.00	29.06	293.94	0.09	0.91
Nalcohol2	1.41	317.06	68.40	248.66	0.22	0.78
Amine-all	-1.50	738.57	131.62	606.95	0.18	0.82
Amine monomer	-0.22	209.51	39.09	170.41	0.19	0.81
Bis-succinimide	0.40	322.74	103.50	219.24	0.32	0.68
PIB_{18}	25.50	1523.92	0.00	1523.92	0.00	1.00
PIB monomer	2.20	260.08	0.00	260.08	0.00	1.00
Sulfonate head	-1.12	237.84	162.41	75.43	0.68	0.32
Phenyl sulfonate	1.68	339.98	142.51	197.48	0.42	0.58
Detergent	10.83	978.95	142.51	836.44	0.15	0.85

5.3 Validation of Computational Method and Force Field Approach

For all computational methods in Material Studio and LAMMPS software used for simulations. COMPASS Class II consistent force field was used in MD simulations. First, 366 base oil molecules were placed into the cell to validate the accuracy of the base oil structure and methodology as demonstrated in Figure 5.8. Experimental density for the base oil is given as 0.86-0.87 g/cm^3 by the company. This density was utilized as the validation parameter. 50000 steps of geometry and cell parameter optimizations were performed for the cell with 0.5 initial density with the convergence criteria given as 2.0e-5 kcal/mol for energy, 0.001 for force kcal/mol/Å,

1.0e-5 Å for displacement. Density of the base oil in unit cell was increased from 0.50 g/cc to 0.85 g/cm^3 after geometry optimization and 0.86 after annealing cycles. Thus, the validity of the base oil structure and computational method was confirmed (Figure 5.9).

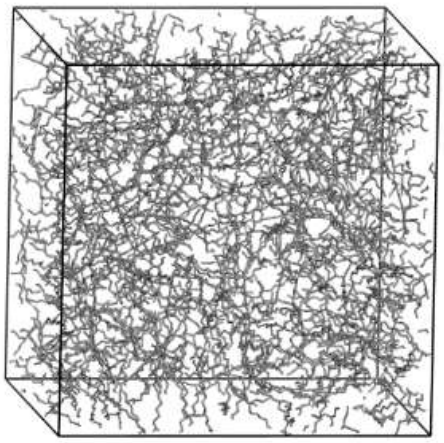

Figure 5.8. The unit cell with 366 base oil molecules.

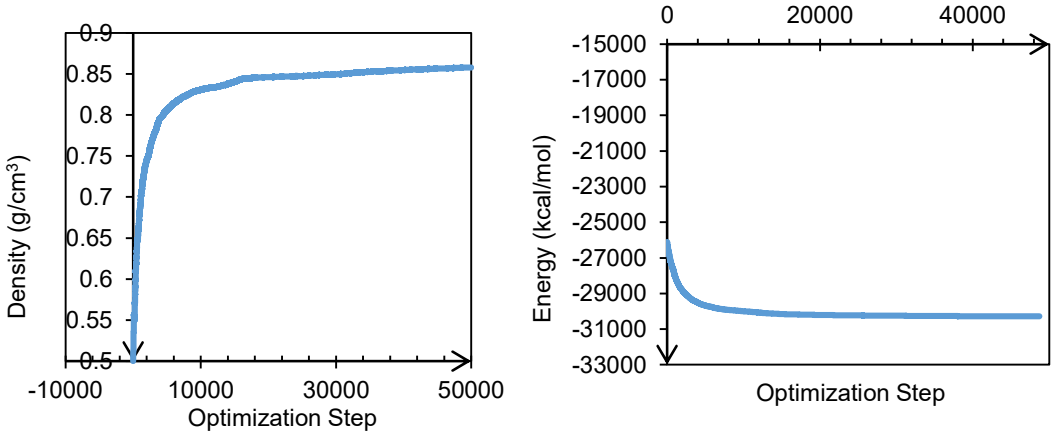

Figure 5.9. Density changes of base oil structure after 50000 step cell optimizations.

5.4 Interaction Energies

5.4.1 DFT Calculations

All possible interaction energies between components were calculated based on the B3LYP/6-31+g(d) level DFT calculations (Figure 5.10). Dispersants were represented by amine, bis-succunimide (bis-suc), polyisobutylene (PIB) groups; detergents were represented by phenyl sulfonate (Psulfonate) and alkyl tail; functional groups on the insoluble nanoparticle surface were represented by carboxylic acid substituted (Nacid), ketone substituted (Nketone), alcohol (Nalcohol) and dialcohol (Nalcohol2) substituted branched alkane groups, base oil were represented by alkyl group by ignoring limited contribution of branching and alkene groups. Our calculations showed that strongest interactions are the ones formed by phenyl sulfonate on detergent, bis-succinimide groups on dispersant, amine groups on dispersants with the functional groups on the insoluble nanoparticles. Alkyl groups showed the weakest interactions with the functional groups on the nanoparticle surface. Alkyl groups show higher interactions with alkyl and PIB compared to their interactions with these functional groups. Although alkyl groups have relatively high interactions with amine groups, the interaction of these amine groups with nanoparticle surface is much higher. It should be noted that number of interactions were ignored here that alkyl-alkyl interactions are dominant interactions due to the higher ratio of the base oil in the system.

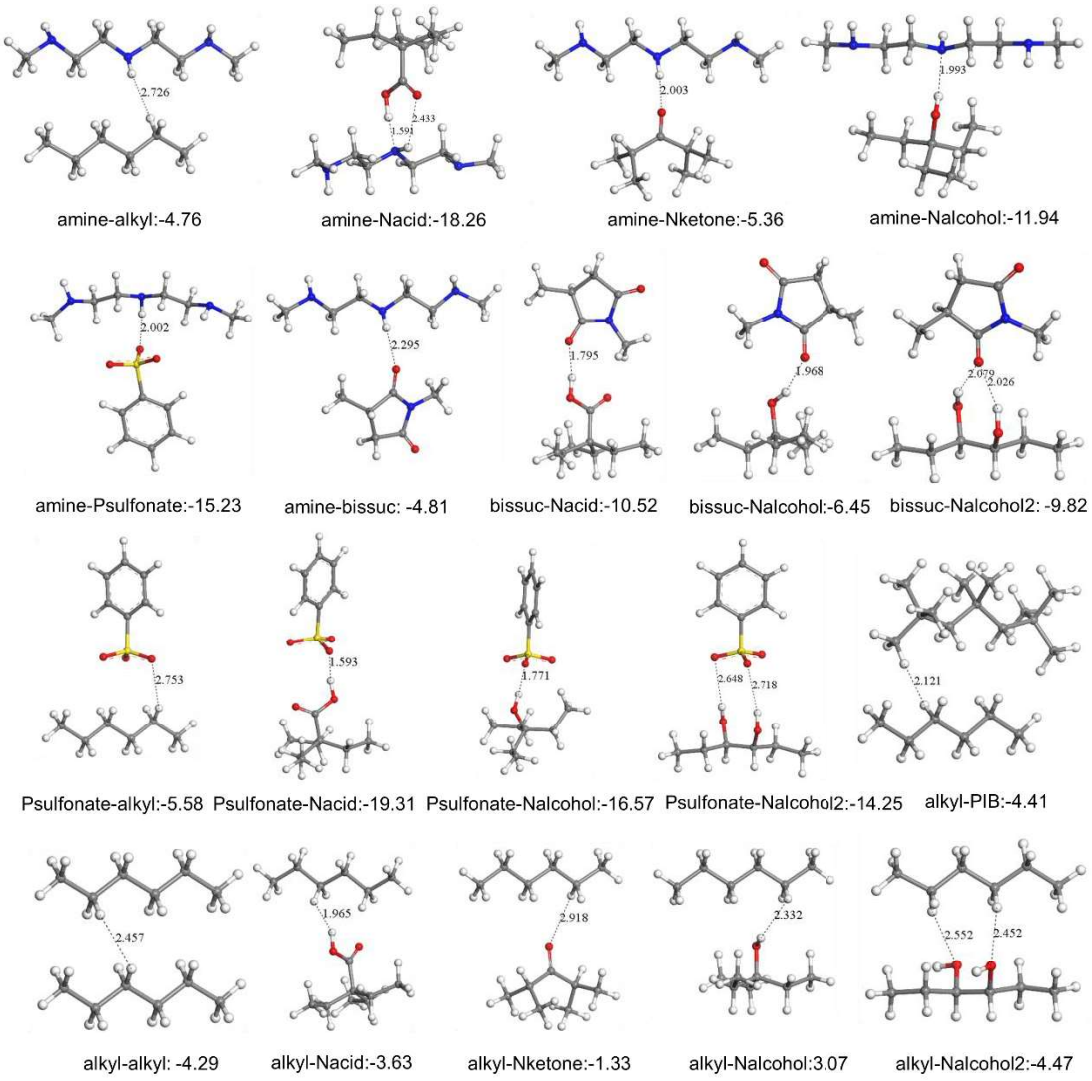

Figure 5.10. Interaction energies (kcal/mol) between components based on the DFT calculations.

5.4.2 Pairwise interactions via Molecular Mechanics Methods

Another calculation that performed is classical calculation of pairwise interaction energies between components, shown in Table 5.3. Dispersants have amine, succinimide and polyisobutylene parts. Detergent has alkyl and phenyl sulfonate part. Base oil has alkyl and alkene groups. The interaction energy between sulfonate and phenyl sulfonate was positive since their interaction is repulsive due to the negative charge on both groups. Secondly, there was highly negative interaction

between amine and phenyl-sulfonate due to the hydrogen bonding between amine and sulfonate oxygens. Additionally, between phenyl-sulfonate and succinimide part of the dispersant, again there was highly negative interaction due their high polarities of these groups. In this way, this calculation demonstrates how interaction energies work and they give opinion to eliminate fewer probable interactions. Moreover, these interactions were used to map molecular interactions into the larger scale coarse-grained simulations.

Table 5.3. Binary interaction energies.

i	j	E_{ij} avg (298 K)
alkyl6C	phenyl	-1.19
alkyl6C	isobutyl	-0.93
alkyl6C	succinimide	-1.46
alkene6C	alkyl6	-1.17
alkene6C	phenyl	-1.18
alkene6C	isobutyl	-0.94
alkene6C	succinimide	-1.55
amine	phenyl-sulfonate	-5.33
amine	alkene6C	-1.32
amine	alkyl6C	-1.29
amine	phenyl	-1.48
amine	isobutyl	-1.02
amine	succinimide	-2.16
phenyl-sulfonate	alkene6	-1.43
phenyl-sulfonate	alkyl6	-1.58
phenyl-sulfonate	phenyl	-1.74
phenyl-sulfonate	isobutyl	-1.16
phenyl-sulfonate	succinimide	-6.40
sulfonate	amine	-5.16
sulfonate	phenyl-sulfonate	28.73
sulfonate	alkene6C	-0.99
sulfonate	alkyl6C	-1.08
sulfonate	phenyl	-1.56
sulfonate	isobutyl	-0.83
sulfonate	succinimide	-6.58
alkyl6C	phenyl	-1.19
alkyl6C	isobutyl	-0.93
alkyl6C	succinimide	-1.46
phenyl	isobutyl	-0.92
phenyl	succinimide	-2.05
isobutyl	succinimide	-1.17

5.5 Solvation Free Energy Calculations

To calculate free energy of solvation a nanoparticle was placed in unit cell fill with base oil in Figure 5.11. The solvation free energy was calculated as +32.43 kcal/mol, which indicates that nanoparticle does not tend to dissolve in base oil. This is the main origin of its self-aggregation, which explains deposit formation.

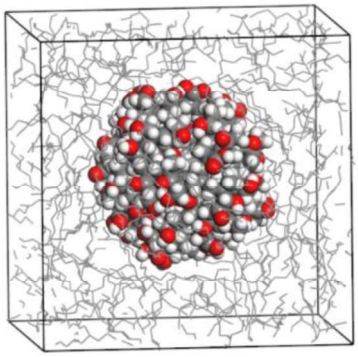

Figure 5.11. A nanoparticle in a unit cell to calculate solvation free energy of nanoparticle.

5.6 Monte Carlo Simulations

The cell structures that were used in molecular dynamics simulations were prepared by packing calculations based on the Monte Carlo algorithm. In these calculations, energy and structure-based criteria were defined to add molecules into the cells. Since the nanoparticle-oil-dispersant-detergent mixture model was formed by all amorphous structures, it was possible to use random packing of each additive to prepare the initial cell structures for MD simulations. The packing of molecules into the amorphous cell allowed us to pack a given mixture of molecules randomly at a specific loading and density into a three-dimensional periodic cell, with some constraints such as energy criteria, close contacts avoiding or ring spearing. An empty cell or a cell already accommodate structures, such as a group of nanoparticles, can serve as a template structure for packing. The atoms that are already in the unit cell were kept at fixed coordinates during the packing process. As

a result, free volume around the structure in the cell were filled by this Monte Carlo algorithm. In short, it was possible to create cells by packing oil or additives into an existing empty or partially filled cells at any mole ratio determined by user. The number of molecules packed into the cell were automatically determined by the density and weight ratio of the components.

Two different methods were used in construction of initial cell structures for MD simulations.

In the first method, dispersants and detergents were packed into the cell where only nanoparticles were present to validate our packing approach. We showed that, after 2000 times of packing followed by the geometry optimizations; polar group of the dispersant and detergent were coordinated onto the nanoparticle surface at the lowest energy cell geometry which agrees with first principle calculations (Figure 5.12 and 5.13).

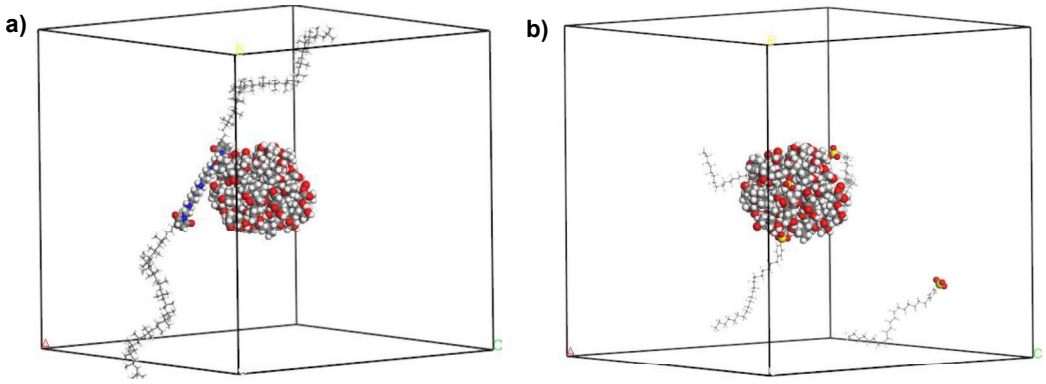

Figure 5.12. The lowest energy cell geometry which agrees with first principle calculations with one nanoparticle and a) one dispersant molecule, b) one detergent molecule.

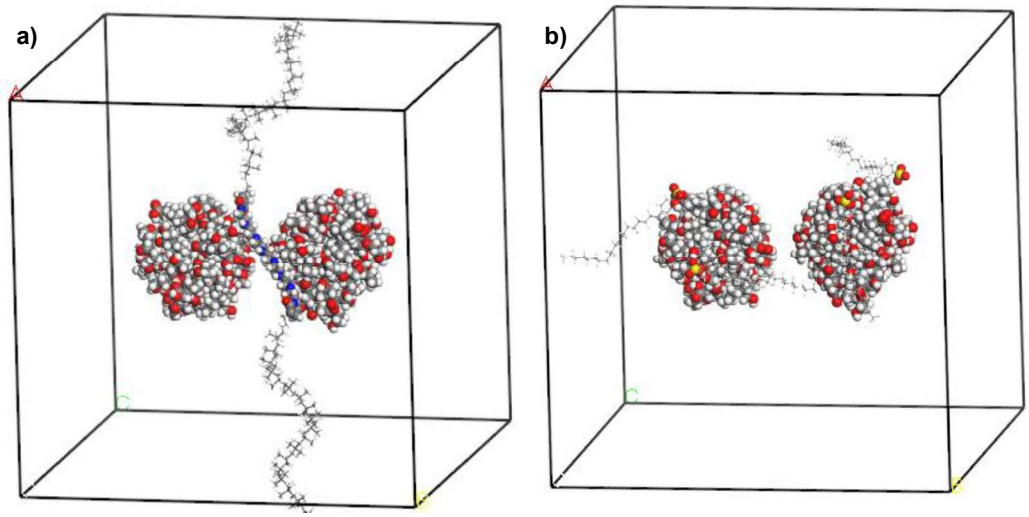

Figure 5.13. The lowest energy cell geometry which agrees with first principle calculations with two nanoparticles and a) one dispersant molecule, b) one detergent molecule.

Next, this template was used in further packing of the oils into the cells. Oil was added to these template cells by using similar Monte Carlo algorithm where the dispersant and detergent were already in the cell in their most stable forms. Similarly, all the initial cells having different number of nanoparticles were created by oil addition to this cell as a final step of construction where sulfonate head group and dispersant amine group are on the nanoparticle surface as expected (Figure 5.14).

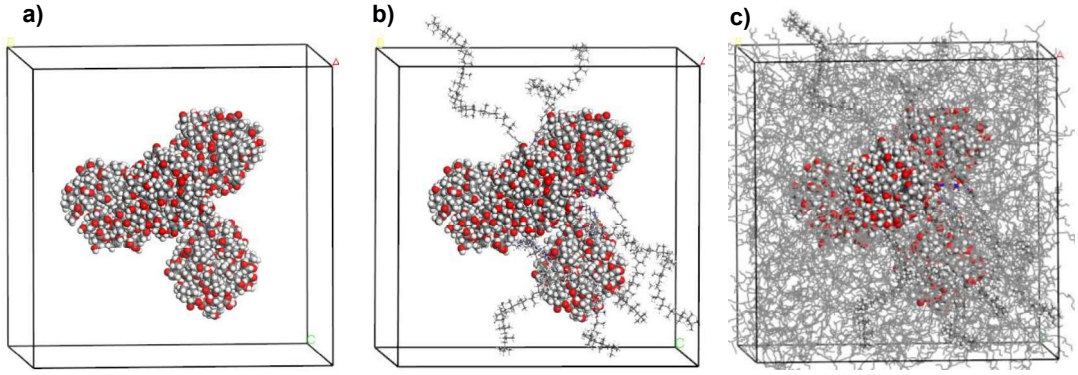

Figure 5.14. Packing of a) four nanoparticles in a unit cell with b) four dispersant molecules followed by c) base oil addition by Monte Carlo calculation.

In the second method, dispersants and detergents were added into the cell that formed after the oil added first to the cell with nanoparticles. As an example, four dispersant molecules were added by Monte Carlo method to these cells followed by the selection of lowest energy cell that was depicted in Figure 5.15. In this example, a cubic structure with a size of 6x6x6 nm^3 with four nanoparticles was used. First, the modeled four nanoparticles were placed into the center of unit cell with an average distance of 5 Å. As a second step, the base oil molecules were packed into the structure with the final density 0.8 g/cm^3. There were 232 base oil molecules in the unit cell to reach this density. The final density was arranged in a way that it increased from 0.80 to experimental 0.86 g/cm^3 after the addition of dispersant molecules.

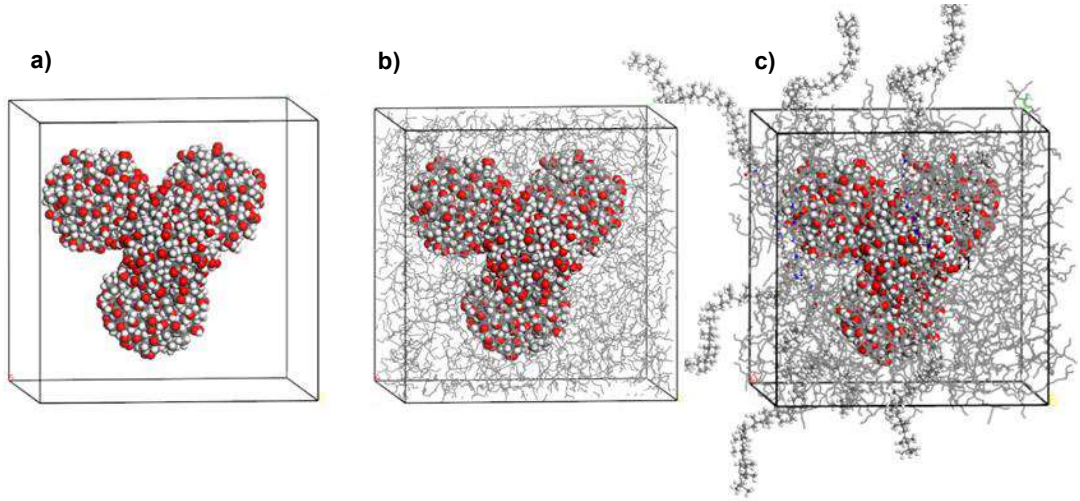

Figure 5.15.a) Placing four nanoparticles in a unit cell, b) packing with 232 base oil molecules, and c) followed by four dispersant molecules.

Next, 20 sulfonate anions and 10 divalent calcium cations for charge equilibrium were added to the same structure with four nanoparticles, which was then the lowest energy structures in base oil-detergent packing is selected for the MD simulations given in Figure 5.16. For packing of base oil and additives, over the 1000 cells have been constructed. All the cells were optimized for 5000 steps.

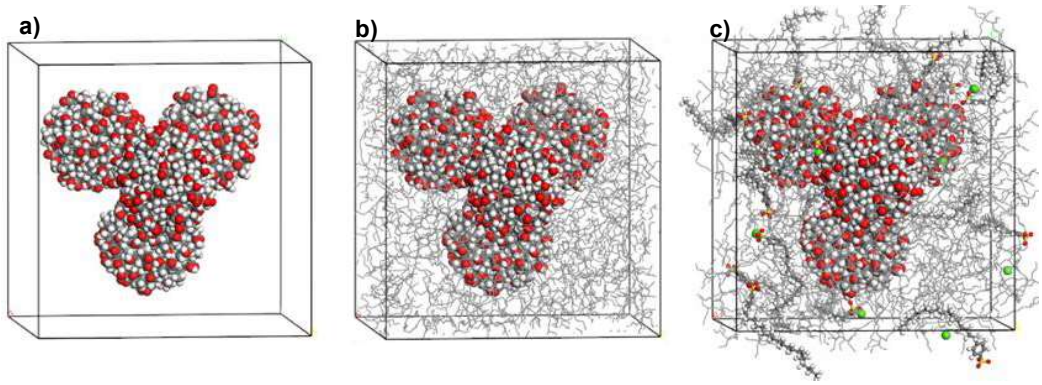

Figure 5.16. Placing four nanoparticles in a unit cell, b) packing of 232 base oil molecule c) followed by ten sulfonate molecules and five calcium cations.

Both methods gave similar initial cell structures. However, first method was selected since lower energy structures were reached where detergents and dispersants were added first onto the nanoparticle surface followed by the addition of oil packing into the cell. In addition, free volume on the polar surface of the nanoparticle was prevented by oil molecules that polar groups of dispersant and detergents cannot position perfectly on the surface.

After the packing of additives and base oil, geometry optimizations were performed for the cell structures. It was observed that the polar succinimide amine groups in the middle part are always in interaction with the surface of the insoluble nanoparticle. Polyisobutylene tails were extending away from the surface into the non-polar base oil. Same result was also valid for the head and alkyl tail groups of the detergents.

Another important result about the dispersant and detergent was that they preferred to intercalate between two or more nanoparticles having 0.5 nm distance in the most stable geometries. For dispersant molecule, only the amine and succinimide groups intercalated between the insoluble nanoparticles. For sulfonate detergent, it was observed that sulfonate head groups were intercalating between the insoluble nanoparticle interfaces. These observations were also supported by the interaction energy calculations.

Initial structures were prepared by packing calculations of two, three and four-nanoparticles systems (Figure 5.17-5.22). Then lowest energy cells were selected for molecular dynamics simulations.

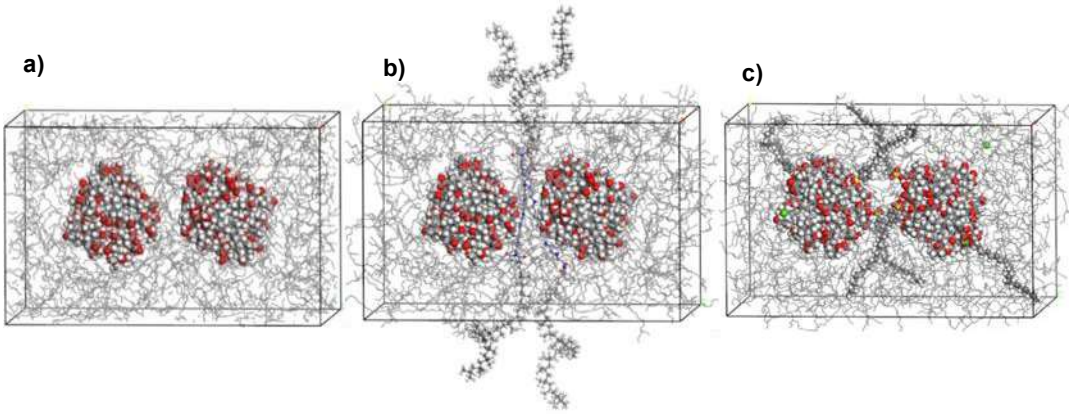

Figure 5.17. Two nanoparticle system packed with a) 261 base oil molecules b) base oil and two dispersant molecules c) base oil and six detergent molecules and 3 calcium cations.

The unit cell with two nanoparticles has 5x8x5 nm^3 lattice dimensions. First, it was packed with 277 base oil molecules, secondly another cell with two nanoparticles were packed with 261 base oil and 2 dispersant molecules, and at last a cell packed with 269 base oil and 6 sulfonate molecules with 3 calcium cations.

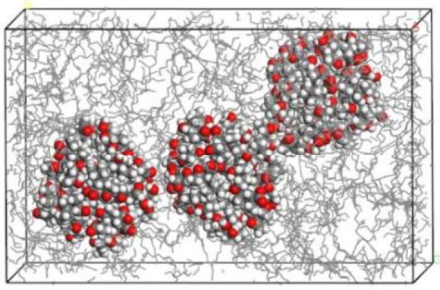

Figure 5.18. Three nanoparticle system packed with 277 base oil molecules in a unit cell.

Three nanoparticle unit cell with same lattice parameters has been packed at first with only 277 base oil molecules. Then, three, six and nine dispersant molecules were packed into the same structure with oil molecules to examine the effect of the dispersant density. Number of base oil molecules are 237, 213 and 190, respectively for 3-6-9 dispersant systems (Figure 5.19). Due to the long chain structure of the

dispersant, as the number of dispersants increased, the number of base oil molecules decreased to provide fixed engine oil density at 0.86 g/cm^3.

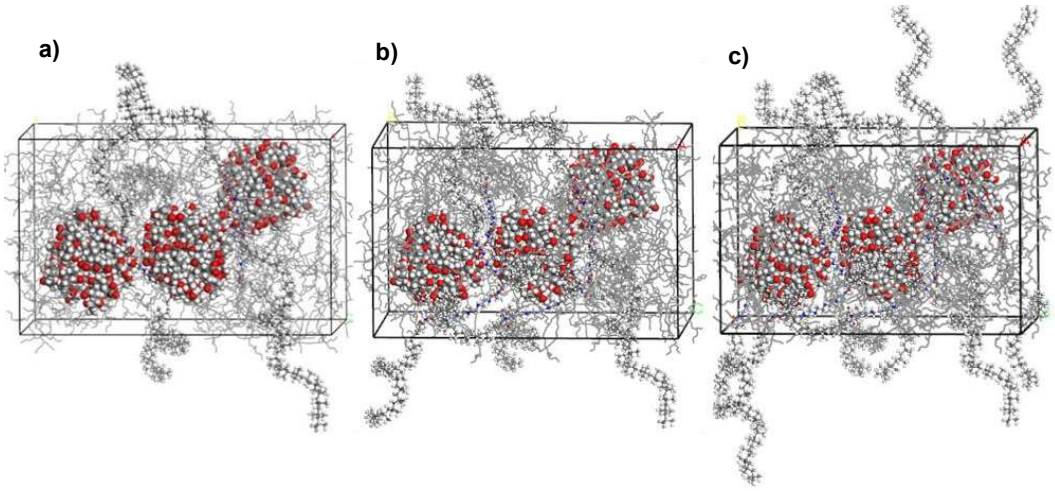

Figure 5.19. Three nanoparticle system with a) three dispersant and 237 base oil molecules, b) six dispersant and 213 base oil molecules, c) twelve dispersant and 190 base oil molecules.

Next, six, twelve and eighteen detergent molecules were packed into the same cell structure to examine the effect of the number of the sulfonate detergents (Figure 5.20). Number of base oil molecules are set 252, 244 and 235 in the unit cells, respectively, for six, twelve, and eighteen sulfonate molecules.

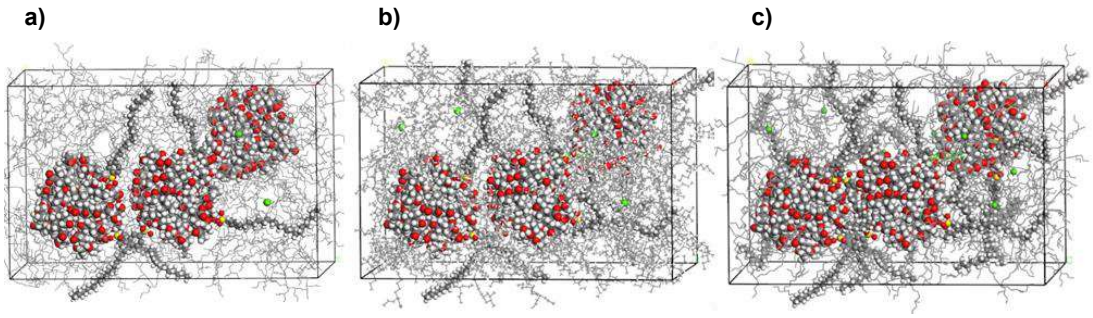

Figure 5.20. Three nanoparticle system with a) six detergent and 252 base oil molecules, b) twelve detergent and 244 base oil molecules, c) eighteen detergents and 235 base oil molecules.

Finally, four nanoparticle systems were prepared. The four nanoparticles were placed into the center of 7.5x7.5x7.5 nm^3 cubic cell with approximately 5 Å interparticle distance between them. The system was first prepared for four dispersant and eight detergent molecules, separately in Figure 5.21 and 5.22.

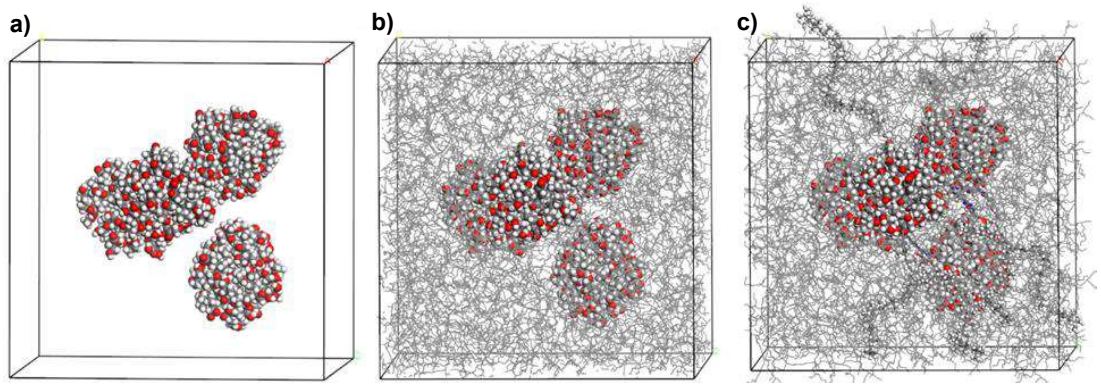

Figure 5.21. Four nanoparticle system a) in cubic cell, b) packing with 728 base oil molecules, c) packing with four dispersant and 697 base oil molecules.

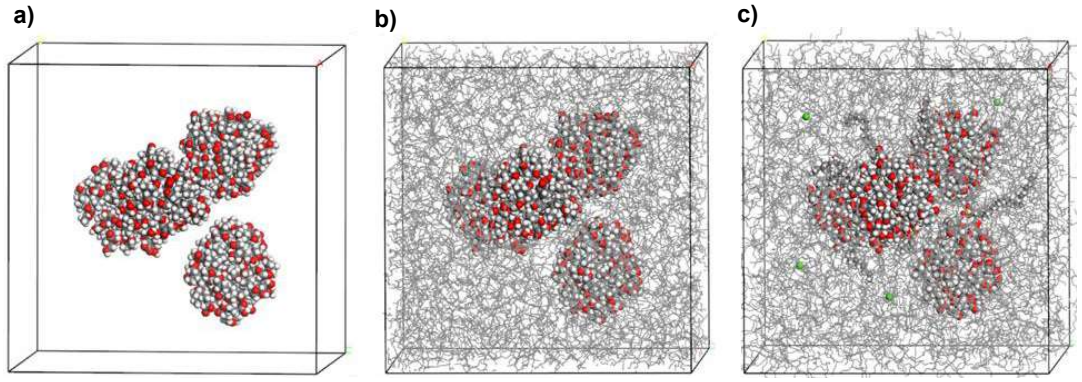

Figure 5.22. Four nanoparticle system a) in cubic cell, b) packing with 728 base oil molecules, and c) packing with eight detergent molecules, four calcium cations and 717 base oil molecules.

After completion of all the oil and additive packing calculations for two, three and four-nanoparticle systems, the final structures were prepared after the final 5000 step geometry optimizations. These final structures were ready for Molecular Dynamics Simulations.

5.7 Molecular Dynamics Simulations

Molecular dynamics simulations were initiated by placing nanoparticles into an empty cell at size 8x8x8 nm^3, followed by geometry optimization at 5000 steps. After the calculation of the free energy of solvation for nanoparticles in base oil, it was calculated as value 32.43 kcal/mol that the nanoparticle did not dissolve in the base oil and aggregate due to hydrophobic and hydrophilic interactions. Not only in base oil but also in the empty cell, nanoparticles have agglomerated. The first, middle and the last frames of the molecular dynamic simulation of this cell is given in the Figure 5.23 and Figure 5.24, below. The simulation parameters were set as NVT as an ensemble, 423 K as temperature, NHL as thermostat with 1 fs step size and 2 ns total simulation time.

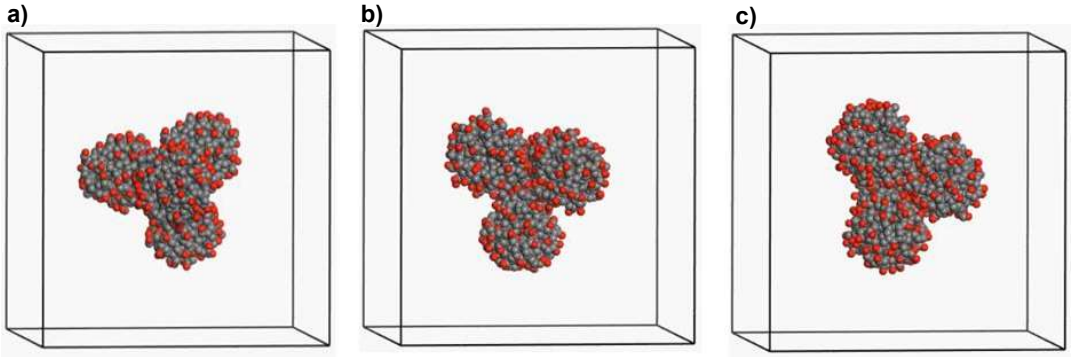

Figure 5.23. a) The first, b) middle and c) final frames of MD simulations of aggregated four nanoparticles in empty unit cell for 2 ns simulation time.

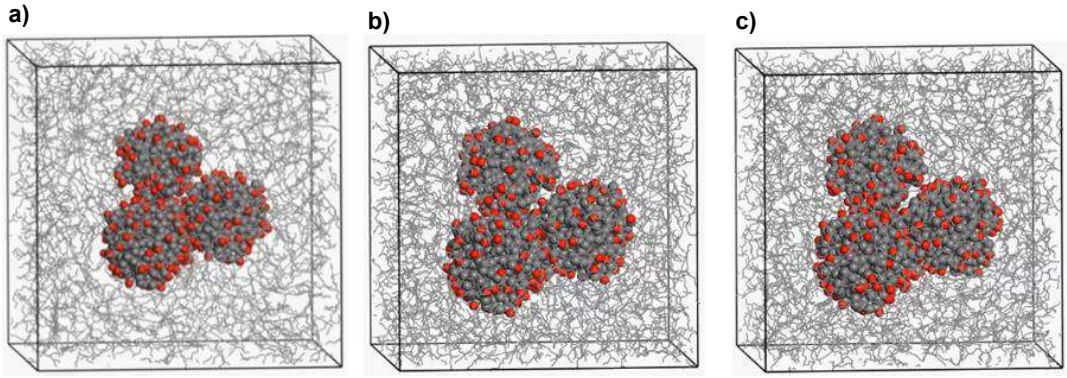

Figure 5.24. a) The first, b) middle and c) final frames of MD simulations of aggregated 4 nanoparticles in unit cell packed with 697 base oil molecules for 2 ns simulation time.

As a first step, the aggregated 4 insoluble nanoparticles were placed into the empty unit cell. Then, cell with aggregated 4 nanoparticles packed with base oil were subjected to molecular dynamics simulations. They both preserve their aggregated structure. Mean square displacement was calculated for both cases.

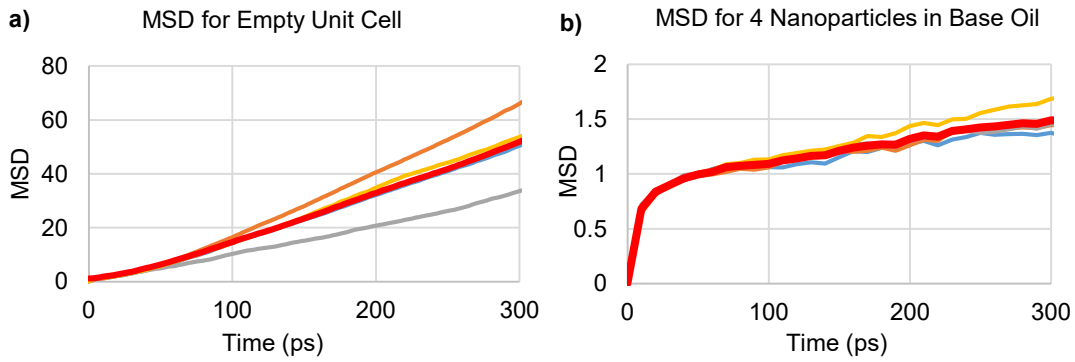

Figure 5.25. MSD calculations of four nanoparticles in a) empty unit cell and b) unit cell with base oil.

The displacement of the nanoparticles in an empty cell is greater than as in base oil as seen in the Figure 5.25. Surfaces of the nanoparticles were polar and hydrophilic and have strong tendency to aggregate both in oil and in vacuum. We concluded that these particles were highly insoluble in oil.

As a second step, four nanoparticles were positioned in an empty cell center with approximately 4 Å distance. After 5000 times geometry optimization, molecular dynamics simulation was performed. Similarly, aggregation behavior was observed. The first, middle, and the last frames of simulation was given in Figure 5.26 for total 2 ns simulation.

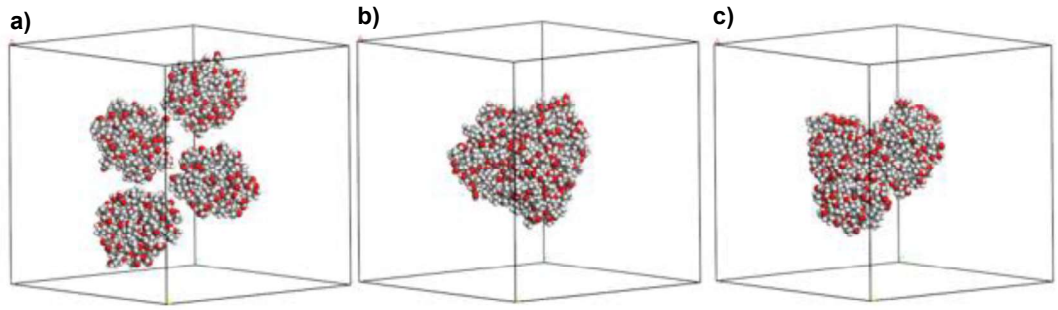

Figure 5.26. a) The first, b) middle and c) final frames of MD simulations of separately placed four nanoparticles in empty unit cell for 2 ns simulation time.

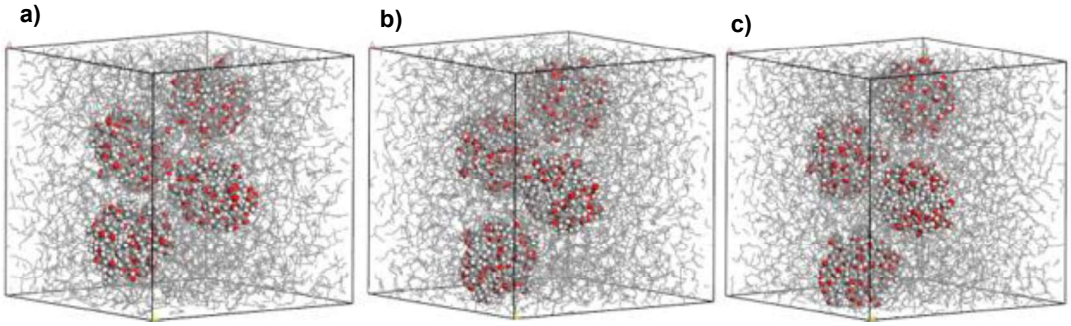

Figure 5.27. a) The first, b) middle and c) final frames of MD simulations of separately placed four nanoparticles in unit cell packed with 581 base oil molecules for 2 ns simulation time.

In the first case without any base oil, aggregation was observed quickly in less than 1 ns simulation time. In addition, it was calculated that the nanoparticles placed at 4 Å distance, approached each other over time and reached 1 to 2 Å as depicted in radial distribution function (RDF). The peak at around 2 Å indicates the hydrogen bond formation which is exactly 2.11 Å in theoretical calculations (Figure 5.28). In Figure 5.29, the last frame of the simulation was shown and the hydrogen bonds between nanoparticles were presented. We concluded that hydrogen bonding between nanoparticles is the second reason for the aggregation mechanism in addition to the positive free energy of solvation.

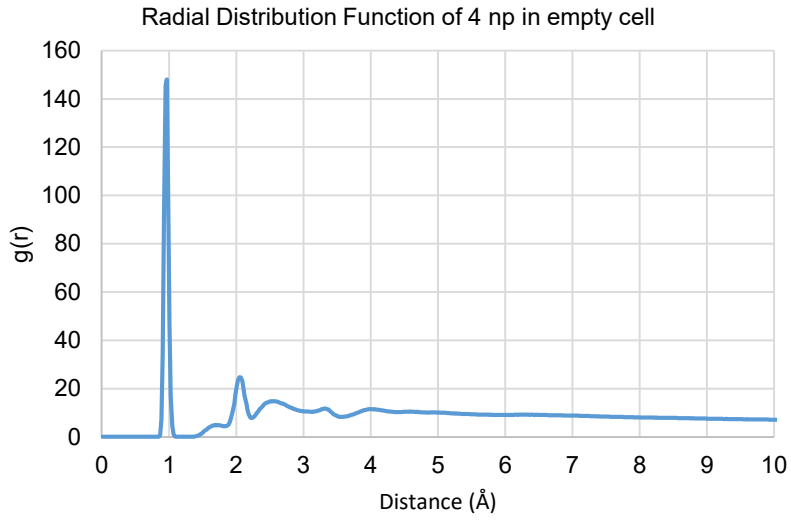

Figure 5.28. Radial distribution function between hydrogen and oxygen atoms of nanoparticles.

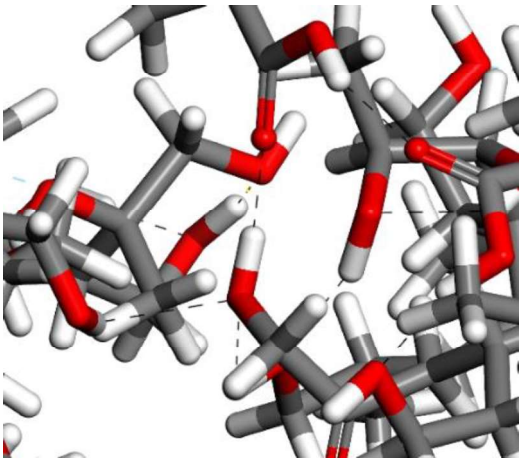

Figure 5.29. Hydrogen bonding between nanoparticles shown as black dashed lines.

It was expected to observe the same aggregation behavior of nanoparticles in the base oil environment; however, they did not aggregate in the simulation time (Figure 5.27). This MD simulation for four nanoparticle system was repeated many times. Each time, a different mechanism was observed such as coming closer distance but do not aggregate. This may cause from the non-homogeneous polar surface of the nanoparticle that contains many different functional groups; in real case this polarity may not be uniformly distributed. Since in this study nanoparticle has almost uniformly oxygen distributed, all the surfaces can interact with each other and base

oil and affect the attraction forces. This influences the aggregation mechanism. Until this point, it was shown that the nanoparticles, which had already been simulated in an aggregated state, continued to show aggregation behavior, not dispersed. Additionally, nanoparticles placed separately from each other also showed aggregation behavior in all cases in vacuum and in some of the cases in base oil.

After determining hydrogen bonding between particles and positive solvation free energy as the main reasons behind aggregation mechanism between nanoparticles in base oil, the lowest energy structures were selected from the Monte Carlo based packing simulations that were used as initial structures in MD simulations. The cell with two nanoparticle structures was first simulated only in the base oil (Figure 5.30), followed by further simulations in which two dispersant (Figure 5.32) and six detergent molecules (Figure 5.35) were placed between nanoparticles in different simulations adopted from the lowest energy structures.

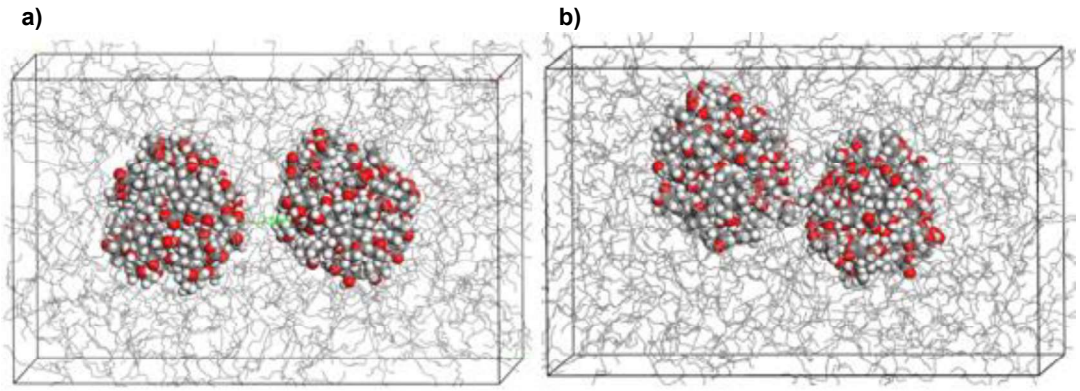

Figure 5.30. The first frame of MD simulations of two nanoparticles with 7 Å distance, b) the last frame of MD simulations of two nanoparticles with 2 Å distance.

Distance evolution analysis were carried out with random distance measurements between the surface atoms of nanoparticles. This analysis was made for 900 ps time of the simulation. It was observed that all the distances decreased with time. Some of these distances reached close to the 2 Å indicate the presence of hydrogen bonding as indicated in Figure 5.31.

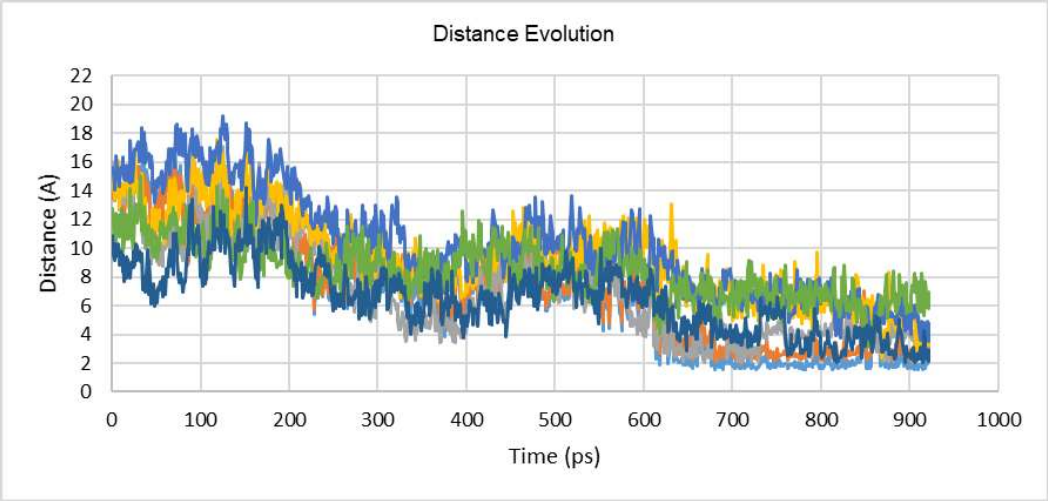

Figure 5.31. Distance evolution graph of two nanoparticles in the unit cell with base oil.

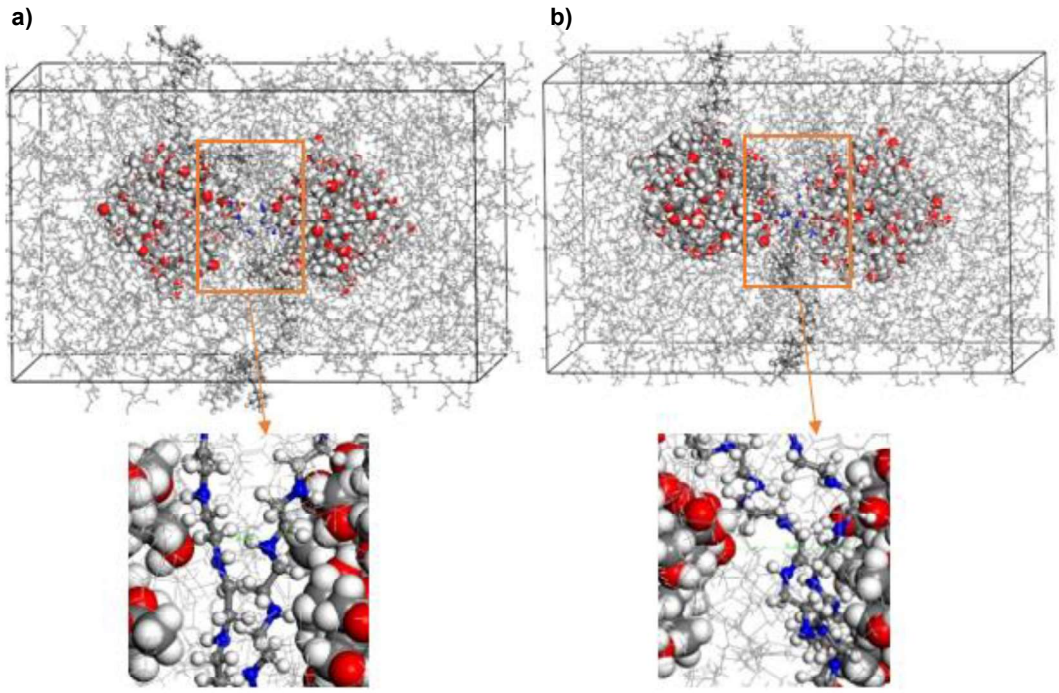

Figure 5.32. a) The first frame of MD simulations of two nanoparticles with 7 Å distance and two dispersant molecules, b) the last frame of MD simulations of two nanoparticles with 9 Å distance with two dispersant molecules. Inset figures show detailed captures.

In the simulations where the dispersant molecules were added, we observed not only the prevention of the nanoparticles from reaching each other, but also increased

distance between them. We determined that non-polar isobutylene tails were extending into the base oil. We found that the observed distance increase between nanoparticles was due to the two reasons. First one was the intercalation of the polar amine succinimide group between the nanoparticles and secondly the movement of this longer poly-isobutylene tails of the dispersant molecule in base oil that created shear.

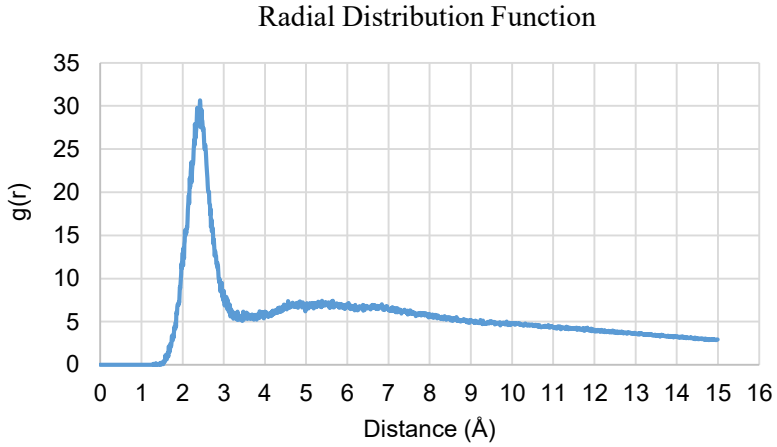

Figure 5.33. Radial distribution function between amine of dispersant molecules and hydrogen of nanoparticles.

From the RDF analysis given in Figure 5.33, it was clearly shown that hydrogen and oxygen atoms of the nanoparticles have 2 Å distances with the nitrogen and hydrogen atoms of dispersant in Figure 5.34.

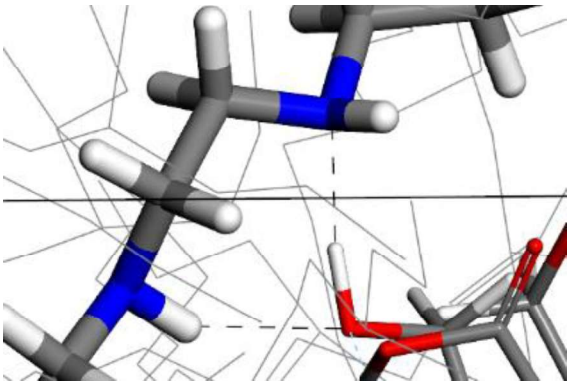

Figure 5.34. Hydrogen bonding between nitrogen of dispersant amine group and hydrogen of nanoparticle hydroxyl group shown as black dashed lines.

Next, two nanoparticle structures with six sulfonate and three calcium cations were studied. In all molecular dynamics simulations which has included sulfonate detergent, head group that is the polar anionic sulfonate group, was positioned on the nanoparticle surface ready to interact with the nanoparticle where they preferred to position between the two-nanoparticle interface in majority supporting the structures generated by Monte Carlo type random packing results.

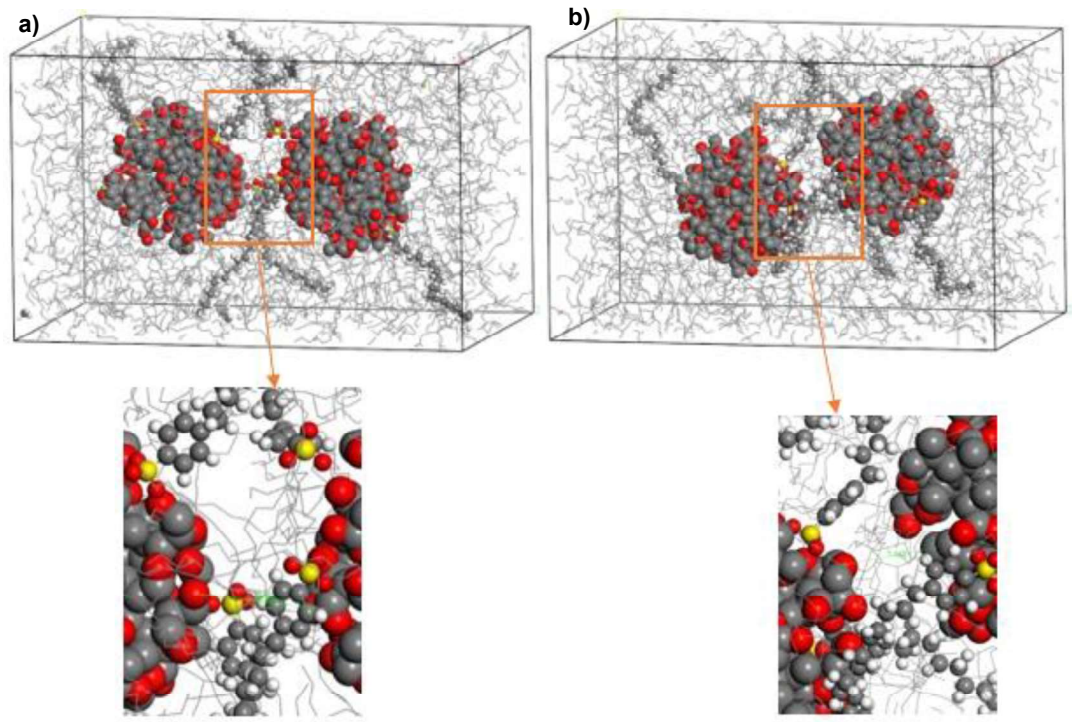

Figure 5.35. a) The first frame of MD simulations of two nanoparticles with 8 Å distance, and b) last frame of MD simulations of two nanoparticles with 7 Å distance with six detergent molecules. Inset figures show detailed captures.

Due to the presence of sulfonate detergent between the nanoparticles, the nanoparticles did not show any aggregation behavior even though they get slightly closer. Additionally, since sulfonate head groups of the detergents were highly polar, they interacted with the polar surfaces of nanoparticles via hydrogen bonding. The head group of detergents were thus positioned toward the surface of the nanoparticle while their tails were extending into the oil. The tails of sulfonate detergent in the base oil kept the other nanoparticle away from one another by covering the surface which was the main working mechanism of the dispersant.

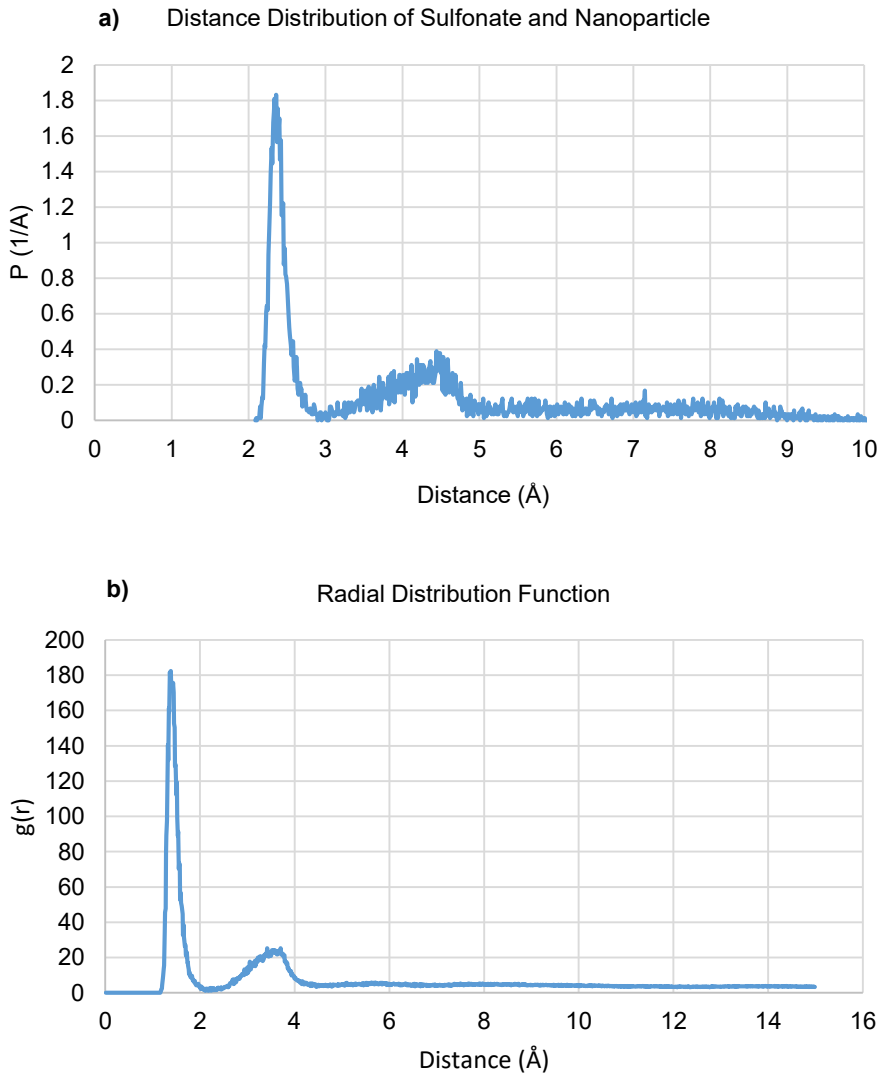

Figure 5.36. a) Distance distribution and b) RDF for the sulfonate head group and nanoparticle surface.

The distance distribution and RDF analysis for the intermolecular distance between the oxygen atoms of the sulfonate head group and any atoms on the nanoparticle surface was given in Figure 5.36. At the end of the 2 ns simulation, this distance was calculated to be 2.34 Å at highest probability. This information supports the hydrogen bond formation between sulfonate head and nanoparticle surface similar with the polar group of the dispersants. Then hydrogen bonds were visualized as given in Figure 5.37 below.

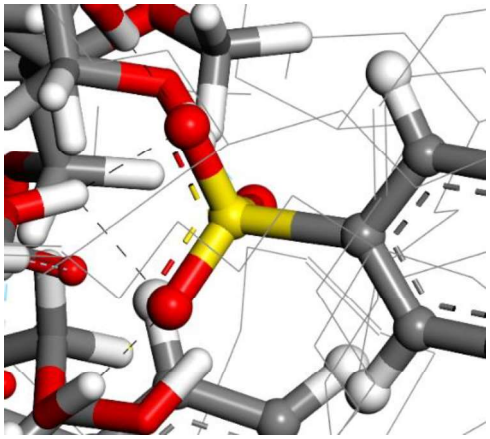

Figure 5.37. Hydrogen bonding between oxygen atoms in sulfonate head group and hydrogen atoms in nanoparticles surface for two nanoparticle system shown as black dashed lines.

The new structures were constructed where the number of nanoparticles increased to three. Similar with previous simulations, unit cell with only base oil and nanoparticles was performed first in MD simulations (Figure 5.38).

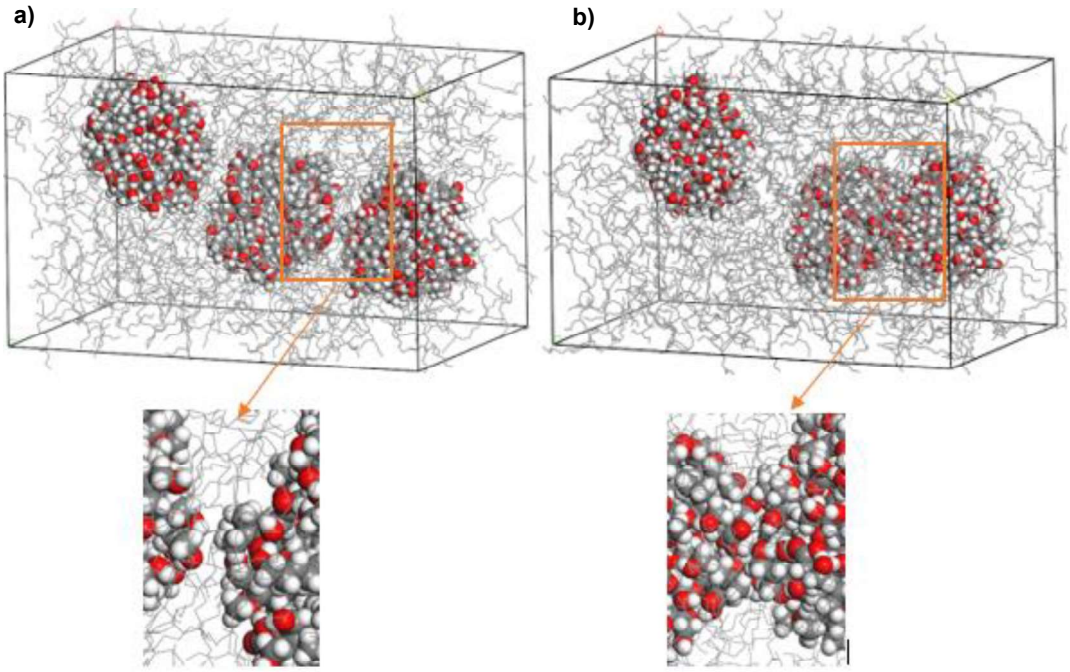

Figure 5.38. a) The first frame of MD simulations of three nanoparticles with 5 Å distance, b) the last frame of MD simulations of aggregated three nanoparticles. Inset figures show detailed captures.

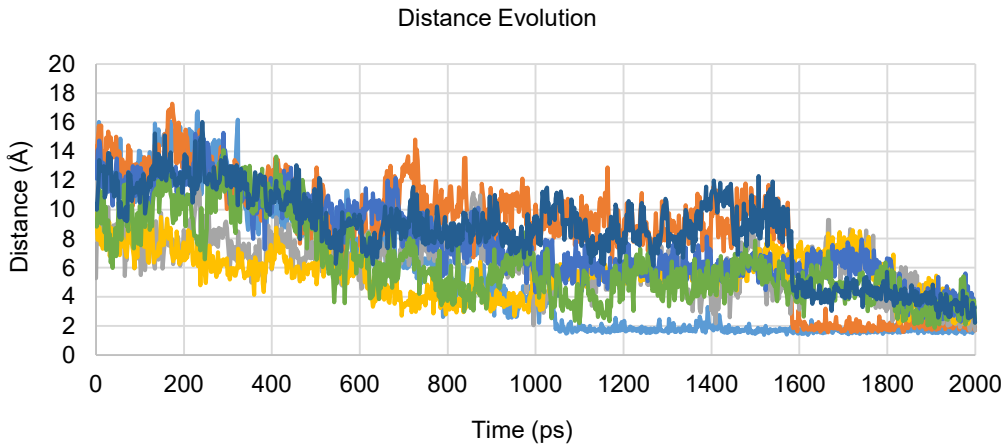

Figure 5.39. Distance evolution of the intermolecular distance between nanoparticles in three nanoparticle system.

Randomly selected distances between surface atoms of the nanoparticles were evaluated for 2 ns simulation time. All the distances showed decreasing trend. Some of these distances reached as low as 1.7 Å distance as depicted in Figure 5.39. In closer image given in Figure 5.40, it was shown that hydrogen bonds were formed between aggregated nanoparticles.

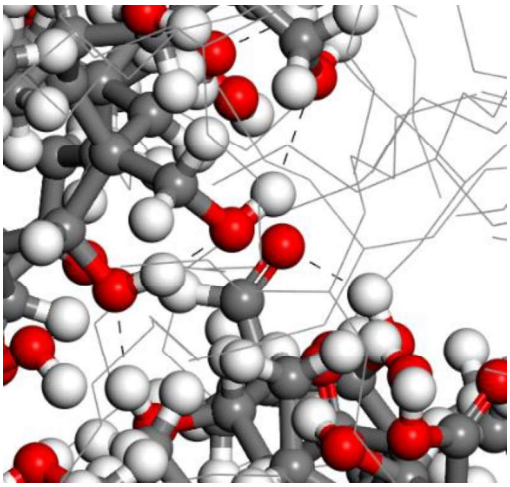

Figure 5.40. Hydrogen bonding between nanoparticles shown as black dashed lines.

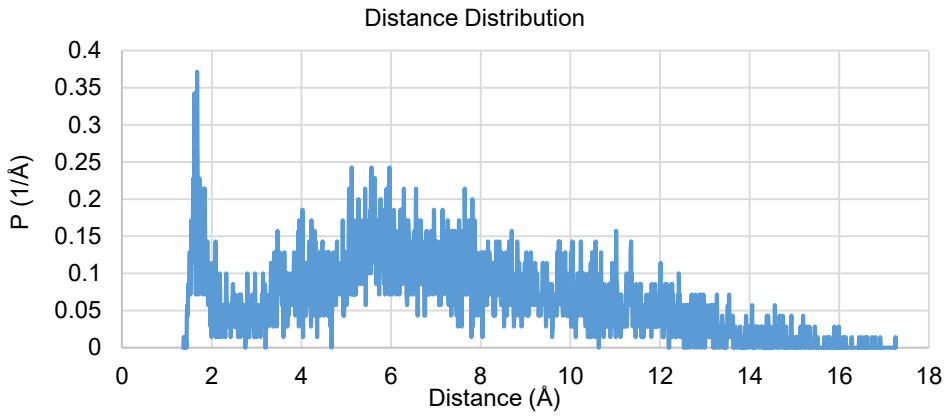

Figure 5.41. Distance distribution of randomly chosen distances between aggregated nanoparticles.

It was presented in Figure 5.41 that the distances between aggregated nanoparticles have the highest probability at 1.68 Å distance which pointed out strong aggregation behavior.

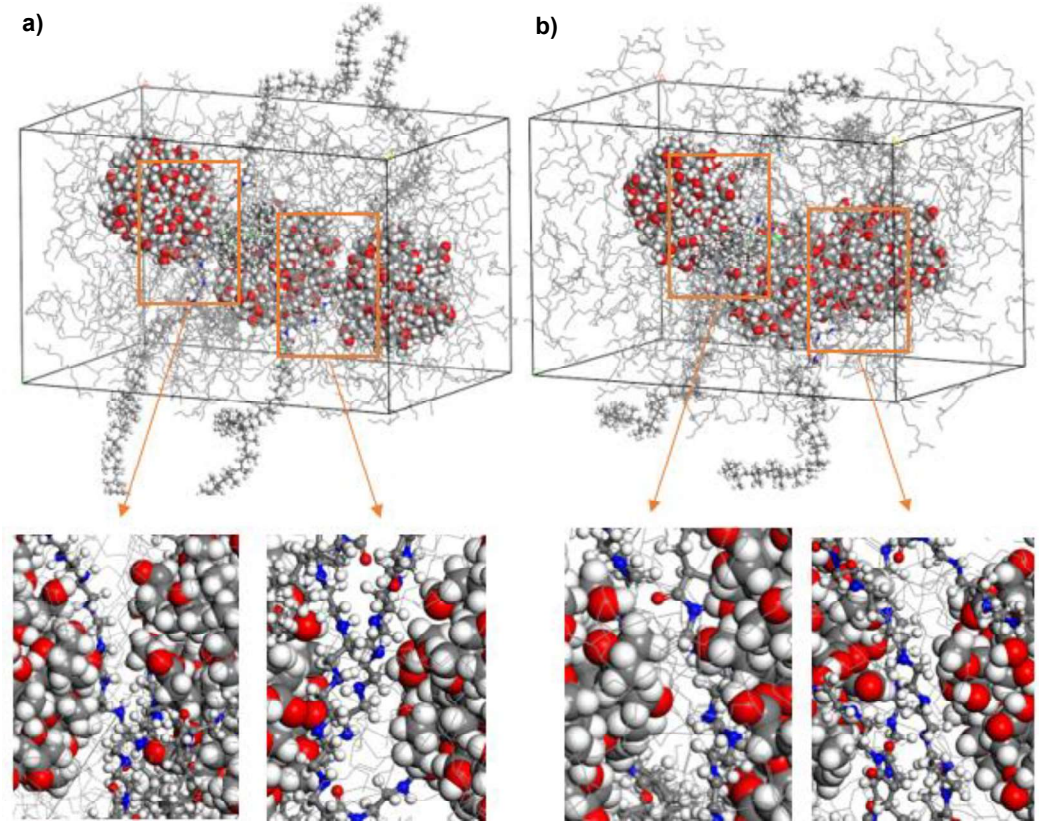

Figure 5.42. a) The first frame and b) the last frame of MD simulations of three nanoparticles with three dispersant molecules. Inset figures show detailed captures.

In order to observe the effect of dispersant addition in the three-nanoparticle system, three, six and nine dispersant molecules were packed separately into the same cell (Figure 5.42-5.44). For the generated unit cells in all cases with different number of dispersants, the additives were always positioned in such a way that their middle polar part, namely the polar amine bis-succinimide structures were in interaction with the nanoparticle surfaces. In the MD simulations, this structure was preferred due to the packing calculations that show cell with the lowest energy have the dispersant structures were placed in this way.

Dispersant molecules were then simulated with the same parameters between the nanoparticles in "three nanoparticles three dispersant molecules system" (Figure 5.42). Since the distance between the nanoparticles were relatively small, dispersant molecules were intercalated and interacted with both nanoparticles at the same time.

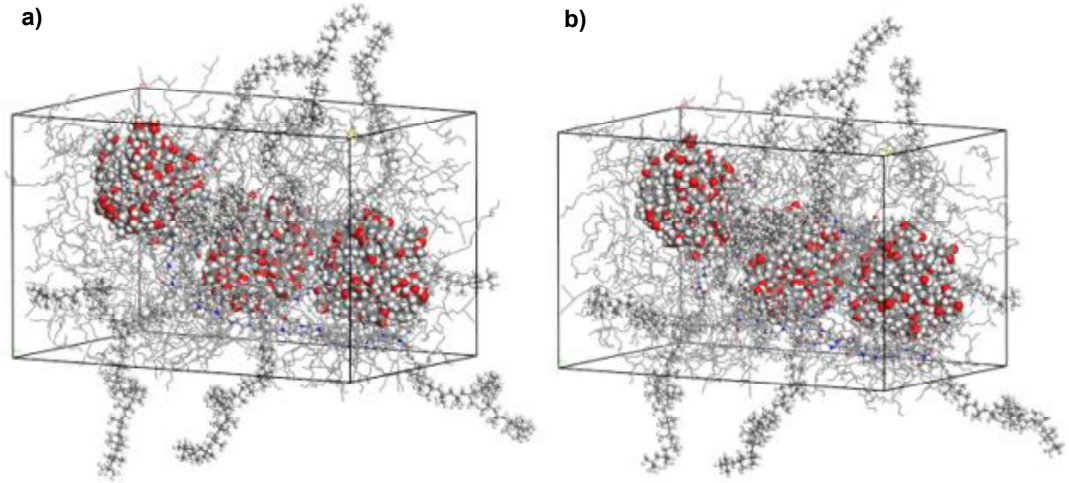

Figure 5.43. a) The first frame and b) the last frame of MD simulations of three nanoparticles with six dispersant molecules.

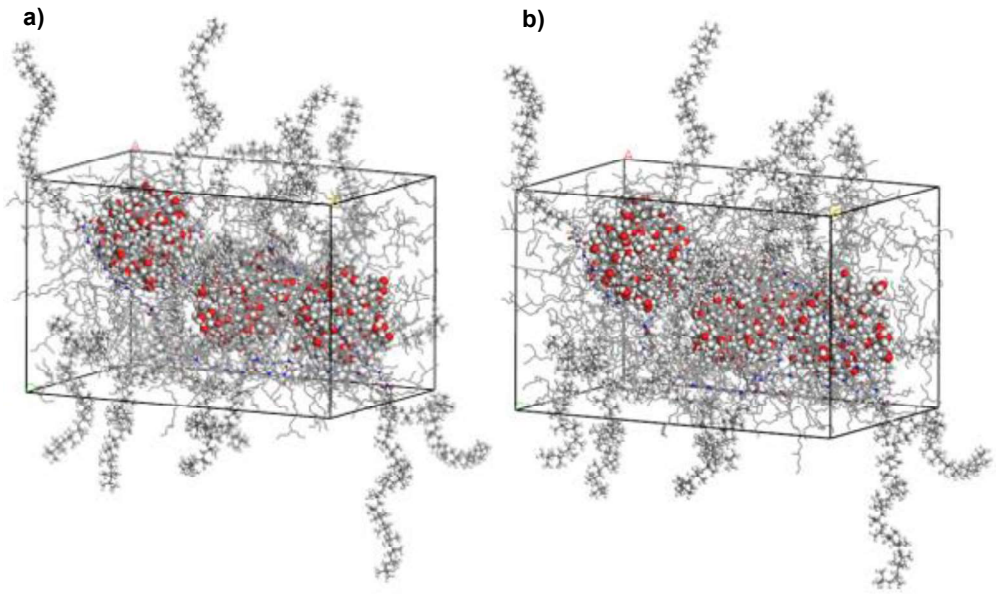

Figure 5.44. a) The first frame and b) the last frame of MD simulations of three nanoparticles with nine dispersant molecules.

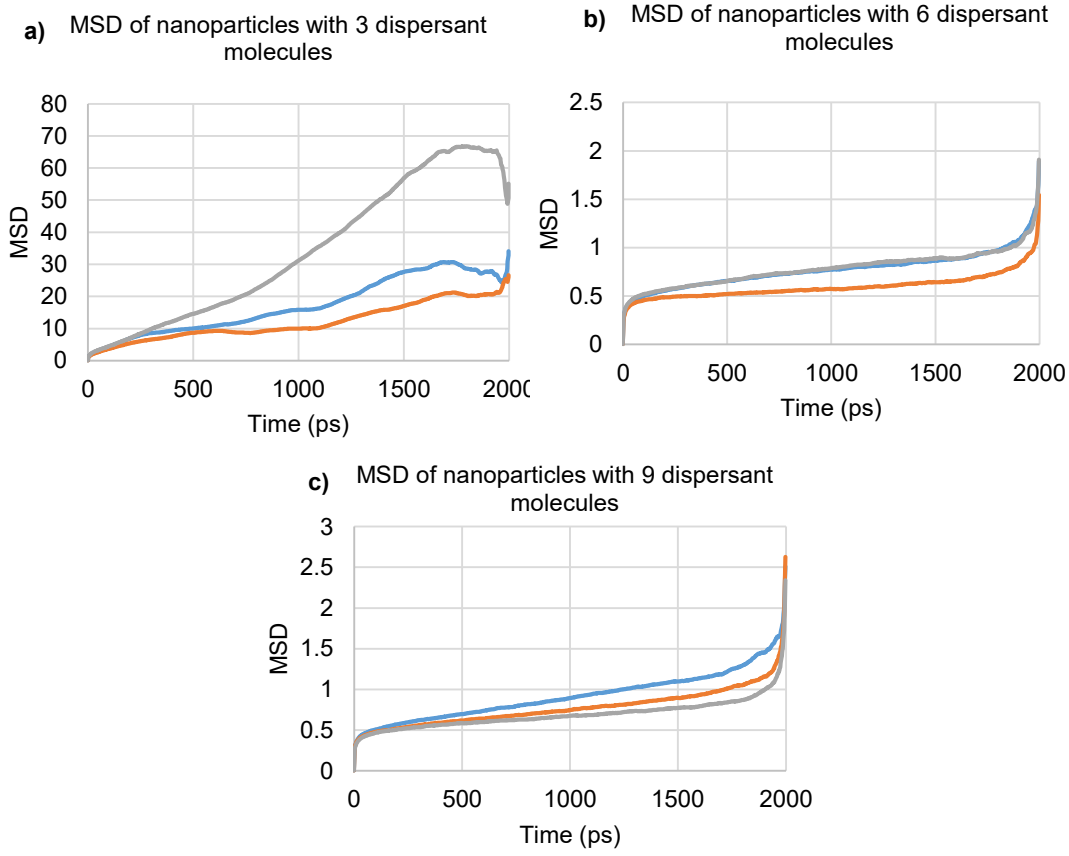

Figure 5.45. MSD graphs of three nanoparticles for a) three, b) six, and c) nine dispersant molecule structures.

Mean square displacement analysis for the mobility of the nanoparticles show that, the first system with three dispersant molecules has the highest value (Figure 5.45). This means that when the number of the dispersant molecules increases, mobility of the nanoparticles decreases as expected. It was believed that covered nanoparticles form a colloid like structures which do not prefer to aggregate and stay stable in base oil solution.

In the three-nanoparticle cell structure, different numbers of detergent molecules were added to determine the effect of sulfonate density on the aggregation mechanism. Packing of the cell with six, twelve, eighteen detergents were prepared (Figure 5.46-5.48).

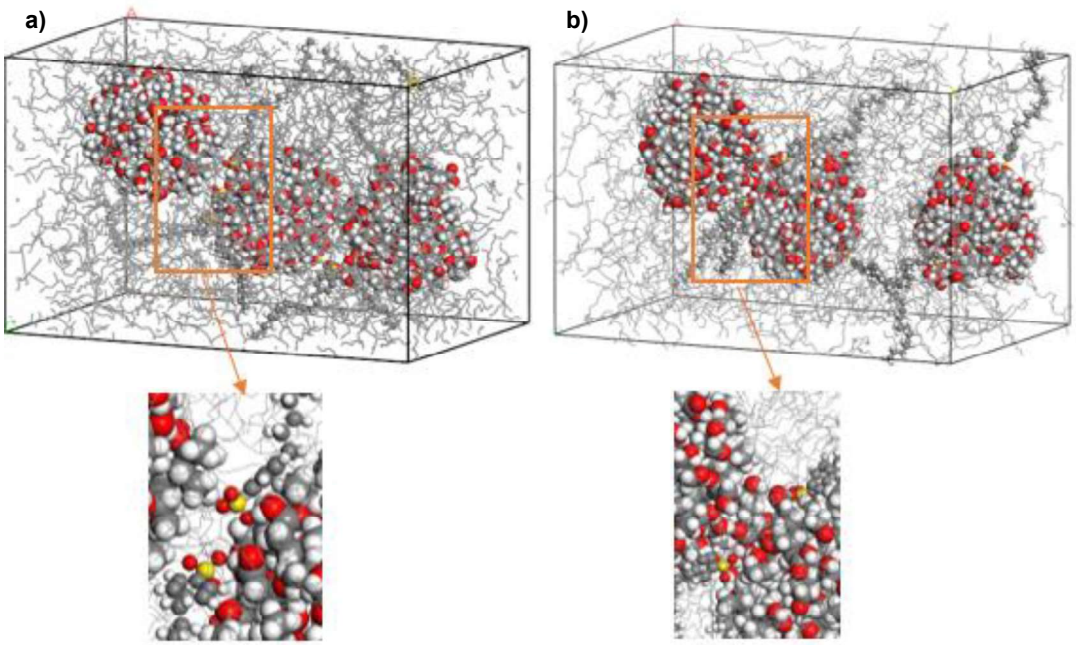

Figure 5.46. a) The first frame and b) the last frame of MD simulations of three nanoparticles with six sulfonate detergent molecules. Inset figures show detailed captures.

Similar with the previous simulations with two nanoparticles, hydrogen bond formation between oxygen atoms in sulfonate head group and hydrogen atoms in nanoparticles surface were determined. Complete aggregation was not observed with

the high number of sulfonates covering the nanoparticle surface given for addition of twelve and eighteen sulfonate detergents. RDF results supported the formation of strong hydrogen bonds at the surface with the sulfonate head groups with the extended tail into the base oil phase (Figure 5.49).

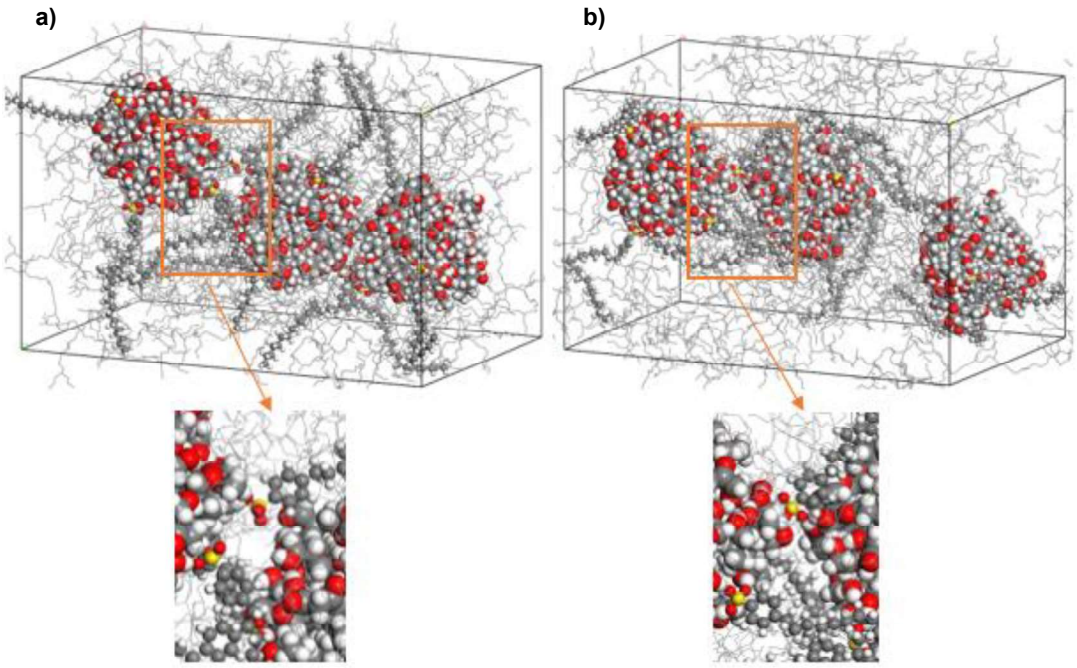

Figure 5.47. a) The first frame and b) the last frame of MD simulations of three nanoparticles with twelve sulfonate detergent molecules. Inset figures show detailed captures.

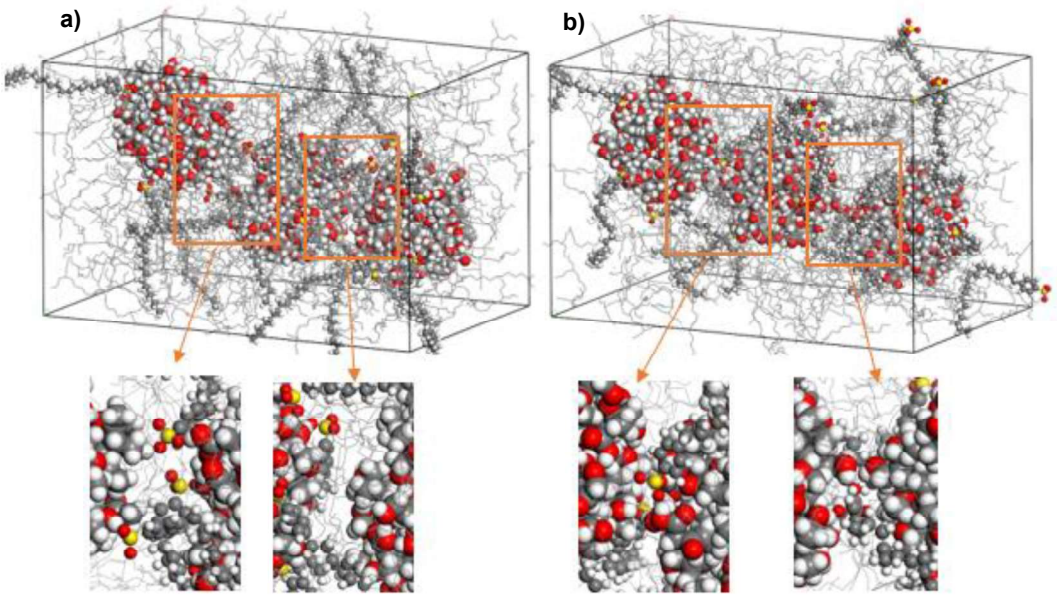

Figure 5.48. a) The first frame and b) the last frame of MD simulations of three nanoparticles with eighteen sulfonate detergent molecules. Inset figures show detailed captures.

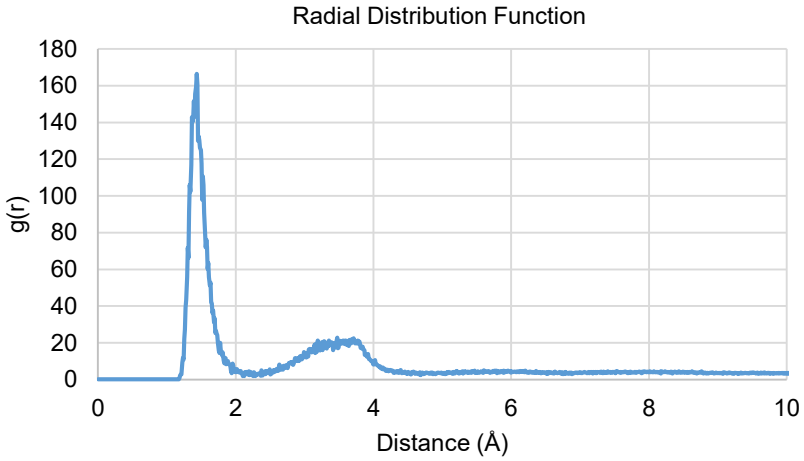

Figure 5.49. RDF of oxygen atoms of detergent head group and hydrogen atoms at the nanoparticle surface.

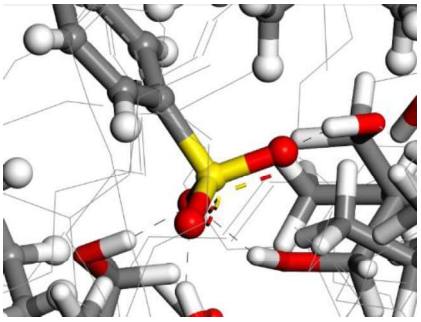

Figure 5.50. Hydrogen bonding between oxygen atoms in sulfonate head group and hydrogen atoms at nanoparticle surface for two nanoparticle system, shown as black dashed lines.

The cell structure with the addition of eighteen detergent molecules has the smallest MSD value (Figure 5.51). Since displacement data indicated the mobility of the selected nanoparticles over the time, it can be concluded that eighteen detergent molecules can mitigate the mobility of the nanoparticles to prevent the aggregation.

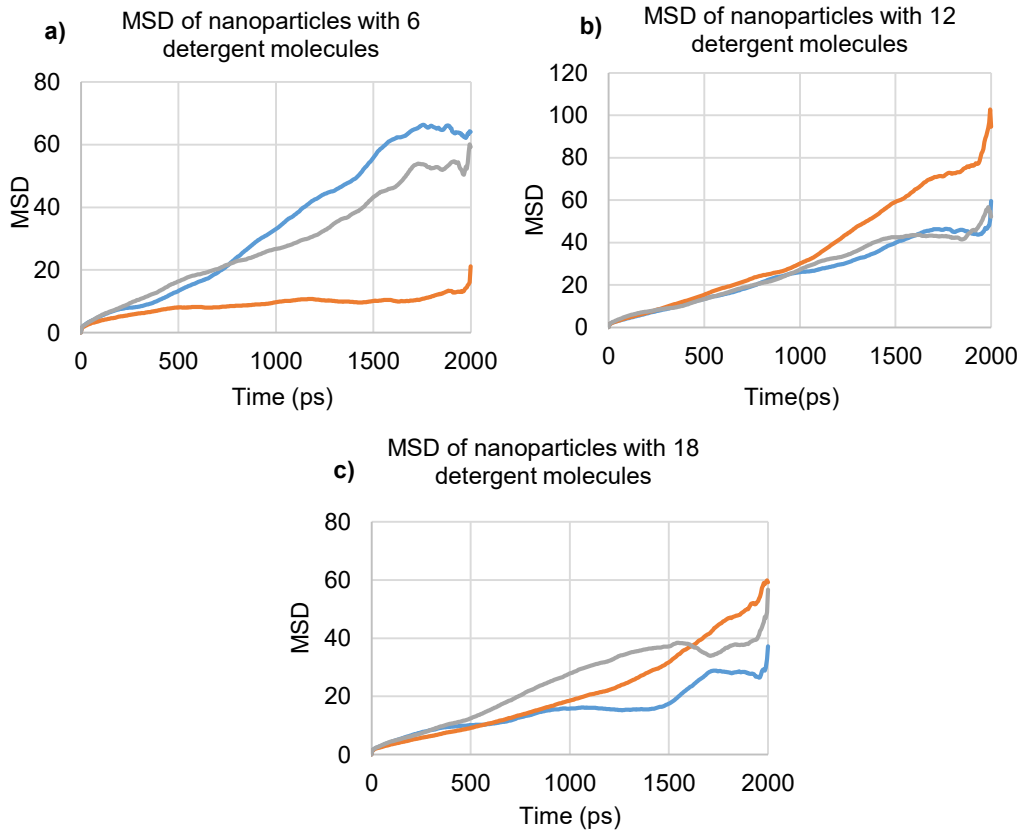

Figure 5.51. MSD graphs of three nanoparticles for a) six, b) twelve, and c) eighteen detergent molecule structures.

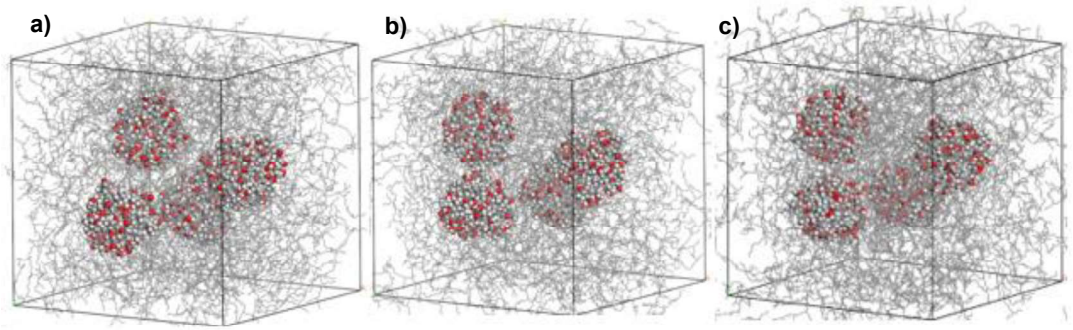

Figure 5.52. a) The first frame of MD simulations of four nanoparticles with 8 Å distance, b) the last frame of MD simulations of four nanoparticles after 2 ns, c) last frame of MD simulations of four nanoparticles in base oil after 4 ns.

After the cell with four nanoparticle structure was constructed, base oil added to the cell with the experimental density followed by 5000 steps of geometry optimization. Next, MD simulation with a total simulation time of 2 nanoseconds was performed. However, aggregation behavior was not observed for nanoparticles contrary to our expectations. Considering that 2 nanoseconds might be insufficient, the total duration of the simulation was increased to 4 nanoseconds. However, it was still not sufficient to observe aggregation behavior (Figure 5.52). It should be noted that when simulations started from the cell with aggregated nanoparticles, the aggregate was stable for the simulation time and did not dissolve in base oil.

As a result of this, it can be said that for this prepared structure, the nanoparticles must be positioned closely for a total of 2 nanoseconds simulation, or the simulation time should last longer than 4 nanoseconds. This time, the structure with nanoparticles at a distance of 5 Å was prepared and MD simulation was performed, given in Figure 5.53. However, this structure did not show aggregation behavior unless the temperature was increased. They aggregated when the temperature was increased to 823 K. This leads to the conclusion that physical factors in engine can affect the aggregation mechanism. It should be noted that average base oil temperature at 423 K were used in simulations and the temperature in the engine can reach much higher temperatures. This could be one of the reasons we did not observe self-aggregation process in simulations.

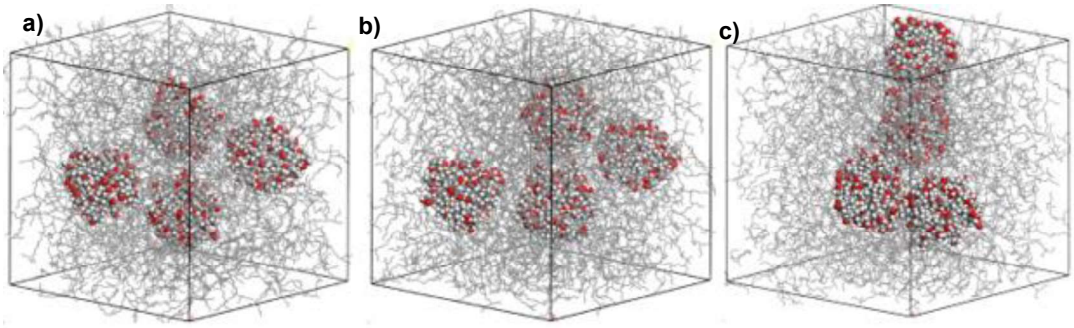

Figure 5.53. a) The first frame of MD simulations of four nanoparticles with 5 Å distance in 423 K, b) the last frame of MD simulations of four nanoparticles after 2 ns in 423 K, c) last frame of MD simulations of four nanoparticles in base oil after 2 ns in 823 K.

There was about 4 Å distance between nanoparticles in Figure 5.53.b. In the last frame, where temperature was significantly higher, aggregate formation were observed. Increasing temperature in this system has led increasing molecular kinetic energy of the molecules and their mobility which decreases the simulation time required for the aggregation.

In order to study the motion of nanoparticles when dispersant was added, four PIBSI was added to the 4-nanoparticle cubic unit cell (Figure 5.54) and MD simulation was performed again at 423 K temperature, since engine environment have 150 ℃ average temperature.

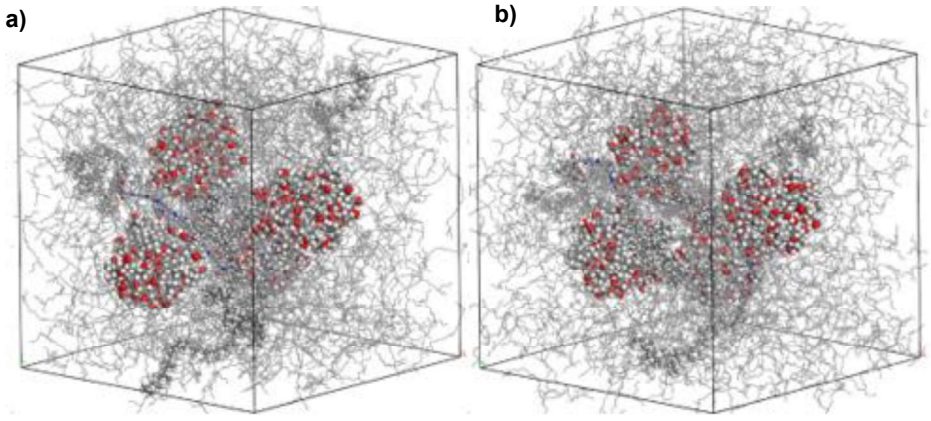

Figure 5.54. The first and b) the last frame of MD simulations of four nanoparticles with four dispersant molecules in 423 K.

The dispersants placed between the nanoparticles prevented them from aggregation even though the distance between them was lowered. This indicates that the mechanism of dispersant was not complete separation of the aggregates, rather than preventing the formation of larger aggregates. Radial Distribution Function analysis was performed on the assumption that the amine and succinimide atoms of the dispersant are the ones formed hydrogen bonds with the nanoparticles (Figure 5.55). Peaks around 2 Å indicated that this estimate was accurate. RDF show that amine part is mainly responsible with the interaction of dispersant with nanoparticle. Then hydrogen bonds were calculated and visualized given in Figure 5.56.

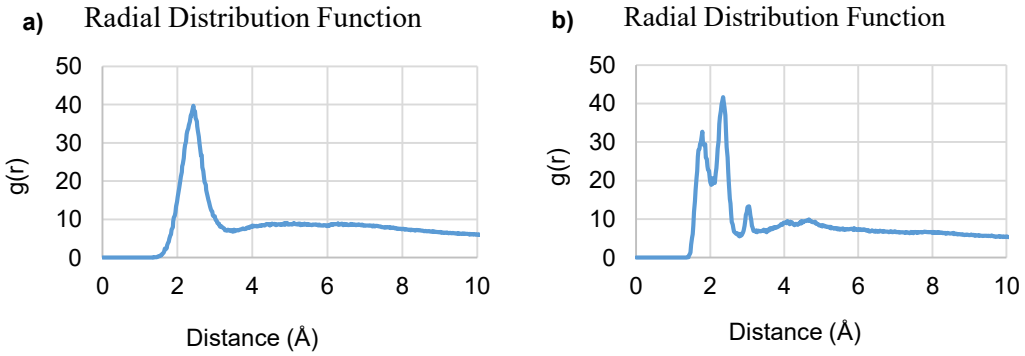

Figure 5.55. RDF between hydrogen atoms in nanoparticle surface and a) nitrogen atoms amine portion b) oxygen atoms in succinimide portion.

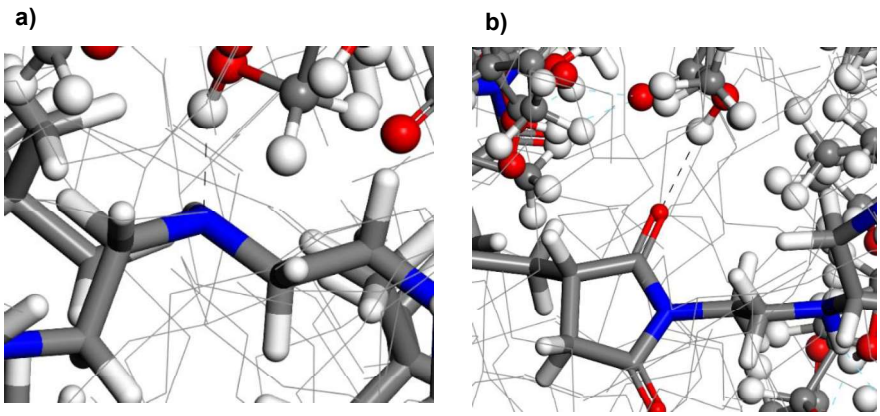

Figure 5.56. Hydrogen bonding between a) the nitrogen atoms in dispersant amine group and hydrogen atoms in nanoparticles surface b) the oxygen atoms in dispersant succinimide group and hydrogen atoms in nanoparticles surface, shown as black dashed lines.

Simulations with eight sulfonate addition to the cell with four nanoparticle showed that there was not any complete aggregation for the nanoparticles (Figure 5.57). Similar with the two and three nanoparticle systems, it has been demonstrated that hydrogen bonding formed in cells with dispersant, were also observed with sulfonate detergents, however with different strength and atom types. A large peak around 2 Å was also observed in the radial distribution function analysis for the four nanoparticle system with sulfonate addition (Figure 5.58). Hydrogen bonds were also visualized between nanoparticle surface hydroxyl and carboxylic acid groups with sulfonate head group in Figure 5.59.

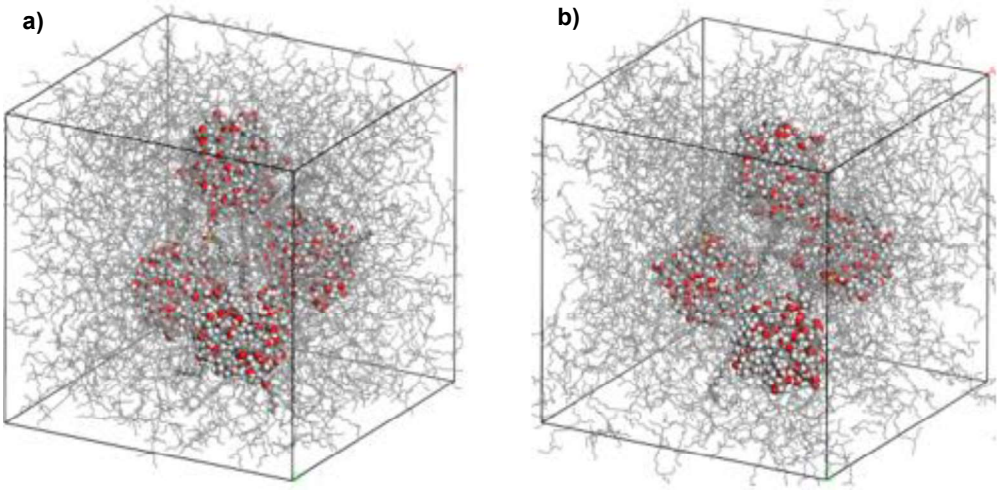

Figure 5.57. a) The first and b) the last frame of the MD simulation of four nanoparticles with eight sulfonate detergent molecules in cubic unit cell.

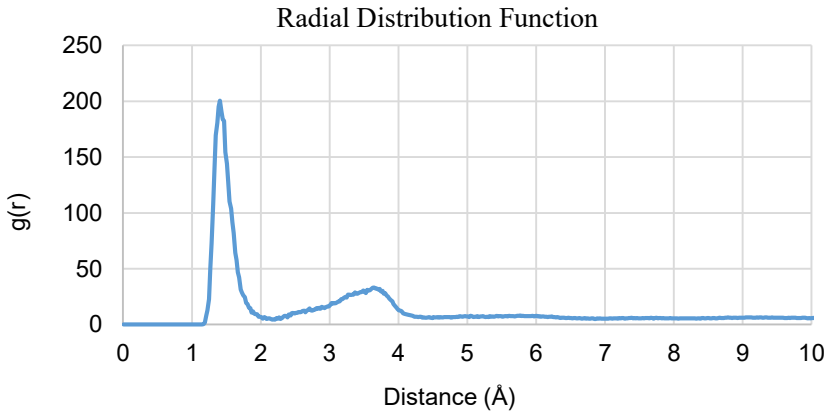

Figure 5.58. RDF between oxygen atoms in the head group of the sulfonate detergent and hydrogen atoms on nanoparticle surface.

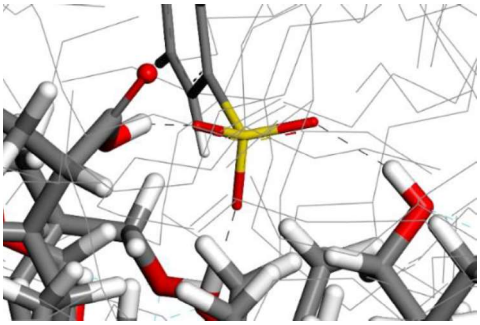

Figure 5.59. Hydrogen bonding between oxygen atoms in the head group of sulfonate detergent and hydrogen atoms at the nanoparticle surface, depicted as black dashed lines.

5.8 Coarse-Grained Simulations

The pairwise coarse-grained interactions between the 4-6 heavy atom units mapped from solubility parameters determined by molecular mechanics were given in Table 5.4. As calculated by both DFT and molecular mechanics methods, strongest attractive interactions are between sulfonate head group (S) and the polar groups of nanoparticles (P and R) as well as succinimide amine groups (N) and the polar groups of nanoparticles (P and R). The most repulsive interactions were between alkyl tails and polar groups of nanoparticle, detergent, and dispersant.

Table 5.4. Coarse-grained interaction parameters mapped into the coarse-grained units.

pair	interaction	pair	interaction	pair	interaction	pair	interaction
AA	-3.0	AP	2.0	AO	2.5	AB	1.0
PA	2.0	PP	-6.5	PO	2.5	PB	6.0
CA	2.5	OP	2.5	OO	0	OB	4.0
BA	1.0	BP	0.6	BO	4.0	BB	0
RA	2.5	RP	-7.0	RO	3.0	TA	0.5
TP	7.0	TO	2.0	NA	1.0	NP	-8.0
NO	3.0	RB	6.5	TB	-5.0	NB	1.0
AR	2.5	PR	-8.0	OR	3.0	BR	6.5
RR	-7.5	TR	9.0	NR	-8.0	AT	0.5
PT	7.0	OT	2.0	BT	-0.5	RT	9.0
TT	0	NT	7.0	AN	1.0	PN	-8.0
TN	7.0	NN	-2.0	SA	1.0	SP	-11
SO	3.0	SB	1.0	SR	-12	ST	7.0

Spherical nanoparticles were only visualized and none of the additives and base oils were shown in the results of coarse-grained simulations. Morphologies of nanoparticles for increasing nanoparticle fraction in the cell were given in Figure 5.60. It was demonstrated that spherical nanoparticles can aggregate at every fraction with different extent. Aggregates showed increasing size of spherical morphologies for the fraction less than 20%. For higher nanoparticle ratio, we observed the formation of continuous labyrinth and gyroid like porous morphology due to the association of these spherical aggregates.

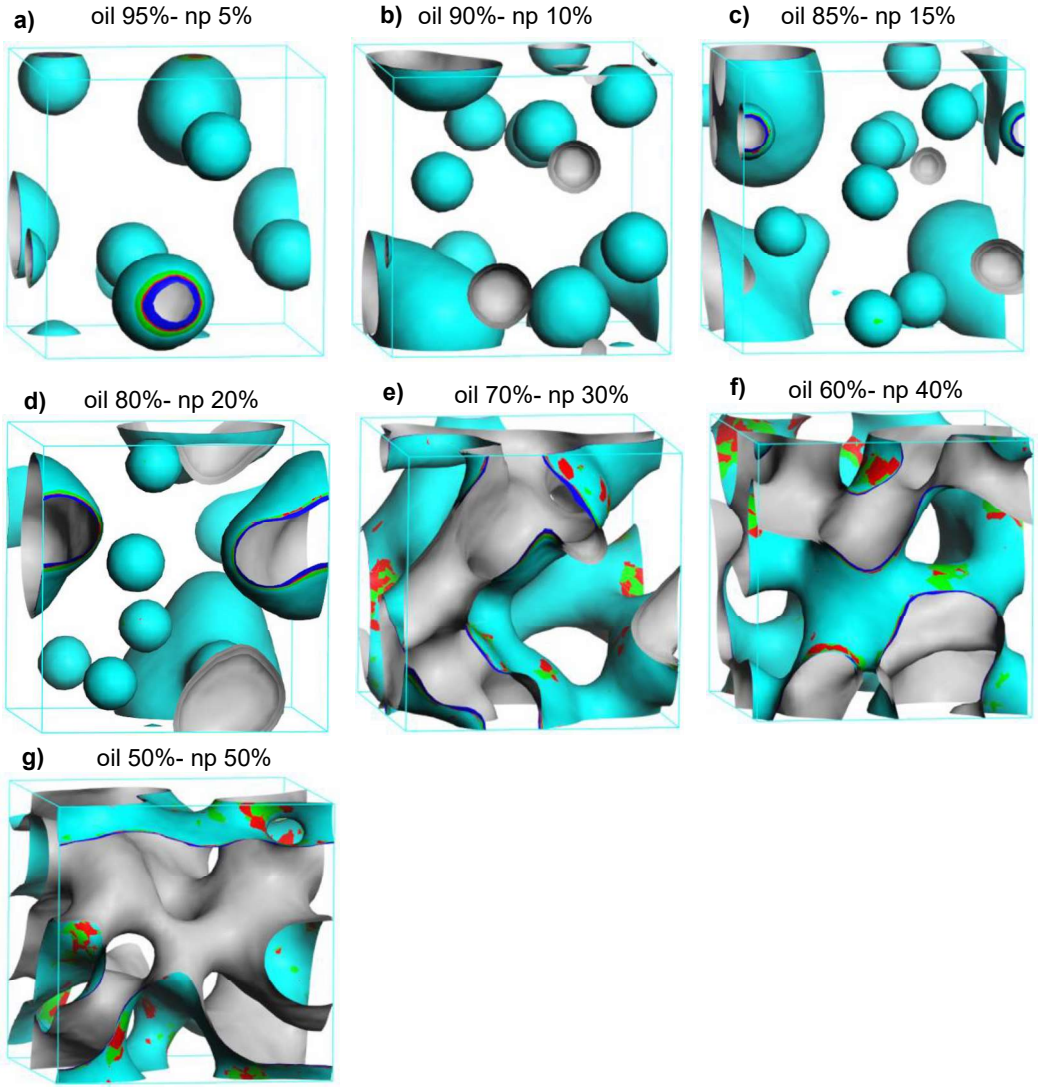

Figure 5.60. Insoluble nanoparticle isosurface structures with a) 95% oil and 5% np, b) 90% oil and 10% np, c) 85% oil and 15% np, d) 80% oil and 20% np, e) 70% oil and 30% np, f) 60% oil and 40% np, g) 50% oil and 50% np ratios.

For the fixed fraction of nanoparticles with increasing dispersant ratio, we observed decreasing aggregation by dispersant addition which indicate the mitigation of deposit formation by the addition of dispersants (Figure 5.61). However, by the extreme addition of dispersant such as 25%, we observed increase of aggregate size again. It was believed that highly hydrophobic surface of nanoparticle due to the PIB tails of dispersant can also cause aggregation.

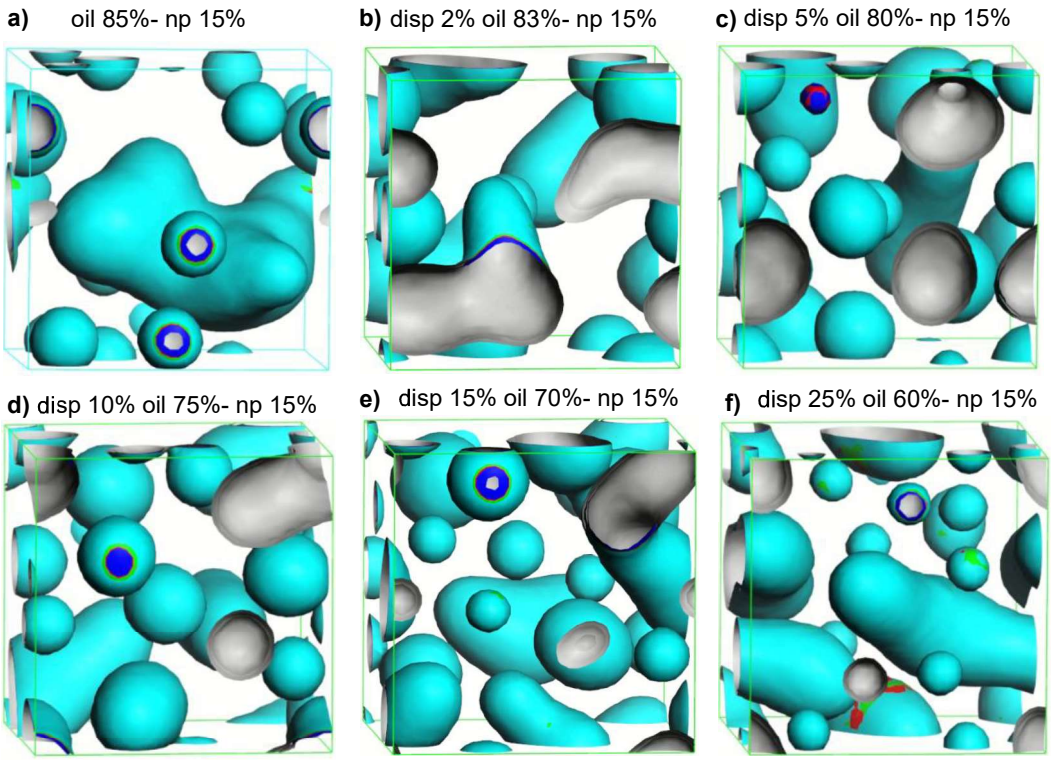

Figure 5.61. Insoluble nanoparticle isosurface structures with a) 85% oil and 15% np, b) 2% disp- 83% oil - 15% np, c) 5% disp- 80% oil - 15% np, d) 10% disp- 75% oil - 15% np, e) 15% disp- 70% oil - 15% np, and f) 25% disp- 60% oil - 15% np ratios.

Similar mitigation of aggregation was also observed by the addition of sulfonate detergents (Figure 5.62). It should be noted that complete dissolution of nanoparticles had never been observed. What we determined was mostly decrease in the size of the aggregates by the addition of detergent and dispersant.

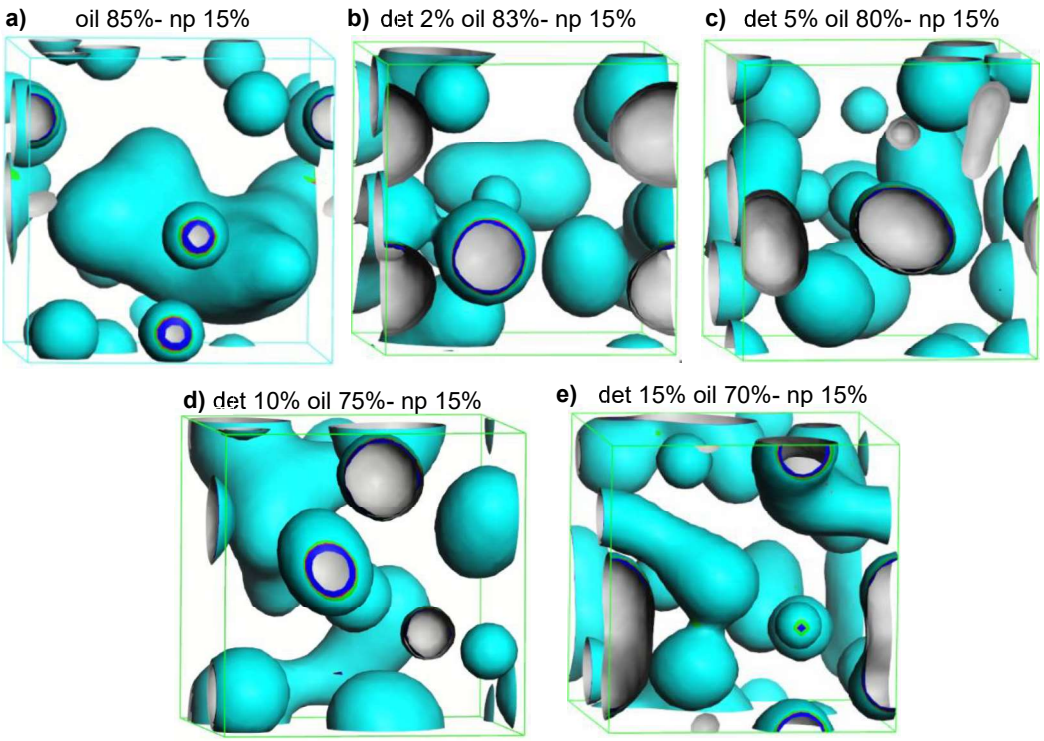

Figure 5.62. Insoluble nanoparticle isosurface structures with a) 85% oil and 15% np, b) 2% det- 83% oil - 15% np, c) 5% det- 80% oil - 15% np, d) 10% det- 75% oil - 10% np, e) 15% det- 70% oil - 15% np ratios.

For the fixed ratio of detergents and dispersants at 10%, the additives were successfully mitigating the effect of aggregation to some point by the increase of nanoparticle ratio (Figure 5.63 and 5.64.). Formation of large aggregates before more than 20% of the nanoparticles was not observed. This result showed that for the deposit formation at very large extent and size, dispersants and detergents in the formula may not be enough to control them completely.

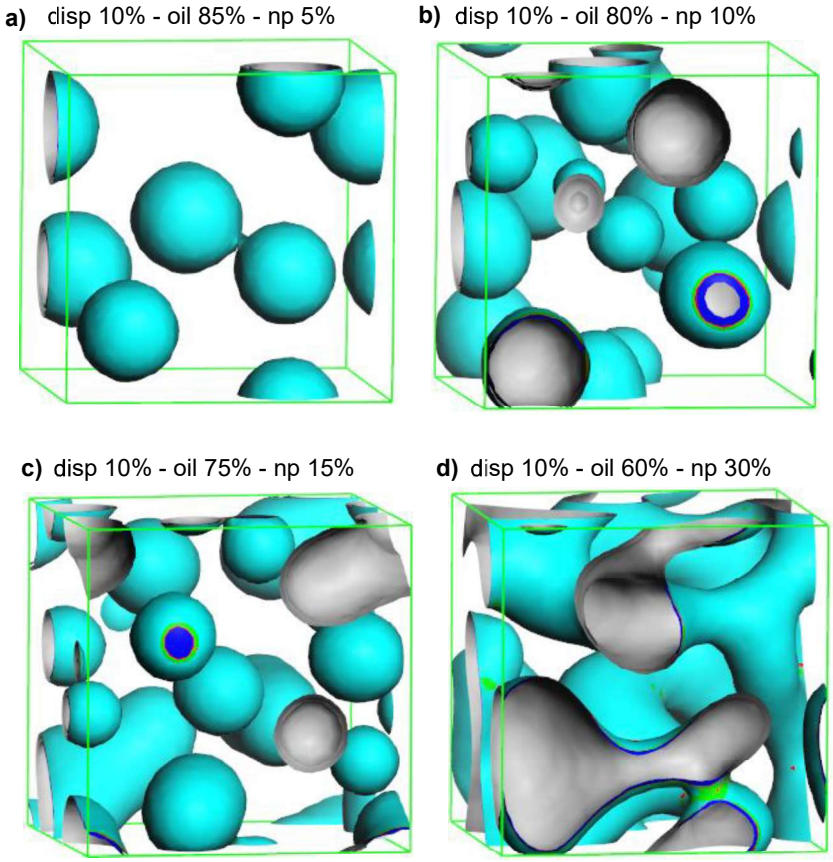

Figure 5.63. Insoluble nanoparticle isosurface structures with a) 10% disp - 85% oil - 5% np, b) 10% disp- 80% oil - 10% np, c) 10% disp- 75% oil - 15% np, d) 10% disp- 60% oil - 30% np ratios.

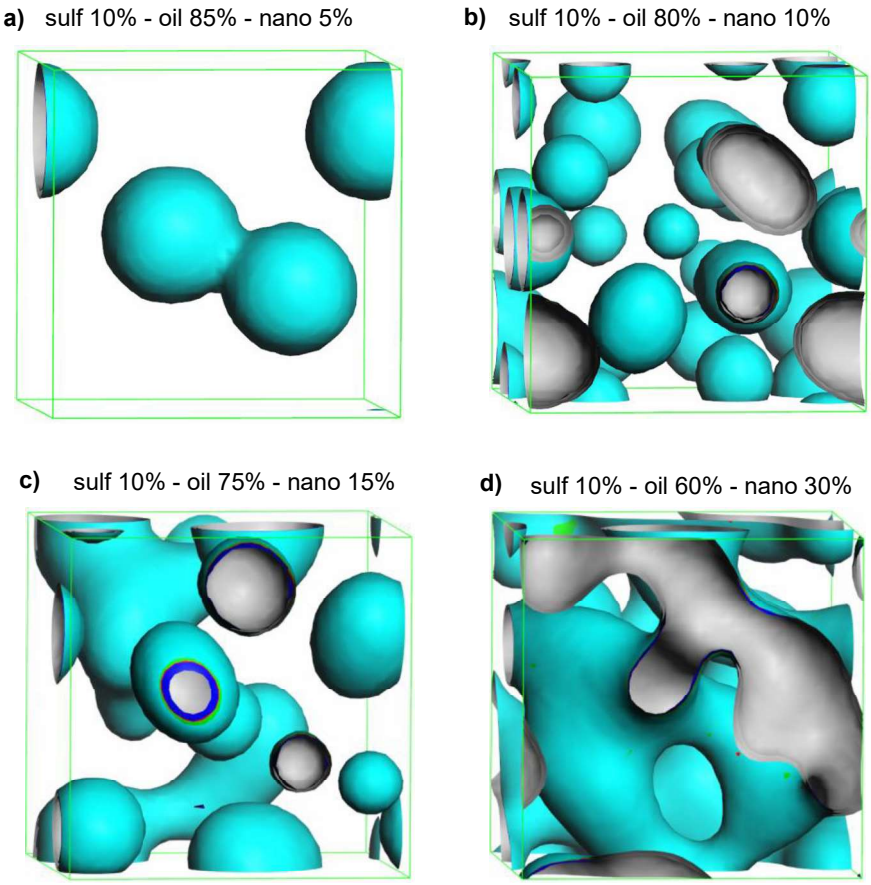

Figure 5.64. Insoluble nanoparticle isosurface structures with a) 10% sulf - 85% oil - 5% np, b) 10% sulf- 80% oil - 10% np, c) 10% sulf- 75% oil - 15% np, d) 10% sulf- 60% oil - 30% np ratios.

As given for the extreme size of continuous aggregates similar with the ones formed on the piston grooves, dispersants and detergents were not clean and control the deposit at their low ratios (Figure 5.65). It can be concluded that different formulations may be required for the different sizes of deposits.

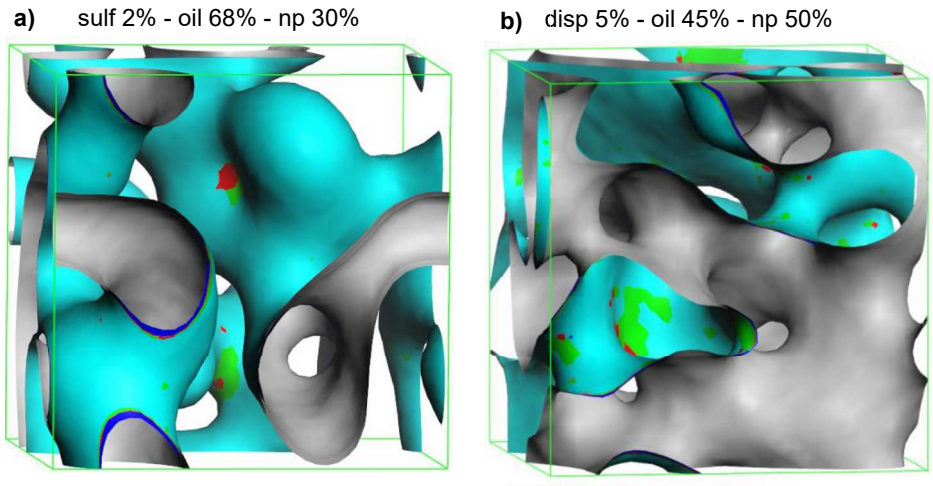

Figure 5.65. a) 2% detergent could not dissolve the 30% nanoparticles, b) 5% dispersant could not dissolve the 50% of nanoparticles.

The effect of increasing temperature has not been observed (Figure 5.66). There are two reasons for this phenomenon. First, our method cannot cover formation of new nanoparticles at high temperatures. Secondly, our method was very coarse that depends on the repulsions and attractions between structures basically. We concluded that this method is too coarse to monitor effect of kinetic factors at great detail.

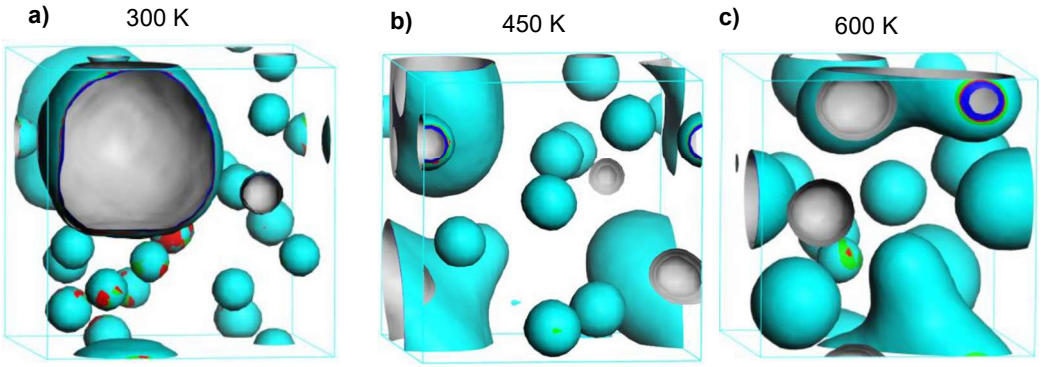

Figure 5.66. Insoluble nanoparticle isosurface structures at a) 300 K, b) 450 K, c) 600 K temperatures.

Field density representation by increasing color tones with and without depiction of dispersant head group is given in Figure 5.67.a and 5.67.c, respectively. Although dispersant polar group shown by green in color is present everywhere in the cell, their concentration was much higher as shown by bright green around the nanoparticle. This result was also valid for the sulfonate head groups of the detergents. The field densities of sulfonate head group show that most of the sulfonate groups are coordinated on the nanoparticle surface demonstrated by brighter green colors in Figure 5.67.d.

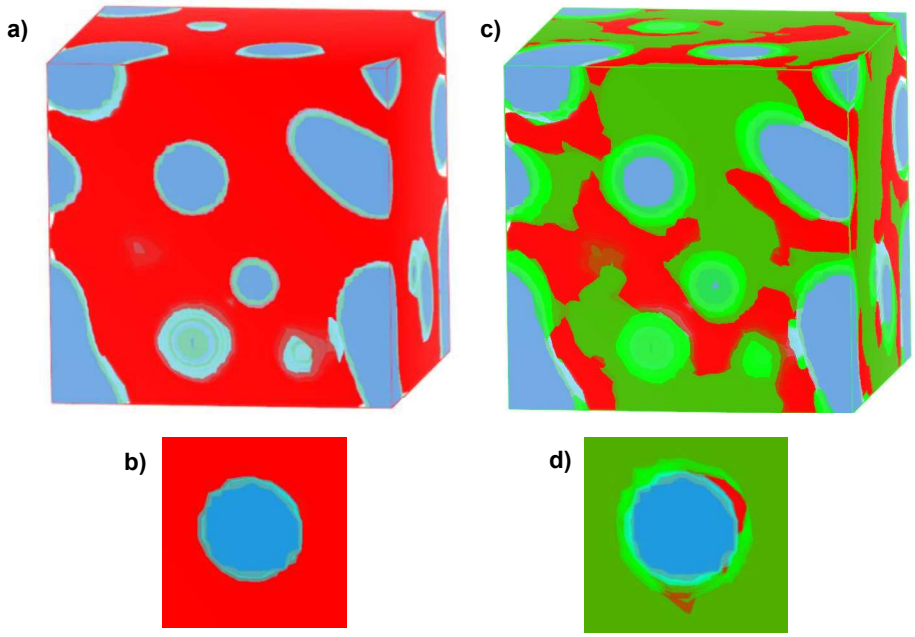

Figure 5.67. The field density distribution of nanoparticles in oil without (a, b) and with (c, d) the depiction of polar amine center in dispersant and sulfonate head group.

CHAPTER 6

CONCLUSION

Multiscale modeling methods was used to explain the working mechanisms of the detergents and dispersants, which are the main additives in engine oils to prevent deposit formation. The effect of different groups in detergents and dispersants on the deposit formation mechanism in multiscale models which include first principle DFT calculations, Monte Carlo methods, all-atom molecular dynamics simulations and coarse-grained simulations that were examined successfully first time for this kind of system in the literature.

All experimental results on lubricant oil recipe and insoluble nanoparticles were provided by Lubrizol Corporation. The main experimental results were pointed out the presence of nanoparticle agglomeration in both drain oil and on piston grooves with the similar morphology which form larger size deposits in the first one. It was observed that these deposits accumulate in the piston grooves and clog them over time and prevent engine running. By the elemental analysis methods such as XPS analysis, it was observed that the insoluble nanoparticle surface was mostly composed of carbon and oxygen in amorphous structure. Experimental results showed that detergents and dispersants can mitigate this problem. Experimental results were used as the roadmap for the design of computational experiments in this thesis.

In the engine oil structure, the base oil has the highest volume ratio. In the structure of the Group II base oil which was used in our model, both small percentage of alkene and branching factors were considered. Besides, molecular and electronic structure of polyisobutylene-bis-succinimide dispersant and sulfonate detergent were studied that explains their role even at molecular level. In the PIBSI dispersant structure, electron rich and deficient parts were concentrated in amine and bis-succinimide

groups, which showed that these groups had high polarity. In the sulfonate detergent structure, the electrostatic potential surface showed high electron density on sulfonate head group. High electron density was on the polar sulfonate head group while low electron density was on the alkyl tail. Molecular model for insoluble nanoparticle, which is one of the most challenging parts of this thesis study, has been performed for the first time in the literature. A model that can aggregate in oil with a relatively polar surface made of carbon and different functional groups at experimental ratio were created after many trials. The electronic structures of the chemicals in the engine oil which are base oil, dispersant and detergent, determined by first principle calculations that show hydrophilic and hydrophobic parts as well as atomic charges to validate force field based molecular mechanics calculations in the first step.

Most probable interactions and configurations of molecules were determined in the interaction energy calculations by both DFT and mixing energies based on molecular mechanic methods. Interaction energies and mixing between components gave the idea on the experimental observations before any simulations. Solubility parameters of the different groups on the dispersant and detergent molecules were calculated after modeling the structures of the chemicals. It was found that the solubility parameters of the non-polar dispersant and oil groups and the polar dispersant and sulfonate head groups had values that are relatively close to each other. These findings supported the notion that whereas amine and succinimide prefer to interact with the polar surface of the nanoparticle, the non-polar tail of the dispersion and detergents may extend into the base oil. The mixing energies and solubility parameters were then used as inputs for coarse grained simulations. AlogP calculations were performed to determine hydrophilicity or hydrophobicity of different molecular groups of dispersant and detergents. It was found that succinimide amine, sulfonate head groups and surface components of insoluble particles are relatively hydrophilic; PIB and base oils were hydrophobic structures. Another guide for understanding of the deposit formation mechanism was solvation free energy calculation of nanoparticle. Solvation free energy of nanoparticle in base

oil was calculated positive which points out the molecular origin of the self-aggregation mechanism of deposit formation.

After modeling molecular structures and solubility parameter, hydrophobicity, interaction energy and solvation free energy calculations, construction of amorphous cells were done using Monte Carlo algorithm to prepare initial structures for Molecular Dynamics Simulations. Oil density at experimental value was reached at constant pressure that validate the force field parameters. Two different methods were used in construction of initial cell structures for MD simulations. In the first method, dispersants and detergents were packed into the cell where only nanoparticles were present. In the second method, first oil was added into the cell where only nanoparticles were present followed by detergent and dispersant addition. In both methods, it was observed that polar group of the dispersant and detergent were coordinated onto the nanoparticle surface at the lowest energy cell geometry which agrees with first principle calculations. Although both methods have similar structures, first method was selected since free volume on the polar surface of the nanoparticle was not prevented by oil molecules as in second method that polar groups of dispersant and detergents cannot position perfectly on the surface. The lowest energy structures of the two, three, and four nanoparticle structures which contains dispersant and detergent molecules were prepared for molecular dynamics simulations after geometry optimizations.

Calculations such as radial distribution functions, mean square displacement of nanoparticles, length evolution between nanoparticles were made for each of the two, three, and four nanoparticle structures for the equilibrium structure of MD simulations. It was observed that hydrogen bonds formed between nanoparticles were the second reason for nanoparticle aggregation and deposit formation when the first reason was positive solvation free energy. In addition, it was presented that in structures with dispersant molecules, they prevented aggregation formation by entering between nanoparticles. The central amine and succinimide groups of the dispersant and the sulfonate head group of the detergent intercalate between the nanoparticles and hydrogen bonds were formed with oxygen which were on the

nanoparticle surface. Hydrogen bond formations were determined in the system by radial distribution function analysis quantitatively. Moreover, the long alkyl tails of the dispersant and detergent were extending in the base oil, preventing aggregation of other nanoparticles. Tail groups extended into the base oil contributes to the dispersion and detergency by forming a repulsive layer as well as creating shear by the flow of base oil. It was concluded that the main purpose of the dispersant and detergent was not to completely disperse the nanoparticle clusters, but to prevent the formation of larger aggregates.

Coarse-grained simulations based on the mean field density functional theory showed three results: Aggregation of nanoparticles was inevitable without any detergents and dispersants. Aggregation of nanoparticles can be mitigated by the addition of dispersants and detergents. For the increasing nanoparticles and fixed amount of detergents and dispersants, such as 10% molecular ratio, we observed presence of critical ratio such that detergents and dispersants were not enough to disperse nanoparticles at high nanoparticle concentration. This implied that there was critical molecular ratio for the detergents and dispersants in the mixture. For the low ratio of nanoparticles, increasing dispersants and detergents mitigates aggregation, however we observed aggregations formed again at very high ratio of dispersants which was predicted to sourced from aggregation of PIB tails.

REFERENCES

[1] S. F. Brown, “Base oil groups: Manufacture, properties, and performance,” *Tribol. Lubr. Technol.*, vol. 71, no. 4, pp. 32–35, 2015.

[2] T. M. Herguth, William R. Warne, *Turbine Lubrication in the 21st Century*, no. 1407. Seattle, Washington: ASTM International, 2001. doi: 10.1520/stp1407-eb.

[3] A. Rizvi,Syed Q., “Lubricant Additives: Chemistry and Applications, Second Edition,” 2nd, illustr ed., L. R. Rudnick, Ed. CRC Press, 2009, pp. 123–139.

[4] N. S. Ahmed and A. M. Nassar, “Lubricating oil additives based on polyalkylpolyamines,” *Int. J. Polym. Mater. Polym. Biomater.*, vol. 58, no. 3, pp. 178–190, Mar. 2009, doi: 10.1080/00914030701551071.

[5] E. J. Seddon, C. L. Friend, and J. P. Roski, “Detergents and dispersants,” in *Chemistry and Technology of Lubricants: Third Edition*, Springer Netherlands, 2010, pp. 213–236. doi: 10.1023/b105569_7.

[6] J. F. Kunc and J. P. Hamer, *Lubricants - The surface savers*. SAE International, 1953. doi: 10.4271/530240.

[7] R. G. Bossert, “The metallic soaps,” *J. Chem. Educ.*, vol. 27, pp. 10–15, 1950, doi: 10.1021/ED027P10.

[8] A. Rizvi, Syed Q., *Fuels and Lubricants Handbook : Technology, Properties, Performance and Testing*, ASTM Inter. ASTM International, 2003.

[9] V. Stepina and V. Vesely, “Lubricants and Special Fluids,” Elsevier, 1992, pp. 303–308.

[10] A. Martini, U. S. Ramasamy, and M. Len, “Review of Viscosity Modifier Lubricant Additives,” *Tribol. Lett.*, vol. 66, no. 2, Jun. 2018, doi: 10.1007/S11249-018-1007-0.

[11] D. Sniderman, “The Chemistry and Function of Lubricant Additives,” *Tribol. Lubr. Technol.*, vol. 73, no. 11, pp. 18–28, 2017.

[12] I. Minami, “Molecular science of lubricant additives,” *Appl. Sci.*, vol. 7, no. 5, 2017, doi: 10.3390/APP7050445.

[13] C.-H. Kuo, “Tribology - Lubricants and Lubrication,” in *Tribology - Lubricants and Lubrication*, 2012, pp. 249–266. doi: 10.5772/873.

[14] H. Abdel-Hameed, N. Ahmed, and A. Nassar, *Some Ashless Detergent/Dispersant Additives for Lubricating Engine Oil*, 1st Edition. OmniScriptum GmbH & Co.KG, 2015.

[15] F. Babick, “Dynamic light scattering (DLS),” *Charact. Nanoparticles Meas. Process. Nanoparticles*, pp. 137–172, Jan. 2020, doi: 10.1016/B978-0-12-814182-3.00010-9.

[16] W. Thiel and G. Hummer, “Nobel 2013 Chemistry: Methods for computational chemistry,” *Nature*, vol. 504, no. 7478, pp. 96–97, 2013, doi: 10.1038/504096A.

[17] H. F. Schaefer, “Methylene: A Paradigm for Computational Quantum Chemistry,” *Science (80-.).*, vol. 231, no. 4742, pp. 1100–1107, Mar. 1986, doi: 10.1126/SCIENCE.231.4742.1100.

[18] S. Karabasov, D. Nerukh, A. Hoekstra, B. Chopard, and P. V. Coveney, “Multiscale modelling: approaches and challenges,” *Philos. Trans. R. Soc. A Math. Phys. Eng. Sci.*, vol. 372, no. 2021, Aug. 2014, doi: 10.1098/RSTA.2013.0390.

[19] N. L. Zhang and X. M. Guo, “Review on multiscale modeling and computation,” *Jisuan Lixue Xuebao/Chinese J. Comput. Mech.*, vol. 28, no. SUPPL. 1, pp. 1–5, 2011.

[20] M. F. Horstemeyer, “Multiscale modeling: A review,” *Pract. Asp. Comput. Chem. Methods, Concepts Appl.*, pp. 87–135, 2010, doi: 10.1007/978-90-481-2687-3_4/FIGURES/11_4.

[21] J. Foresman, “Exploring chemistry with electronic structure methods,” Second Edi., January, J. Foresman and A. Frisch, Eds. Pittsburgh, PA: Gaussian, Inc, 1996, pp. 111–123.

[22] T. Van Mourik, “First-principles quantum chemistry in the life sciences,” *Philos. Trans. R. Soc. A Math. Phys. Eng. Sci.*, vol. 362, no. 1825, pp. 2653–2670, Dec. 2004, doi: 10.1098/RSTA.2004.1469.

[23] J. A. Pople, “Nobel lecture: Quantum chemical models,” *Rev. Mod. Phys.*, vol. 71, no. 5, pp. 1267–1274, 1999, doi: 10.1103/REVMODPHYS.71.1267.

[24] A. Zangwill, “The education of Walter Kohn and the creation of density functional theory,” *Arch. Hist. Exact Sci.*, vol. 68, no. 6, pp. 775–848, Nov. 2014, doi: 10.1007/S00407-014-0140-X.

[25] R. J. Hinde, “Quantum Chemistry, 5th Edition (by Ira N. Levine),” *J. Chem. Educ.*, vol. 77, no. 12, p. 1564, Dec. 2000, doi: 10.1021/ED077P1564.

[26] L. Pauling and E. B. Wilson, “Introduction to Quantum Mechanics with Applications to Chemistry - Linus Pauling, E. Bright Wilson,” New York: Dover, 1985, pp. 50–77.

[27] T. Schlick, “Molecular Modeling and Simulation: An Interdiciplinary Guide,” in *Transport*, 2nd Editio., vol. 8, S. S. Antman, J. E. Marsden, and L. Sirovich, Eds. Springer, 2009, p. 1067.

[28] P. Carsky and M. Urban, *Ab Initio calculations: methods and applications in chemistry*. Springer Science & Business Media, 2012, 2012. doi: 10.1007/978-3-643-93140-6.

[29] B. M. Rode, S. M. Islam, and Y. Yongyai, "Computational methods in solution chemistry," *Pure Appl. Chem.*, vol. 63, no. 12, pp. 1725–1732, Jan. 1991, doi: 10.1351/PAC199163121725.

[30] P. Hohenberg and W. Kohn, "Inhomogeneous electron gas," *Phys. Rev.*, vol. 136, no. 3B, 1964, doi: 10.1103/PHYSREV.136.B864.

[31] W. Kohn and L. J. Sham, "Self-consistent equations including exchange and correlation effects," *Phys. Rev.*, vol. 140, no. 4A, 1965, doi: 10.1103/PHYSREV.140.A1133.

[32] I. Y. Zhang, J. Wu, and X. Xu, "Extending the reliability and applicability of B3LYP," *Chem. Commun.*, vol. 46, no. 18, pp. 3057–3070, Apr. 2010, doi: 10.1039/C000677G.

[33] R. G. Parr and W. Yang, "Density-functional theory of the electronic structure of molecules," *Annu. Rev. Phys. Chem.*, vol. 46, no. 1, pp. 701–728, 1995, doi: 10.1146/ANNUREV.PC.46.100195.003413.

[34] S. Grimme, J. Antony, S. Ehrlich, and H. Krieg, "A consistent and accurate ab initio parametrization of density functional dispersion correction (DFT-D) for the 94 elements H-Pu," *J. Chem. Phys.*, vol. 132, no. 15, Apr. 2010, doi: 10.1063/1.3382344.

[35] N. Metropolis and S. Ulam, "The Monte Carlo Method," *J. Am. Stat. Assoc.*, vol. 44, no. 247, pp. 335–341, 1949, doi: 10.1080/01621459.1949.10483310.

[36] H. Sun, "The COMPASS force field: Parameterization and validation for phosphazenes," *Comput. Theor. Polym. Sci.*, vol. 8, no. 1–2, pp. 229–246, 1998, doi: 10.1016/S1089-3156(98)00042-7.

[37] A. K. Rappé, C. J. Casewit, K. S. Colwell, W. A. Goddard, and W. M. Skiff, "UFF, a Full Periodic Table Force Field for Molecular Mechanics and Molecular Dynamics Simulations," *J. Am. Chem. Soc.*, vol. 114, no. 25, pp. 10024–10035, Dec. 1992, doi: 10.1021/JA00051A040.

[38] M. A. González, "Force fields and molecular dynamics simulations," *École thématique la Société Française la Neutron.*, vol. 12, pp. 169–200, 2011, doi: 10.1051/SFN/201112009.

[39] J. R. Maple *et al.*, "Derivation of class II force fields. I. Methodology and quantum force field for the alkyl functional group and alkane molecules," *J. Comput. Chem.*, vol. 15, no. 2, pp. 162–182, Feb. 1994, doi: 10.1002/JCC.540150207.

[40] A. Y. Toukmaji and J. A. Board, "Ewald summation techniques in

perspective: a survey," *Comput. Phys. Commun.*, vol. 95, no. 2–3, pp. 73–92, Jun. 1996, doi: 10.1016/0010-4655(96)00016-1.

[41] S. Nosé, "A molecular dynamics method for simulations in the canonical ensemble," *Mol. Phys.*, vol. 52, no. 2, pp. 255–268, 1984, doi: 10.1080/00268978400101201.

[42] S. Nosé, "A unified formulation of the constant temperature molecular dynamics methods," *J. Chem. Phys.*, vol. 81, no. 1, pp. 511–519, 1984, doi: 10.1063/1.447334.

[43] S. Nosé, "Molecular Dynamics Simulations at Constant Temperature and Pressure," *Comput. Simul. Mater. Sci.*, pp. 21–41, 1991, doi: 10.1007/978-94-011-3546-7_2.

[44] Y. Chen, J. Zimmerman, A. Krivtsov, and D. L. McDowell, "Assessment of atomistic coarse-graining methods," *Int. J. Eng. Sci.*, vol. 49, no. 12, pp. 1337–1349, Dec. 2011, doi: 10.1016/J.IJENGSCI.2011.03.018.

[45] M. Christen and W. F. Van Gunsteren, "Multigraining: An algorithm for simultaneous fine-grained and coarse-grained simulation of molecular systems," *J. Chem. Phys.*, vol. 124, no. 15, 2006, doi: 10.1063/1.2187488.

[46] V. A. Harmandaris, N. P. Adhikari, N. F. A. Van Der Vegt, and K. Kremer, "Hierarchical modeling of polystyrene: From atomistic to coarse-grained simulations," *Macromolecules*, vol. 39, no. 19, pp. 6708–6719, Sep. 2006, doi: 10.1021/MA0606399.

[47] S. J. Marrink, H. J. Risselada, S. Yefimov, D. P. Tieleman, and A. H. De Vries, "The MARTINI force field: Coarse grained model for biomolecular simulations," *J. Phys. Chem. B*, vol. 111, no. 27, pp. 7812–7824, Jul. 2007, doi: 10.1021/JP071097F.

[48] P. M. Chaikin and T. C. Lubensky, "Principles of Condensed-Matter Physics," *MRS Bull.*, vol. 26, no. 11, pp. 940–941, Nov. 2001, doi: 10.1557/MRS2001.250.

[49] A. Tkatchenko and M. Scheffler, "Accurate molecular van der Waals interactions from ground-state electron density and free-atom reference data," *Phys. Rev. Lett.*, vol. 102, no. 7, Feb. 2009, doi: 10.1103/PHYSREVLETT.102.073005.

[50] E. Yildirim, G. Erciyes, and M. Yurtsever, "Theoretical approach to the structural, electronic, and morphological properties of poly(ε-caprolactone) grafted polypyrroles," *Macromol. Res.*, vol. 21, no. 9, pp. 949–957, Sep. 2013, doi: 10.1007/S13233-013-1111-9.

[51] A. F. M. Barton, "Solubility Parameters," *Chem. Rev.*, vol. 75, no. 6, pp. 731–753, 1975, doi: 10.1021/cr60298a003.

[52] T. Steinbrecher, I. Joung, and D. A. Case, “Soft-core potentials in thermodynamic integration: Comparing one-and two-step transformations,” *J. Comput. Chem.*, vol. 32, no. 15, pp. 3253–3263, Nov. 2011, doi: 10.1002/JCC.21909.

[53] P. J. Hoogerbrugge and J. M. V. A. Koelman, “Simulating microscopic hydrodynamic phenomena with dissipative particle dynamics,” *EPL*, vol. 19, no. 3, pp. 155–160, Jun. 1992, doi: 10.1209/0295-5075/19/3/001.

[54] J. G. E. M. Fraaije *et al.*, “The dynamic mean-field density functional method and its application to the mesoscopic dynamics of quenched block copolymer melts,” *J. Chem. Phys.*, vol. 106, no. 10, pp. 4260–4269, Mar. 1997, doi: 10.1063/1.473129.

[55] A. S. Sarpal, M. I. S. Sastry, V. Bansal, I. Singh, S. K. Mazumdar, and B. Basu, “Correlation of structure and properties of groups I to III base oils,” *Lubr. Sci.*, vol. 24, no. 5, pp. 199–215, Aug. 2012, doi: 10.1002/LS.1172.

[56] B. H. Besler, K. M. Merz, and P. A. Kollman, “Atomic charges derived from semiempirical methods,” *J. Comput. Chem.*, vol. 11, no. 4, pp. 431–439, 1990, doi: 10.1002/JCC.540110404.

[57] A. Tomlinson, T. N. Danks, D. M. Heyes, S. E. Taylor, and D. J. Moreton, “Interfacial characterization of succinimide surfactants,” *Langmuir*, vol. 13, no. 22, pp. 5881–5893, 1997, doi: 10.1021/la970550j.

[58] J. A. Griffiths and D. M. Heyes, “Atomistic simulation of overbased detergent inverse micelles,” *Langmuir*, vol. 12, no. 10, pp. 2418–2424, 1996, doi: 10.1021/la950816r.

[59] A. Berthod and S. Carda-Broch, “Determination of liquid-liquid partition coefficients by separation methods,” *J. Chromatogr. A*, vol. 1037, no. 1–2, pp. 3–14, May 2004, doi: 10.1016/J.CHROMA.2004.01.001.

[60] J. C. Dearden and G. M. Bresnen, “The Measurement of Partition Coefficients,” *Quant. Struct. Relationships*, vol. 7, no. 3, pp. 133–144, 1988, doi: 10.1002/QSAR.19880070304.

[61] A. K. Ghose, V. N. Viswanadhan, and J. J. Wendoloski, “Prediction of hydrophobic (lipophilic) properties of small organic molecules using fragmental methods: An analysis of ALOGP and CLOGP methods,” *J. Phys. Chem. A*, vol. 102, no. 21, pp. 3762–3772, May 1998, doi: 10.1021/JP980230O.